3-2002

Examination of Contact Width on Fretting Fatigue

Russell S. Magaziner

EXAMINATION OF CONTACT WIDTH ON FRETTING FATIGUE

THESIS

Russell S. Magaziner, Lieutenant, USAF

AFIT/GAE/ENY/02-8

DEPARTMENT OF THE AIR FORCE

AIR UNIVERSITY

AIR FORCE INSTITUTE OF TECHNOLOGY

Wright-Patterson Air Force Base, Ohio

Report Documentation Page

Report Date	Report Type	Dates Covered (from... to)
26 Mar 02	Final	Aug 2001 - Mar 2002

Title and Subtitle Examination of Contact Width on Fretting Fatigue	**Contract Number**
	Grant Number
	Program Element Number
Author(s) 2lt Russell S. Magaziner, USAF	**Project Number**
	Task Number
	Work Unit Number
Performing Organization Name(s) and Address(es) Air Force Institute of Technology Graduate School of Engineering and Management (AFIT/EN) 2950 P Street, Bldg 640 WPAFB, OH 45433-7765	**Performing Organization Report Number** AFIT/GAE/ENY/02-8
Sponsoring/Monitoring Agency Name(s) and Address(es) Dr. Jeffrey Calcaterra AFRL/MLLMN 2230 Tenth Street, Suite WPAFB OH 45433-7817	**Sponsor/Monitor's Acronym(s)**
	Sponsor/Monitor's Report Number(s)

Distribution/Availability Statement
Approved for public release, distribution unlimited

Supplementary Notes
The original document contains color images.

Abstract
The primary goal of this study was to find the effects on the fretting fatigue life when systematically holding the fretting fatigue variables, peak contact pressure, maximum/minimum nominal bulk stress, and the ratio of shear traction to pressure force constant while varying the contact semi-width through changes in pad radius and normal load. Experimental tests were performed on a test setup capable of independent pad displacement. Analytical and finite element simulations of the different experimental tests were performed. The local mechanistic parameters were inspected. Five different critical plane based fatigue predictive parameters lacked effectiveness in predicting changes in life with changes in contact width. The Ruiz parameter, and a modified version of the Ruiz parameter performed better than the five critical plane based parameters. Correlations between slip amplitude and fretting fatigue life were found. Tests experiencing infinite fatigue life, in contrast to the typical shortened fretting fatigue life, were experiencing the gross slip condition, which led to fretting wear instead of fretting fatigue.

Subject Terms
Fretting Fatigue, Fretting Wear, Critical Contact Width

Report Classification unclassified	**Classification of this page** unclassified
Classification of Abstract unclassified	**Limitation of Abstract** UU
Number of Pages 186	

The views expressed in this thesis are those of the author and do not reflect the official policy or position of the United States Air Force, Department of Defense, or the U. S. Government.

AFIT/GAE/ENY/02-8

EXAMINATION OF CONTACT WIDTH ON FRETTING FATIGUE

THESIS

Presented to the Faculty

Department of Aeronautic and Astronautics

Graduate School of Engineering and Management

Air Force Institute of Technology

Air University

Air Education and Training Command

In Partial Fulfillment of the Requirements for the

Degree of Master of Science in Aeronautical Engineering

Russell S. Magaziner, B.S.M.E.

Lieutenant, USAF

March 2002

AFIT/GAE/ENY/02-8

EXAMINATION OF CONTACT WIDTH ON FRETTING FATIGUE

Russell S. Magaziner, B.S.M.E.
Lieutenant, USAF

Approved:

Dr. Shankar Mall (Chairman) — 3/11/02 date

Robert A. Canfield, Lt Col, USAF (Member) — 3-13-02 date

Dr. Vinod K. Jain (Member) — 3-11-02 date

Acknowledgements

Firstly I would like to thank God for providing me the opportunity to attend AFIT and for greatly supporting me through my time here. I would also like to sincerely thank my 2LT friends for always being there for me. Josh, Ever, Carolyn, and Matt, I could not have made it without you. Thanks mom, dad, and bro for all the phone calls and emails of encouragement. I love you guys!

Academically I would first like to thank Dr Shankar Mall for his vast patience and his confidence in me. Shantanu Namjoshi became a good friend and role model for me. Ohchang Jin was helpful to me as I started to learn about experiments on fretting fatigue. My two close Turkish officer friends, Halil Yuksel and Onder Sahan, were with me all the way. Tesekkur ederim Agabey! I cannot forget to include my favorite teacher at AFIT, LtCol Bob Canfield for ingraining in me the finite element method and for always being there to listen to me and guide me about matters in and out of school. I had a great time learning from you all!

Russell S. Magaziner

Table of Contents

Page

List of Figures

Page

Page

List of Tables

NOMENCLATURE

2a	contact width
A^*	composite compliance
a	contact semi-width
a_{crit}	*critical* contact semi-width
$a_{theoretical}$, $a_{analytical}$	contact semi-width determine from analytical solution
b	specimen thickness
c	stick zone size
d	displacement measured by extensometer, aka experimental slip
E	modulus of elasticity
e	eccentricity
e_{max}	minimum eccentricity
e_{min}	maximum eccentricity
EXP δ_{max}	maximum experimental slip range
f	cyclic frequency
F_1	first Ruiz Parameter
F_2	second Ruiz Parameter
FEA δ_{range}	finite element slip range
FP, F	Findley Parameter
$F_{modified}$, F_{mag}	modified Ruiz Parameter, Magaziner Parameter
k	relative radius of curvature
k	influence factor for Findley parameter
L_1, L_2	load cell readout

L1, L2, b1, b2	slip zone size
m	fitting parameter
$\max\tau_{max}$	maximum maximum shear stress
MSSR	Modified Shear Stress Range
N	number of cycles
N_f	number of cycles until failure, aka life
P	normal load
p(x)	normal pressure distribution
P_0	peak contact pressure
$P_{0,analytical}$	peak contact pressure from analytical solution
$P_{0,FEA}$	peak contact pressure from finite element solution
Q	shear traction force, aka friction force
Qmax	maximum shear traction
Qmin	minimum shear traction
Q/P	the ratio of shear traction to pressure force
R	pad radius
R_1, R_2	radius of the first body and second body
$R\tau$	shear stress ratio
S_1, S_2	principal stresses
SWT	Smith-Watson-Topper
Sxy, τ_{xy}	shear stress
Sxx, σ_{xx}	normal stress parallel with length of specimen
Syy, σ_{yy}	normal stress perpendicular to length of specimen

SSR	Shear Stress Range
teff	Effective Shear Stress Parameter
u1, u2, u3	nodal displacements
V	voltage from extensometer
x	distance along the specimen surface from the center of contact
$\Delta\sigma_L$	local (bulk) cyclic tensile stress
$\Delta\sigma_{L,max}$	maximum local normal stress range
$\Delta\sigma_N$	bulk nominal stress range
$\Delta\tau_L$	local cyclic tangential shear stress at the interface
$\Delta\tau_{L,max}$	maximum local shear stress range
$\Delta\tau$	shear stress range
δ	independent pad displacement, aka span
δ	slip amplitude at the interface
δ, δ_{range}	slip range
δ_{crit}	critical slip range or critical slip amplitude
δ_{max}	maximum slip range
μ	coefficient of friction
ν	Poisson's ration
θ	plane angle
$\sigma_{L,max}$	maximum local normal stress
σ_L	local stress
σ_N, σ	*nominal* bulk stress, remote stress, global stress

$\sigma_{N,max}$	max nominal bulk stress
$\sigma_{N,min}$	min nominal bulk stress
$\tau_{L,max}$	maximum local shear stress
τ_{max}	maximum shear stress
τ_{min}	minimum shear stress

ABSTRACT

The primary goal of this study was to find the effects on the fretting fatigue life when systematically holding the fretting fatigue variables, peak contact pressure, maximum/minimum nominal bulk stress, and the ratio of shear traction to pressure force constant while varying the contact semi-width through changes in pad radius and normal load. Experimental tests were performed on a test setup capable of independent pad displacement. Analytical and finite element simulations of the different experimental tests were performed. The local mechanistic parameters were inspected. Five different critical plane based fatigue predictive parameters lacked effectiveness in predicting changes in life with changes in contact width. The Ruiz parameter, and a modified version of the Ruiz parameter performed better than the five critical plane based parameters. Correlations between slip amplitude and fretting fatigue life were found. Tests experiencing infinite fatigue life, in contrast to the typical shortened fretting fatigue life, were experiencing the *gross slip* condition, which led to fretting wear instead of fretting fatigue.

EXAMINATION OF CONTACT WIDTH ON FRETTING FATIGUE

I. Introduction

1.1 Definition of Fretting Fatigue:

Fretting occurs between components that are together in contact and undergo a small amplitude cyclic-type loading that causes them to have at least some small tangential displacement relative to each other. When the presence of fretting is associated with decreased fatigue performance, such as shorter life or smaller allowable maximum stress range at a given life, the effect is called fretting fatigue [26]. It is widely accepted that fatigue loading coupled with pressure between two touching components causes premature crack nucleation and accelerated crack growth causing components under fretting fatigue to fail unexpectedly at stress levels well below their plain fatigue limit [29] or at fewer life cycles than predicted by plain fatigue analysis. But it is not generally agreed upon as to what specifically is occurring that causes this phenomenon or what can be done to prevent it.

This type of scenario happens most often in bolted and mechanically fastened joints [26]. For example, the bolted flange connections between pipes provide a typical, real world, example of a potential fretting fatigue problem. Hydrostatic pressure from the fluid within the pipe and the pressure from the flange combined with vibrating loads from the pump or cavitations that can lead to failure from fretting. Subsequently a danger of pipes bursting at the flange is caused by the phenomenon being studied.

1.2 Relation to Air Force:

One reason that the United States Air Force is interested in the subject of fretting fatigue is because it is a potential problem in turbine bearing propulsive engines. At the dovetail joint, where each turbine blade connects to the outer annulus wall is another prime example of where components could undergo fretting fatigue. The turbine blades experience cyclic loading in the form of vibrations. At the dovetail joint two surfaces are in contact and potentially rub and slip against each other. Failure of turbine blades cannot be predicted accurately by the conventional plain fatigue analysis. Instead Air Force designers need to over-compensate for this danger in the form of thicker, less efficient blades. Secondly, because of the lack of understanding of fretting fatigue, engine maintenance crews need to spend extra money and effort in looking for cracks that may or may not be propagating on the blades. If cracks are missed, the lives of Air Force pilots and aircrafts are at risk. With a better understanding of the failure mechanism, turbine design engineers could make a more efficient engine, pilots will be safer with a reduced chance of in-flight engine damage, and maintenance costs will be reduced, as detection and prediction will be made easier for repair crews.

1.3 Simplifications From Turbine to Experimental Setup:

Turbine engine geometry and conditions are very complex and it is therefore necessary to make some simplifications to the structure and load in order to investigate the failure mechanism. A test setup has been created in an AFIT laboratory to simulate the same failure mechanism using a servohydraulic test machine, specially designed fretting pads, a fretting fixture to hold the pads, and dogbone test specimens. It is the hope of researchers that an understanding of fretting fatigue will be gained by its study,

and then this clearer picture can be applied to the real world through better engineering designs and predictive methods.

1.4 Introduction to Contributing Variables:

Variables such as the pressure between contacting bodies, the peak pressure between the rubbing components, the magnitude of the rubbing, the area of the contact, and the cyclic loading as well as several other factors, all seem to contribute to failure by fretting fatigue in some unknown collaborative way. Unfortunately it is hard to isolate and examine the effects of specific variables. To accomplish this mammoth undertaking of predicting and preventing, many studies need to be made and their results combined.

1.5 Purpose of this Study:

Several factors are thought to influence the effect of fretting fatigue on the life of a component. It is generally agreed that these variables either directly or indirectly play a role in the fretting fatigue process, but the exact contribution of these factors is not currently known. As a part of the combined effort of several fretting fatigue studies to examine what the recipe is of contributing variables, this study attempts to isolate one variable and look at the effects of changing it while keeping as many other variables constant as possible. The variable that will be systematically studied is the area of contact between the two components, which will be represented by and referred to as the contact semi-width. This study asks the question, what will be the effect on fretting fatigue by varying contact semi-width in tests, but keeping other variables constant.

A secondary goal of this study was to investigate an enigma in the fretting world, the *critical* contact semi-width, and how it applied to the titanium alloy commonly used in jet engine components. It was previously discovered, with copper-aluminum alloy,

that tests run with a contact area smaller than a certain *critical* contact area, had fatigue lives about an order of magnitude greater than those with contact areas larger. Would Ti-6Al-4V also have a critical contact semi-width? If so, what would be causing the dramatic change in life between similar tests with slightly greater and contact semi-widths slightly smaller than the critical width?

Firstly, the efforts of previous researchers in this area were intensely studied. Then experimental tests were designed and conducted. The subject of this investigation was then analyzed through the use of analytical and numerical test simulations, as well as using the latest methods/techniques in predictive fretting parameters.

Experimental tests revealed a difference in fretting fatigue life with changes in contact semi-width. Predictive parameters were also evaluated in their ability to predict these changes in life that occurred with variances in contact semi-width. The results of the analysis were highly interesting, especially with respect to the critical contact semi-width.

II. Background Research

The field of research in fatigue is vast. Even the bank of knowledge and experiments in the subsection of fatigue that is known as fretting fatigue is immense. Because of this enormity the background research for this study will cut straight to the chase and try to avoid any unnecessary information. This chapter will start with distinguishing between two types of fretting: fretting fatigue and fretting wear. Secondly, how fretting fatigue is typically simulated in experiments and the variables involved will be described. Then various experiments and theories germane to this study will be summarized. Next the pertinent analytically developed equations will be presented. Finally, two key assumptions made in past studies will be highlighted.

2.1 Difference Between Fretting Fatigue and Fretting Wear

As touched upon in the last chapter, whenever assemblies of components undergo vibrations, be it in an airplane, automobile, or even household plumbing, there is potential for fretting [28]. Often rubbing and hence slipping takes place between adjacent surfaces within these assemblies, causing one or both of two harms: fretting fatigue and fretting wear. Fretting fatigue is what leads to a reduction in the components' fatigue life from the expected typical fatigue longevity due to plain fatigue [28]. Fretting wear causes deterioration of components' surface finishes and changes their dimensions [33]. Both effects of this slipping can be detrimental, but fretting fatigue seems worse from a

strength and component longevity standpoint. The reduced life caused by fretting fatigue can be as low as one-tenth of the plain fatigue life [7]!

It will become important for the purposes of this study to clearly establish the distinction between the two types of fretting. When the life to failure is drastically reduced, the dominant fretting phenomenon is known as fretting fatigue [1]. When a specimen, that is in a fretting situation, fails at a number of cycles significantly larger than is typical for fretting fatigue, the specimen is said to have *infinite fretting fatigue life*, even if its life is not really infinite or even as long as plain fatigue life. Specimens with infinite fretting fatigue life are probably dominantly influenced by fretting wear. The surfaces are worn due to the rubbing the phenomenon, but the reduction in life of the specimen from plain fatigue is not as dramatic. While specimens with much shorter lives could be experiencing both fretting fatigue and some wear, it seems fretting fatigue is the controlling failure mechanism. For example, if one fretting test specimen in this study fails at 80,000 cycles, but a second does not fail even after a million cycles, the latter has infinite life and is said to be experiencing fretting wear, but the former has failed from fretting fatigue.

2.2 Introduction to Test Setup:

As mentioned in the introduction, with a good understanding of how fretting fatigue affects Ti-6Al-4V, the material of most turbine blades, Air Force aircraft designers can potentially build improved propulsion engines and the benefit in safety and money could be great. To achieve this level of understanding research needs to be done. But due to the complex nature of turbine blades in working jet engines, simplifications are needed to be made in order to experimentally isolate the fretting fatigue phenomenon.

Researchers hope to simulate the same harms that happen to system components such as turbine blades or rivet joints in a more universal way than by testing each specific situation and system in which fretting is potential danger. Therefore over the years fretting fatigue specialists have developed a general test setup to try to isolate the phenomenon in question. The basic test setup can be seen in Figure 2.1 at the end of this chapter.

A hydraulic test machine is used to grip a specimen and apply a cyclic stress load, σ_N, to one end while holding the other end fixed. At the same time pads are pressed against the specimen by a load, P, in the direction perpendicular to the length of the specimen. Often these pads are cylindrical, because analytical solutions of the stress and displacement distributions have been derived for this special case. Due to the elasticity of the material, the specimen expands and contracts under the cyclic load. But at the same time, the pads are held in a fixed position, by a fretting fixture. The two bodies, the pads and the specimen, rub against each other. This setup can lead to failure by fretting fatigue.

In order to understand the different variables involved, it is a good idea to look at the Figure 2.2. It shows a 2-dimensional picture of the fretting fatigue experimental setup. The rectangular shape in the middle represents the specimen and the two rounded bodies on opposite sides of the middle of the specimen are fretting pads. When P is zero, the cylinders have a constant radius, R. The pads are essentially held fixed perpendicular to the specimen by the fretting fixture. Technically they do have slight movement and rotation during the cyclic loads, but this will be discussed in the analysis section in Chapter III. Normal force, P, is applied to the tail ends of the fretting pads by springs,

which are in turn attached to a load cell, which reads the magnitude of the load. The force is translated through the pads and the cylindrical heads of the pads are pressed against the substrate. For cylinder-headed pads, the pressure force has a Hertzian distribution against the specimen. The peak pressure force experienced on the substrate by the pads is known as the peak contact pressure, p_0. When the pad is pressed against the specimen, the materials slightly compress and flatten together. The length of the area of the substrate surface that is actually touching the pad, when normal load is applied, is known as the contact width, 2a. Half of the contact width is the contact semi-width, a. In this study, contact width and semi-contact width are both used to describe the same factor, the amount of contacting area between the pads and specimen. This is shown on Figure 2.2 at the end of this chapter. One end of the specimen is held by a fixed servohydraulic gripping arm, while the other end of the substrate is gripped and a cyclic stress is applied, σ_N. The rubbing effect, which is a key ingredient of fretting, occurs as the substrate is stretched and relaxes. Due to changes in strain induced by the cyclic bulk stress, the specimen moves relative to the pads, which are pressed against it. There is friction between the pads and the specimen. Q is the surface shear force caused by this friction. All three forces just described, P, σ_N, and Q, can be seen on Figure 2.1

It is also important to note that there are different regions within the contact area. In many fretting fatigue tests there are three regions within the contact width, 2a. The central area is where the contacting bodies stick together, as if they had been welded. This is called the stick zone, 2c. On both sides of the sticking region are regions where the contacting bodies slip relative to each other. Regions b1 and b2 are slip zones. The amount of slipping that takes place between the two bodies in these regions is known as

the micro slip range or slip range, δ. Incidentally, just as the contact semi-width is half of the contact width, the slip amplitude is half of the slip range. Outside of the slip zones, the pads and specimen are no longer in contact. Figure 2.3 shows what the slip zones might look like on the specimen surface if one could see through the fretting pad.

2.3 Summaries of Previous Works:

2.3.1 Bramhall:

Back in the 1970's, Oxford researcher, Bramhall noticed both the peak normal pressure, p_0, and contact semi-width, a, varied oppositely with respect to P and cylindrical pad radius, R. Contact semi-width and p_0 are both proportional to $(PR)^{\frac{1}{2}}$. By changing R and P, it is possible to change the size of the contact width while still maintaining a constant p_0 [28]. Furthermore, it is conversely possible to change the P and R in such as way as to maintain a constant 2a, but varying p_0. If P and R change, there is an option to keep either a or p_0 constant while varying the other. Evidence for this will be given in equations (13) and (14) of section 2.4.

In the conclusion of Bramhall's study, were two points relevant to this work. First, was the observation that fretting fatigue life depended both on the contact size and the imposed stress levels. Secondly, it was noted that there was a critical contact size below which fatigue life rapidly goes from short to long. Later University of Oxford researchers, Nowell and Hill, ran experiments in an attempt to explain Bramhall's observations [28].

2.3.2 Nowell and Hill [28]:

Nowell and Hill conducted some very interesting fretting fatigue tests in the late 1980's germane to this study. The material they used was an aluminum/copper alloy. They varied contact size while trying to keep other relevant parameters constant, including the ratio of shear traction to normal load, Q/P. From this

study, they noted that fretting fatigue life was found to be infinite below a certain *critical* contact width, just as Bramhall had found. Using elastic stress analysis and by calculating stresses and displacements they came to their conclusion: the change in life with contact size is a result of a variation in the micro-slip amplitude, the slipping between the pad and the substrate. They used two parameters proposed by Ruiz et al. to weigh the severity of damage caused by fretting and the probability of crack initiation at a specific location.

2.3.3 Iyer [14]: Iyer had a completely different approach to fretting fatigue analysis than that of Nowell and Hill. Former AFIT researcher, Iyer, presented a newer explanation of the effect of contact width on fretting fatigue, which incorporated the use of the numerical technique finite element method.

2.3.3.1 Local Mechanistic Parameters: Also using a cylinder-on-flat contact configuration, Iyer ran a series of experiments to better understand the relative effects of six local mechanistic parameters on which the fretting fatigue life may depend. It was his major claim that the important variables to look at were not the global boundary conditions, such as the applied normal load, the pad radius, or the applied bulk stress. Instead, he thought, "local" variables within the contact region on a microscopic scale should be the primary focus of any fretting life equations. In order to find values for the local parameters, Iyer used finite element analysis to simulate his tests.

Studies of the fretting fatigue contact-induced crack initiation and growth have been made difficult by the complex nature of fretting, which combines both plasticity and wear. Iyer noted several local parameters that had been identified as being related to the overall fretting fatigue degradation process are: local contact pressure, p(x), slip

amplitude at the interface, δ, the coefficient of friction, μ, the local cyclic tangential shear stress at the interface, $\Delta\tau_L$, the local (bulk) cyclic tensile stress just beneath the contacting interface and parallel to it, $\Delta\sigma_L$, cyclic frequency, f, contact width, 2a, and the number of fretting cycles, N. Many of these local parameters are dependant on each other. For example the tangential shear stress is proportional to the coefficient of friction and the contact width changes with differing contact pressures. It is generally agreed that some combination of the above parameters is responsible for the reduction in plain fatigue life, but the exact recipe of which parameters contribute and how much they contribute relative to each other towards fretting fatigue is unknown. In order to examine the maximum values of local stresses in this study, principal stresses were calculated from the finite element output.

2.3.3.2 Principal Stresses [10]: The maximum or minimum in-plane normal stress acting on a point is given by the equation:

$$S_{1,2} = \left(\frac{\left(\sigma_{xx} + \sigma_{yy}\right)}{2}\right) \pm \left(\left(\frac{\left(\sigma_{xx} - \sigma_{yy}\right)}{2}\right)^2 + \tau_{xy}^2\right)^{\frac{1}{2}} \quad (1)$$

S_1 and S_2 are called the principal stresses and the planes on which they act are called the principal planes. There is no shear acting on the principal planes. The planes for maximum shear stress are 45^o from the orientation of the planes for principal stress. This maximum shear stress is

$$\tau_{\max} = \left(\left(\frac{\left(\sigma_{xx} - \sigma_{yy}\right)}{2}\right)^2 + \tau_{xy}^2\right)^{\frac{1}{2}} \quad (2)$$

2.3.4 Jin and Mall [15,16]: The very recent efforts of Jin and Mall in the area of gross slip and independent pad displacement became important towards the end of this study. So the two publications in this area will be briefly summarized.

Jin's test setup was capable of independently moving the pads even with the normal force and bulk stress applied. Incidentally, it was Jin's same test setup that was used in this study. This modified setup could perform both fretting fatigue and fretting wear tests. A more detailed description of how this worked will be presented in the test setup section of chapter III. Jin and Mall also used the cylinder-on-flat configuration, but with only 0.0508 m radius fretting pads. The specimens and pads were made of Ti-6Al-4V, the same material used in this study. Jin varied pad displacement for two different P loads, and a constant cyclic stress range. What he found was that, for lower values of independent pad displacement, his tests would fail by fretting fatigue. But for higher values of independent pad displacement, his tests would be dominated by fretting wear and have infinite fretting life. In these infinite life tests he described the type of slipping that occurred between the pads and specimen as "gross slip."

2.3.5 Namjoshi, Mall, Jain, and Jin (Predictive Parameters): Contemporary fretting fatigue researchers Namjoshi, Mall, Jain, and Jin have been making efforts in the development of predictive criteria for fretting fatigue. If they can accurately predict the location, crack initiation angle and number of cycles until crack initiation caused by fretting fatigue, then they can reduce the danger of unexpected failures. Furthermore, these predictive parameters being created can be used to narrow down what the actual causes of fretting fatigue are and help engineers design components that will be more resistant to fretting fatigue's detrimental effects.

2.3.5.1 Definition of critical plane: The most recent predictive criteria are based on the stresses found on the critical plane. If the principal axes rotate during the cyclic loading, the cyclic loads occur at more than one frequency, or if there is a difference in phase, other than 180^{o}, between loads, then fatigue problems are often approached by looking at the critical plane. Generally speaking, the critical plane approach is done by finding the maximum shear strain amplitude and the plane on which it acts and then using the maximum normal stress acting upon this plane to obtain the effect of a mean stress [4].

Many conventional fretting fatigue researchers recommend using critical plane based predictive parameters and criteria, because crack nucleation and initiation in fretting fatigue occur in a contact region between two bodies which is governed by a state of stress that is multi-axial in nature. It was the recent opinion of Namjoshi et al. [23] that fretting fatigue crack initiation is function of the shear stress on the critical plane and that fretting fatigue life is related to the normal stress on the critical plane. However, because the stresses required for these parameters cannot accurately be measured using test equipment, they need to be determined through simulations of tests. These simulations can be based on the analytical solutions as well as numerical methods, such as finite element analysis.

The following critical plane based fatigue parameters were looked at in this study with regard to the tests conducted:

2.3.5.2 Smith-Watson-Topper (SWT) Parameter: Szolwinski and Farris modified the Smith-Watson-Topper parameter for application to fretting fatigue crack initiation [31]. The modified parameter is the product of the normal strain amplitude and

the maximum normal stress. For this parameter, the critical plane is defined as the plane in which the modified SWT parameter is a maximum. Therefore the critical plane approach, using this parameter, gives both the location and orientation angle of fretting fatigue crack initiation.

2.3.5.3 Shear Stress Range (SSR) Parameter: The second parameter is known as the shear stress range critical plane parameter. The shear stress range,

$$\Delta\tau = \tau_{max}-\tau_{min} \quad (3)$$

was calculated using a program written by Namjoshi, which will be known as the *Namjoshi parameters program* [24]. The program computed the $\Delta\tau$ on all planes at all points on the substrate's contact region and chose the plane, where this range was maximum, to be the critical plane. τ_{max} and τ_{min} are the shear stress values due to the maximum and minimum axial loadings. Just as was the case with the SWT parameter, the maximum shear stress range was determined in the program on all planes ranging from $-90^{o} \le \theta \le 90^{o}$ in 0.1^{o} increments.

2.3.5.4 Effective Shear Stress Parameter: In order to include the effect of the mean axial/shear stress on the fretting fatigue this parameter was slightly modified using the amendment proposed by Walker [32],

$$\Delta\tau_{crit,effective} = \tau_{max}(1-R\tau)^{m} \quad (4)$$

where τ_{max} means the maximum shear stress on the critical plane, $R\tau$ refers to the shear stress ratio, τ_{min}/τ_{max}, on the critical plane, and m is a fitting parameter. From plain fatigue data, the value of μ was found to be 0.45, which is the value used in this equation. This accounts for the mean shear stress ratio effect on the critical plane. The following are two parameters are based on both shear and normal stresses and the critical plane.

2.3.5.5 Findley Parameter: The Findley Parameter, FP, was created in the 1960's for plain fatigue analysis. It involves both the shear stress amplitude and the maximum stress normal to the orientation of the maximum shear plane multiplied by an influence factor, k, such that:

$$FP = \tau_{average} + k\sigma_{max} \quad (5)$$

As before, this was calculated using the parameters program designed by Namjoshi. The critical plane was such that crack initiation was assumed to occur on the plane with the maximum Findley Parameter value. The parameter was determined, as the others were, on all planes from –90 to 90 degrees on increments of 0.1^{o}. It was shown by Namjoshi that this parameter could not discern between plain and fretting fatigue when determining fatigue life, which is obviously in error. So it is probably not the best choice of a predictive fretting fatigue parameter.

2.3.5.6 Modified Shear Stress Range (MSSR) Parameter: The final critical plane parameter evaluated in this study is considered by some to be the premier fretting fatigue predictive parameter [23]. It is a modified version of the shear stress range critical plane parameter, MSSR, which combined the better features of the other critical plane parameters. It is thought that this parameter is the best for determining the effects of fretting fatigue for several reasons. It is based on both normal and shear stresses, so therefore it eliminates the effect of pad geometry. Also it includes aspects of the shear stress range parameter, which was the only parameter mentioned thus far shown by Namjoshi to be satisfactory for determination of both crack location and orientation [23].

$$MSSR = A\Delta\tau^{B}_{crit} + C\sigma^{D}_{max} \quad (6)$$

A, B, C, and D are constants obtained experimentally and were found to be A = 0.75, B = 0.5, C = 0.75, and D = 0.5 from previous studies. In this approach the critical plane is determined by the maximum value of the shear stress range, not by the maximum value of the MSSR parameter.

2.4 Analytical Model:

Over the years, material theorists and mathematicians have created analytical solutions, under idealized conditions such as cylinder-on-flat fretting geometry. It is because there are analytical solutions for this geometry that many researchers choose it as opposed to flat fretting pads or other geometry.

Before setting up any experimental tests for this study, analytical computations were made to estimate what boundary conditions should be chosen. In order to calculate the peak contact pressure and contact semi-width for given material properties, geometries, boundary conditions, and loads, analytical equations for the cylinder-on-flat contact scenario were used.

R_1 is the radius of the first body and R_2 is the radius of the second body in contact. k is their relative radius of curvature such that:

$$k = \frac{1}{R_1} + \frac{1}{R_2} \tag{7}$$

In this study, the radius of the specimen was infinite, so:

$$k = \frac{1}{R} \tag{8}$$

A^* refers to the composite compliance of the materials in contact:

$$A^* = 2 * \left[\left(\frac{\left(1 - v_1^2\right)}{E_1} \right) + \left(\frac{\left(1 - v_2^2\right)}{E_2} \right) \right] \tag{9}$$

Or if the materials are both the same, such as in the case of this study:

$$A^* = 4 * \left(\frac{\left(1 - v^2\right)}{E} \right) \tag{10}$$

The normal pressure distribution is Hertzian [9]:

$$p(x) = p_0 * \left(1 - \left(\frac{x}{a} \right)^2 \right)^{\frac{1}{2}} \tag{11}$$

Assuming that the contacting materials are elastically similar, the peak pressure is given as:

$$p_0 = \frac{(2 * P)}{(\pi * a)} \tag{12}$$

or

$$p_0 = \left(\frac{(P * E)}{2 * \pi * \left(1 - v^2\right) * R} \right)^{\frac{1}{2}} \tag{13}$$

The relationship:

$$P = \frac{\left(\pi * k * a^2\right)}{\left(2 * A^*\right)} \tag{14}$$

was used to theoretically predict contact semi-width. The above listed equations were used initially to set up the experimental boundary conditions. But for the analytical analysis, a Fortran program, called the "Ruiz" program, was used in this study to calculate stress distributions based on further analytical solutions for the cylinder-on-flat geometry [2].

2.5 Fretting Fatigue Analysis Assumptions:

Finally, before moving on to the next chapter it is important to briefly mention two assumptions fretting fatigue researchers typically make. Obviously many more

assumptions are made throughout the experiments and analysis, but these two assumptions seem significant as potential sources of error. It is conceivable that if one of these assumptions is not closely met in real world fretting fatigue, that the assumption should not be made and analysis based on the assumption would therefore be invalid.

The first major assumption is the so-called half-space assumption, which will be described and related to this study in the section on finite element validation in the next chapter, section 3.4.1. Nowell and Hill published a rebuttal to Iyer's paper, which claimed that Iyer did not adequately discuss how his model met the criteria for this half space assumption [27]. So it is a potential source of error, but it will be tabled until the next chapter.

2.5.1 Steady-State Assumption: The second major assumption, that could lead researchers to mistakes, is the idea that pseudo-steady-state conditions are quickly met in fretting fatigue experiments and that the values of the test variables in that steady-state are held throughout the life of their tests. In order to come to their conclusions many researchers, including Nowell and Hill and Iyer, have made this assumption that the variables in the fretting fatigue tests do not significantly change throughout the life of the tests. Iyer assumed that initial conditions were maintained [14]. This steady-state assumption may be dangerous if indeed conditions do change significantly during tests and that change is related to what is causing the fretting phenomenon.

2.5.2 Iyer on Steady-State [14]: Of the local mechanistic parameters, Iyer noted several trends. The peak contact pressure, p_0, and the contact semi-width remained approximately constant throughout the duration of his specific tests. The maximum slip range, local maximum shear stress, and local maximum shear stress range all varied

during the test due to local compliance with interfacial wear and crack initiation. This variation itself varied depending upon the different test conditions. Therefore his finite element values of δ_{max}, $\tau_{L,max}$, and $\Delta\tau_{L,max}$ were only applicable for the initial stage of the test. The values of $\sigma_{L,max}$ and $\Delta\sigma_{L,max}$ were held constant throughout his tests.

In regard to this steady state assumption, Iyer noted that in all of his testing, the test conditions reached steady state in less than 1000 cycles and the change from the initial conditions was small. Jin found that Q stabilized in his tests within a few hundred cycles [16]. If the analytical and finite element solution for the contact region is to be of any value, the actual experimental conditions must not vary much from the analyzed conditions. This is because the finite element model and analytical solution only simulate the conditions for one sample cycle in the test, which could run anywhere from 40000 to well over a million cycles. All other cycles are assumed to have the same stresses and displacements as this one sample cycle.

2.6 Transition to Chapter 3:

The experimental tests created for this study were specifically designed so that the results could be compared to that of Nowell and Hill. The material used in this study was titanium alloy, instead of aluminum/copper, but much of the other basic test conditions are similar. Just like the Nowell and Hill tests, experiments in this study were designed to keep p_0, the bulk stresses and the ratio of Q/P constant while looking at the effects of variances in 2a. The primary goal of this study was to make a systematic investigation into the effects of variances in contact semi-width on fretting fatigue. Experimental test boundary conditions were calculated using the analytical solutions. It was hoped that a critical contact width would be found for Ti-6Al-4V, and that it could be examined using

various analytical approaches. The critical plane predictive parameters suggested by Namjoshi et al. would be evaluated from finite element simulations of the experiments. An explanation of the cause of the critical contact semi-width's effect on fatigue life will be sought.

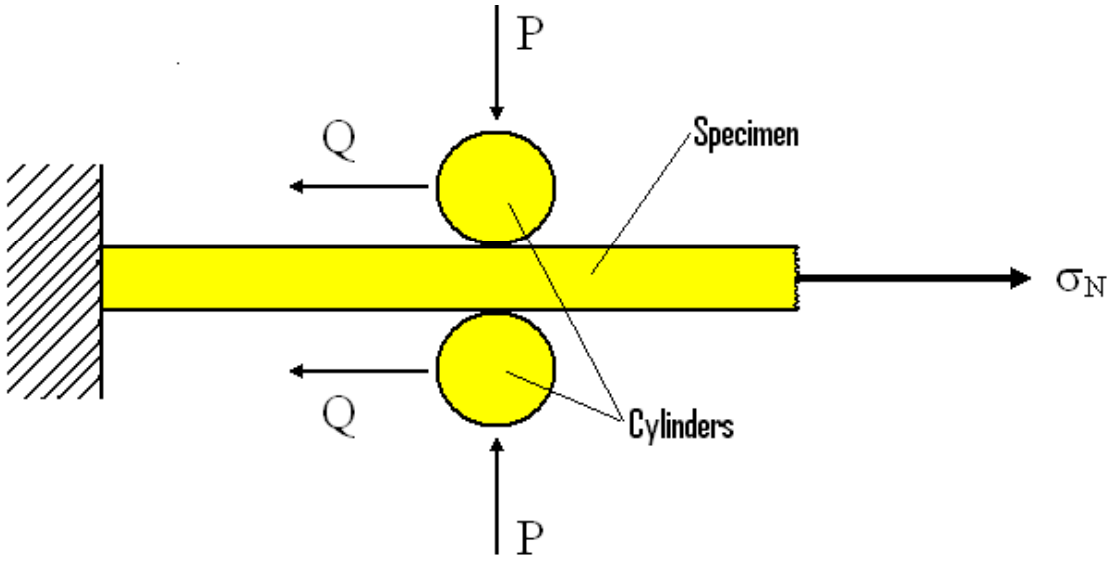

Figure 2.1 Simplified Diagram of Fretting Fatigue Test

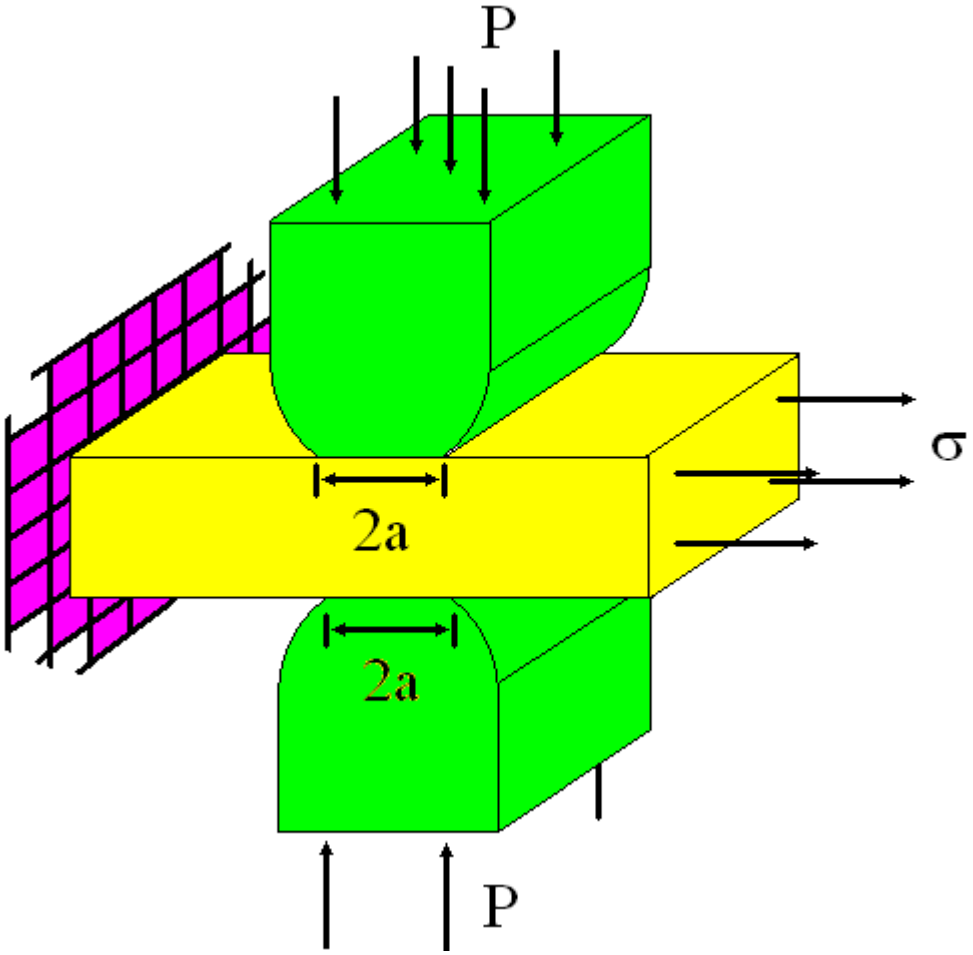

Figure 2.2 Diagram of Experimental Test Setup Illustrating Contact Semi-width, a

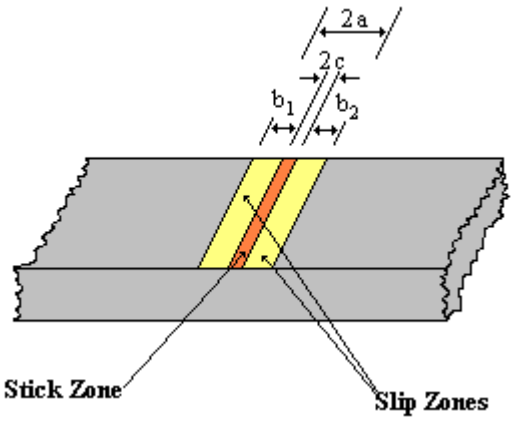

Figure 2.3 Illustration of the Stick and Slip Zones in the Contact Region

Chapter III: Experiments/ FEA Validation

This chapter narrows the focus from general background to the actual work performed for this study. It contains a more detailed explanation of the tests' setup. The program of experiments performed is presented. The finite element model used in the analysis is described and validated.

3.1. Test Setup:

3.1.1 Setups from Previous Studies: The test setup used in this study was created as a result of the experiences of previous research efforts. As fretting fatigue experiments have been performed for decades, this machine allows for cylinder-on-flat tests. But it also incorporates the one of the latest hydraulic control programs, Teststar II, and a newly developed fretting fixture, which allows for independent pad displacement. Independent pad displacement is a relatively new technique that has not been fully explored.

3.1.1.1 Bramhall and Nowell and Hill [28]: Both the experiments run by Bramhall and those by Nowell and Hill were conducted with similar testing set-ups. They used parallel-sided specimens and loaded them in a test machine such that they received a bulk stress, which varied sinusoidally in time. Two cylindrical fretting pads of a certain radius, R, were pressed against the sides of the specimen by a normal force, P. The tests in this study were the same up to this point. To prevent movement of the cylinders when the fatigue specimen displaced, springs were used to provide a tangential force restraint, Q. A simple diagram incorporating the essence of this test setup can be seen in Figure 2.1 of the last chapter.

3.1.1.2 Iyer [14]: For his fretting fatigue experiments Iyer used the cylinder-on-flat arrangement of pads specimens. A reason for using cylinder-on-flat contact is that closed-form analytical solutions of the elastic stress and displacement fields for cylinder-on-flat contact geometries have been developed [17], whereas a flat pad on flat specimen, for example, has a singularity at the edge of contact. To apply the remote stress Iyer used a uniaxial, servohydraulic testing machine and a fixture for positioning the fretting pads. Using the fretting pad fixture he simultaneously applied a constant normal load, P, to the each of the cylinders pressing them against the substrate. Then he set the test machine to load one end of the substrate with a cyclic stress, $\sigma_{N,max}/\sigma_{N,min}$, while keeping the other end fixed. A similar technique was used in this study.

3.1.1.3 Jin [16]: The fretting fatigue testing apparatus recently used in this study was the same one used by Jin et al. for his studies of Independent Pad Displacement and Gross-Slip. The schematic diagram of the test setup is shown in Figures 3.1 and 3.2. The maximum loading and frequency capabilities of the servohydraulic test machine used in this study are an applied load of 100kN and a cyclic frequency of 20 Hz. A second servohydraulic actuator, 13 kN, was added to the main test frame and linked into the fretting fixture. The purpose of the second actuator was to allow independent cyclic movement of the fretting fixture, which was at the same time undergoing a pad-applied normal load and cyclic shear traction forces. In order to measure the tangential forces experienced by the ends of the specimen, a 100 kN load cell was placed on the top grip and 22 kN load cell was attached to the bottom grip. A half-inch extensometer was used to measure relative displacement of the fretting pads and substrate. Figure 3.3 shows how the extensometer was put in place. The letters on Figure 3.3 relate to the equations

presented by Wittkowsky et al. for the purposes of denoting how slip amplitude is measured [34].

3.1.2 Setup for this Study: The test machine could be used to provide independent pad displacement. Different from the typical fretting fatigue test setups two separately controllable actuators on the tensile test machine were used in this study. The upper or leading edge of the specimen was held by a fixed hydraulic grip. The upper actuator of the servohydraulic test machine could then be set to apply a cyclic displacement upon the fretting pad fixture while, the lower actuator applied tensile loads to the trailing end of the specimen. During the testing the upper actuator was set to run on the signal provided by the lower control. This way both actuators ran in unison with each other. Figures 3.1 and 3.2 show a front view of the test set-up.

All tests done for this work were conducted at a rate of 2 cycles per second. The tests in this study were stopped if failure had not occurred by a million cycles, while, in Jin's research on gross slip tests were considered to have infinite life by 300000 cycles [16].

3.1.2.1 Material [16]: Both the specimen and fretting pads were made of titanium alloy, Ti-6Al-4V. Prior to specimen machining the material was heated: solution heat-treatment at 935^{o}C for 1:45 hours, cooling in air, annealing at 700^{o}C for 2 hours in vacuum, and cooling in argon. The grain size was about 10 $\mu m \pm 2 \mu m$. The modulus of elasticity of the material was approximately 118 GPa, with a yield strength of 930 MPa and ultimate tensile strength of 978 MPa.

3.1.2.2 Specimen and Pad Geometry [16]: Dog-bone type specimens of this material were used. Figure 3.4 shows the dimensions of one such specimen. The width

and thickness of the reduced area were 0.00635 m and 0.00381 m. Wire electric discharge method was used to cut the specimens. Then low stress grinding was used to reduce stresses due to the machining. The specimens were then polished using 600 grit silicon carbide papers. Cylindrical pads of 0.0508 m, 0.04445 m, 0.0381 m, 0.03175 m, 0.02540 m, 0.01905 m, 0.01524 m, 0.0127 m, 0.01016 m, 0.00762 m, and 0.00508 m radii were used. The heads of the pads were cylindrical, but the lengths were square, 0.009525 m by 0.009525 m. Figure 3.5 shows a typical fretting pad.

3.1.3 Controlling the Variables: The fretting fatigue variables, in this study, held constant were p_0, $\sigma_{N,min}$, $\sigma_{N,max}$, $\Delta\sigma_{N,max}$, and the ratio of Q to P. The variables 2a, slip range, P, Q, and R all varied for the different tests.

3.1.3.1 Constant Stresses: Keeping the bulk nominal stresses ($\sigma_{N,max}$ and $\sigma_{N,min}$) and stress ranges ($\Delta\sigma_{N,max}$) constant was the simplest. These were the loads applied to the ends of the test specimen in the parallel direction of the length of the specimen by the servohydraulic test machine. Controlling these stresses was done by setting the Teststar II control system, which was sending commands to the servohydraulic test machine, to oscillate about the desired mean load with the desired load amplitude. Each experiment in this study ran at a maximum remote stress of 550 MPa and a minimum of 18 MPa. This meant that the external stress range was 532 MPa, with a mean stress of 284 MPa and a 266 MPa stress amplitude. The load input into the control system was simply the product of the desired stress and the specimen's cross sectional area. In this way the external boundary condition of applied tensile stresses was held constant.

3.1.3.2 Constant Peak Contact Pressure: The second variable held constant in the experiments of this study was the peak contact pressure. This was done assuming that the

analytical equations presented by Nowell and Hill could be accurate in a real experiment. R and P were manipulated such that p_0 was a constant for each test using equation (13). The value of p_0 equal to 5.269E+8 Pa was chosen because the fretting fixture could be set to all the different P values required by the different radii to achieve this peak pressure. Notice that as R increases, increasing values of normal load need to be applied in order to achieve the same p_0. For the test using the .0508m radius pads, a P load of 4000N needed to be applied. Table 3.1 shows these values in a table.

3.1.3.3 Constant Q/P Ratio: The boundary conditions had to be calibrated to achieve a constant ratio of Q/P. There have been two different approaches used to calibrate the ratio of shear traction to normal load.

3.1.3.3.1 *Nowell and Hill Approach:* Nowell and Hill maintained a constant Q/P ratio for their tests by attaching their fretting fixture to a spring with a linear spring constant. The force of the spring fully absorbed the shear tractions, Q. As long as the displacements of the fretting fixture, and hence the displacements of the spring which absorbed Q, were constant and the normal pressure load was constant, the ratio of Q/P was held constant. An illustration of the Nowell and Hill fretting fixture configuration is drawn in Figure 3.6 and can be compared to this test setup in Figures 3.1 and 3.2

3.1.3.3.2 *Approach of this Study:* At AFIT fretting fatigue researchers have developed a different way of calibrating the ratio of Q/P. It was found by Jin and Mall that the magnitude of shear traction force could be controlled using independent pad displacement, also known as adjusting the span [15]. From previous studies it had been observed that as span increased, the amount of shear traction also increased [16]. First the maximum Q/P ratio, of all the different pad radii tests, that occurred without

independent pad displacement was found. The Q/P ratio of 0.85, found for the 0.01016 m pads, was considered the highest Q/P ratio without independent pad displacement. All other pad radii were calibrated for magnitudes of independent pad displacement such that their Q/P ratio was approximately 0.85. A much more detailed description of the calibration process can be read in Appendix A.3: Q/P Calibration and Test Diary.

3.2 Program of Experiments:

The program of experiments to be conducted was created with several things in mind. This being a systematic study of the effects of changes in contact semi-width with changes in cycles until failure, it was important to keep as many variables constant as possible. Using analytical equation (13), the amount of P for each different radius pad, necessary to produce a constant p_0 was calculated. Table 3.1, located at the end of this chapter after the figures, is the program of experiments, a summary of the important input boundary conditions of all the twelve tests that were conducted. It should be noted that Jin performed the 1st test in the table, with the 0.0508 m radius pads, for a separate study.

3.3 FEA Description:

Analytical Equations and the "Ruiz" program are good at estimating the effects of fretting with the cylinder-on-flat loading arrangement. However, they are only considered a good representation if the half space assumption can be made. The details of the half-space assumption will be discussed in the next section 3.4.1. Because there is a violation of the half-space assumption for some tests run in this study, analytical solutions had offered only limited amount of help in illuminating what processes really occurred. However, due to advances in numerical analysis within the past decade, another method of analysis has become practical. Finite element analysis, FEA, seemed

to be a good compliment to the analytical solutions in closely examining the occurrences taking place in this study.

3.3.1 Advantages of FEA: In order to determine detailed descriptions of the local stresses, the present work used finite element models of the experiments performed. Through this type of modeling, local parameters, p_0, a, δ_{max}, $\tau_{L,max}$, $\Delta\tau_{L,max}$, $\sigma_{L,max}$ and $\Delta\sigma_{L,max}$ in the contact region could be determined for any combination of defined boundary conditions, R, P, Q, $\sigma_{N,max}$, $\Delta\sigma_{N,max}$, and coefficient of friction, μ.

The finite element model revealed details about the test set-up that were not evident in analytic model. In the FEA model, the contact semi-width was not symmetric about the center of contact. It had an eccentricity, e. Secondly, there was also a tensile stress concentration on the substrate generated solely by the normal load, P. Iyer thought that this tensile stress concentration was the reason for the critical contact semi-width. It will be discussed in a great deal in the 4th chapter.

3.3.2 Mesh Layout: A picture representing the finite element mesh used in this study can be seen in Figure 3.7. The darker areas, such as the tip of the fretting pad and the area of substrate directly below it are the areas of highest element concentration. Not surprisingly these are also the areas of primary interest in the analysis. They are located in the region where the contact between the pad and the specimen takes place.

The model is comprised of a two-dimensional finite element model of a fretting fixture, or "pad holder," holding a cylindrical pad, which lies directly above a flat substrate of a finite thickness. If the coordinate axis is such that the substrate surface lies along the x-axis, then the cylinder and holder lie above it in the positive y-direction. The cylindrical pad is rigidly fixed to the pad holder, but the negative x side of the pad holder

is free to roll along the y-axis and fixed in the x-direction, as is shown in the figure. A load is applied to the top of the cylindrical pad in the negative y-direction, which act as the normal force, P, in the setup. The x-axis is centered about the center of the substrate, which is lines up with the cylinder tip at the coordinate x=0. The negative x-direction end of the substrate is fixed, while the opposite end is loaded in the positive x-direction by a force simulating the bulk nominal stress. The substrate is free to roll in the x-direction but its bottom surface is fixed in the y-direction. Only half of the setup is needed to be modeled because ideally the fretting test setup is symmetric about the x-axis.

Plane strain, linear quadrilateral elements were used for all three bodies [13] and the distance between adjacent nodes on the unloaded contact surfaces in the x-direction is $6.2255*10^{-6}$ m. To solve the contact inequality constraints, single-noded, non-rigid contact elements were generated internally. Due to symmetry about the x-axis, the thickness of the substrate in the model is half that of the actual substrate, $1.905*10^{-3}$ m. The range of the substrate in the x-direction is $\pm 9.53*10^{-3}$ m and the range of refined mesh for contact analysis on the substrate surface in the x-direction is $\pm 0.794*10^{-3}$ m. The cylindrical pad radii used in the finite element analysis are 0.0508 m, 0.04445 m, 0.0381 m, 0.03175 m, 0.0254 m, 0.01905 m, 0.01524 m, 0.01016 m, and 0.00762 m. The Q, $\sigma_{N,max}$ and $\sigma_{N,min}$, P, R values were taken directly from the experimental tests conducted. The values for E=128 GPa and v=0.32 were the standard values used by previous and current AFIT researchers using finite element analysis. The coefficient of friction, μ, was chosen to be 0.95. It had to be greater than the ratio of Q/P for the numerical solution to converge. The mesh was adjusted for each test's unique loading

and geometry. A table summarizing the inputs for the finite element mesh is located at the end of this chapter, labeled as Table 3.2.

3.3.3 Step 1 Versus Step 2: The generated finite element meshes with their respective loading and boundary conditions were run on the ABAQUS finite element program on Unix computers. For each test numerically simulated, the maximum loading conditions, meaning the maximum bulk stress and corresponding Q value, and the minimum loading conditions, meaning the minimum bulk stress and corresponding Q, were run separately. Furthermore, within each run, ABAQUS produced stress, strain, and displacement data for two cases: firstly, when the only load applied was the normal load to the top of the cylinder and secondly when all of the loadings, Q, σ_N, and P were being applied together. The first case is commonly referred to throughout this study as the "step 1" or "P-only" finite element analysis and the second case is referred to as the "step 2" or "combined loading" analysis. So for each experimental test run on ABAQUS, two separate input files needed to be processed and two separate output files were produced for each input file.

3.4 Finite Element Validation:

The finite element models' outputs were compared to the results predicted by the analytical solution for validation of the FEA meshes. The "Ruiz" program calculated the stress distributions predicted by the analytical solution. This program is generally used as a test to compare with the finite element outputs.

The two methods clearly have differences. The analytical solution can be used to solve for values at points anywhere along the specimen while the finite element model finds stresses and displacements at specific discrete points only, called nodes. Data at

points in between the finite element nodes needs to be interpolated from the surrounding nodal points through the use of shape functions. Neither model is perfect and both are based on assumptions. The finite element solution does not need to assume a half space exists, but in order to even apply the analytical solutions to the cases in this study, it had to be proven that the test conditions met the half space assumption [27].

3.4.1 Half-Space Assumption: For the analytical solutions, the assumption is made that the two bodies in contact, the cylindrical pad and the substrate specimen, have infinite boundaries [19]. This assumption is known as the half space assumption. Generally it is assumed to be reasonable if one half of the specimen thickness, b, is at least ten times the contact semi-width, a.

$$\frac{b}{a} \geq 10 \tag{15}$$

It is helpful to note that "b" is referring to half of the specimen thickness and not the width of the slip zone, which is also represented by the letter b.

Violation of the half space assumption has been shown to cause deviation from the expected analytical solutions as was demonstrated by Fellows et al. [6]. Figure 3.8 shows how the ratios of specimen width to contact width compared for the various tests in this study. Contact widths were calculated using both the analytical and numerical solutions. Both the analytical and numerical ratios of b/a showed the same results: the half space assumption only holds for some of the solutions. So some of the analytical solutions should have significant error. Note that how the contact widths were calculated is discussed in greater detail in the appendices where the Syy stress distributions are analyzed. Remember also, that the "Ruiz" FORTRAN program, written by Chan and Lee [2], designed to calculate the stress distributions based on the analytical solution, required

the half space assumption to be met in order to produce theoretically accurate results [20].

3.4.2 Comparison of "Ruiz" Program and FEA: Logically the best test to compare results of the analytical to the numerical solution would be the one with the greatest b/a ratio. This is the 0.00762 m pad radius test. Therefore comparisons between the Ruiz program and the Finite Element mesh for this pad radius were made for the purpose of validating the effectiveness of the finite element mesh.

3.4.2.1 Mesh Refinement: The finite element mesh was refined in an iterative manner until magnitudes of p_0 no longer changed by more than 2.6% with further refinement [13]. This mesh was formatted for and then run on the ABAQUS finite element program.

3.4.2.2 Stress Curves: From Figure 3.9 to Figure 3.14 it can be seen that the curves for normal stresses in the x and y directions and shear stresses were similar for both analytical and numerical method solutions. Because of the difference in the geometric constraints, the two solutions can never be identical [13], but they did come close enough to endorse the finite element mesh. The greatest difference was in the Sxx maximum and minimum values. The worst disagreement between the two solutions occurred at the minimum value of the Sxx curve, where there is 14.21% difference of the analytical from the numerical value. But this difference is atypical of the curves. For example, the difference in peak contact pressures for the minimum loading case was only 2.1%. The analytical and numerical solutions seem very similar and the case for the finite element validation is supported by the comparison.

3.4.2.3 Peak Contact Pressures and Contact Semi-widths: The second test for finite element validation was comparing the peak contact pressures and contact semi-widths determined from the finite element output to the theoretical values, which could be determined from the equations presented by Nowell and Hill. Both the theoretical and finite element values for these parameters matched well. There was a maximum difference of only 1.56% of the theoretical contact width to the finite element computed value. The theoretical peak contact pressure varied a maximum difference of only 2.22% from the finite element value. The peak contact pressure and contact semi-widths, calculated from the formulas (13) and (14), independent of the FORTRAN program, matched well the numerical solution.

3.4.2.4. Applied Nominal Stresses: The third check on the finite element model dealt with the combined loading σ_{xx} curves. When the nominal bulk stress is applied, as the distance on the σ_{xx} distribution curves from the stress concentration increases, the amount of stress should level off at the value of the applied load. In every test case the positive x end of the σ_{xx} curve from the finite element output levels off at 550 MPa for the maximum loading conditions and at 18 MPa for the minimum loading case. 550 and 18 MPa are the maximum and minimum applied σ_N. So this checks.

Caparison of the finite element models' results to the "Ruiz" program's output and analytical equations validates the numerical model. The data attained from the finite element program was used next in analysis and discussion.

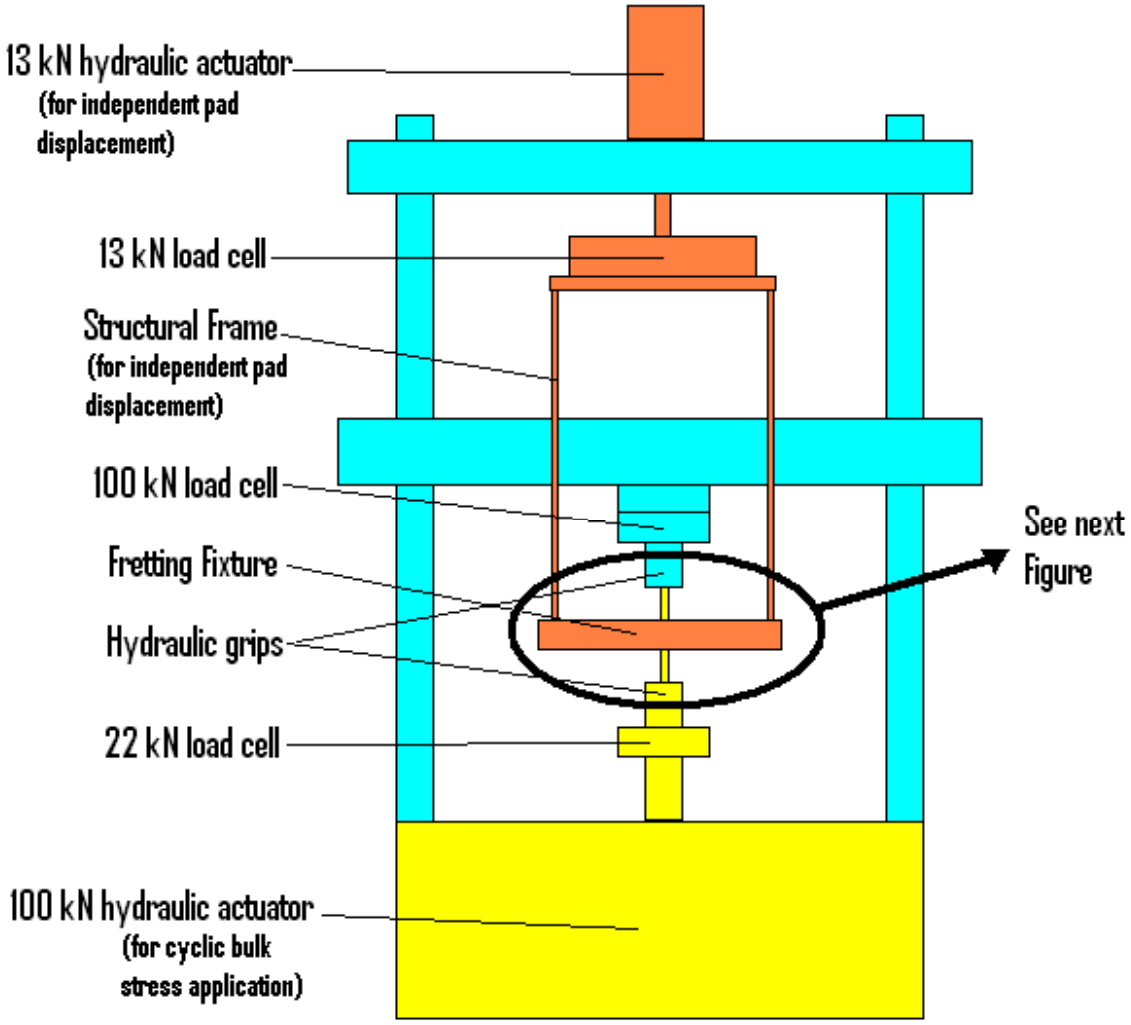

Figure 3.1 Servohydraulic Test Machine Setup for Independent Pad Displacement

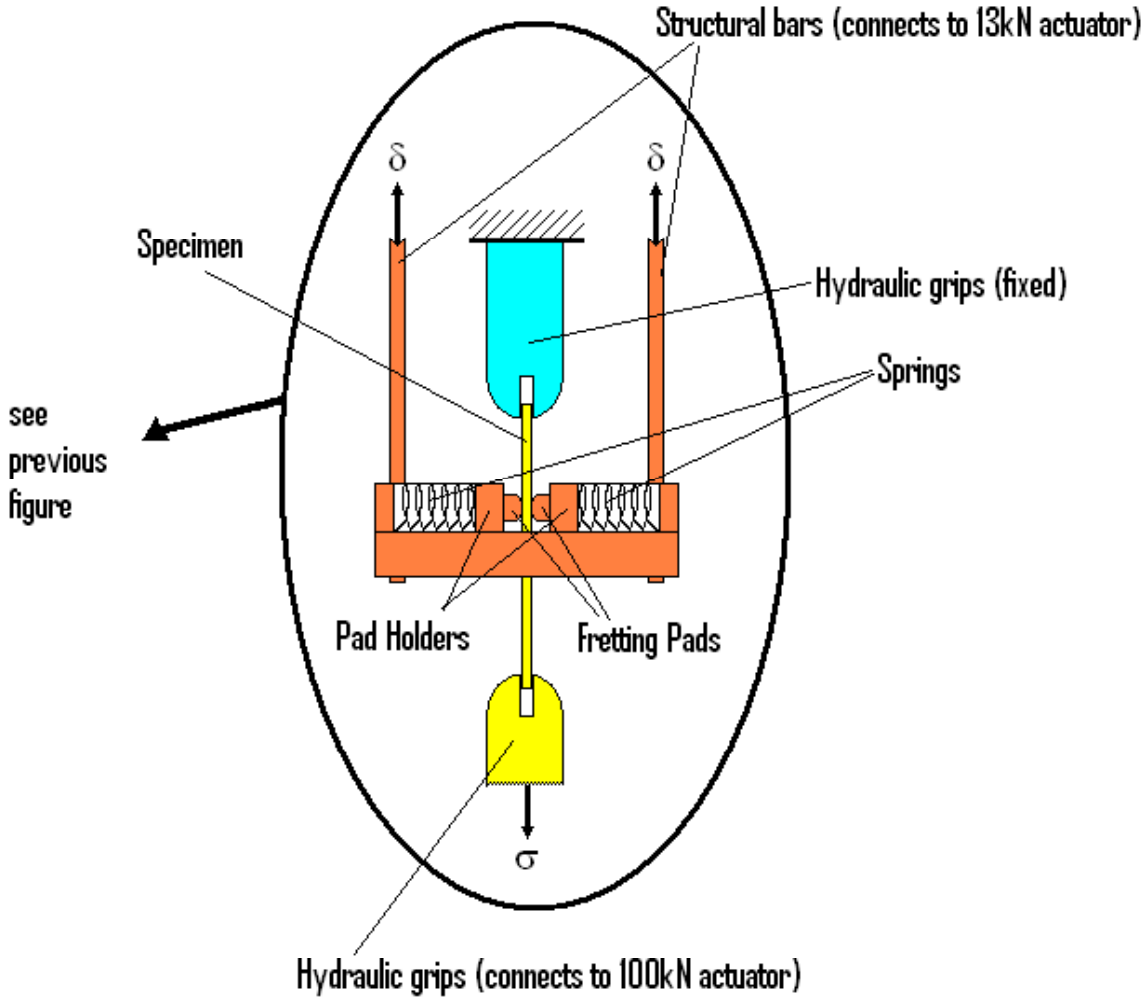

Figure 3.2 Fretting Fixture for Independent Pad Displacement w/o Extensometer

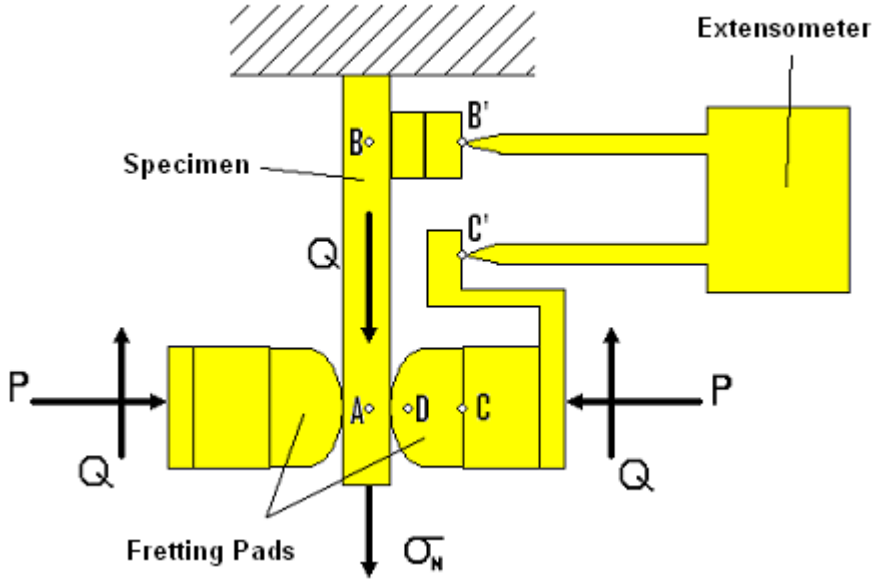

Figure 3.3 Fretting Setup Showing Extensometer Location.

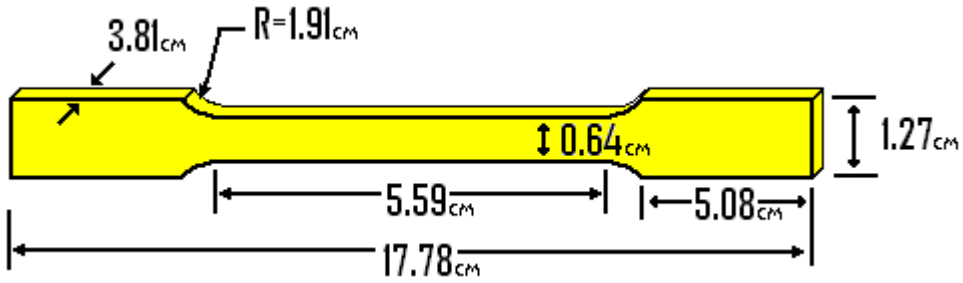

Figure 3.4 Typical Dogbone Specimen with Dimensions

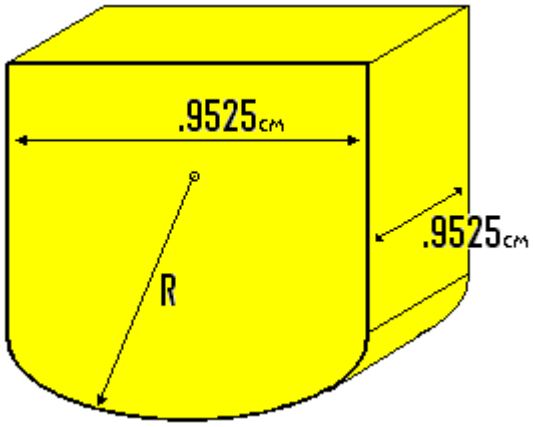

Figure 3.5 Typical Fretting Pad

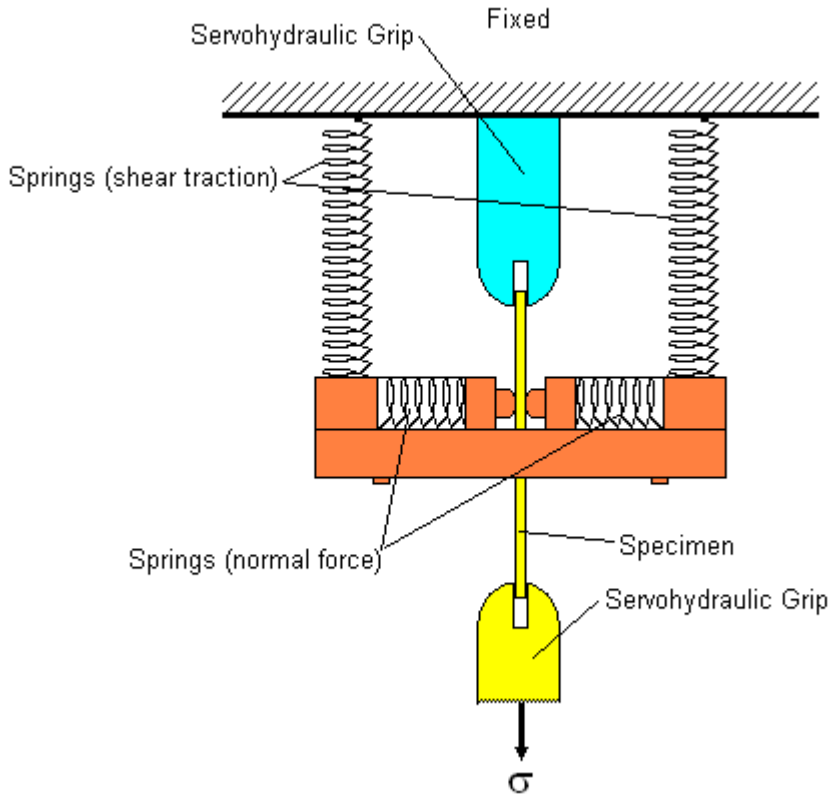

Figure 3.6 Nowell and Hill Fretting Fixture for Constant Q/P Ratio

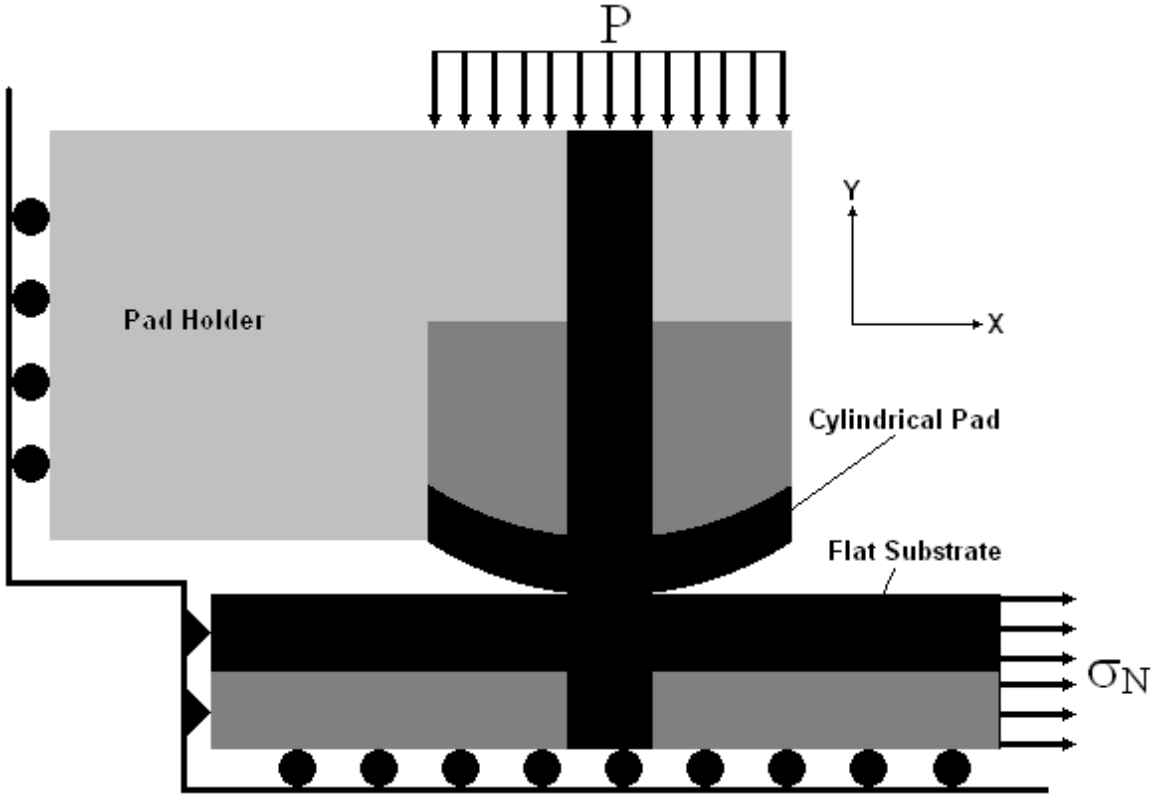

Figure 3.7 Finite Element Model

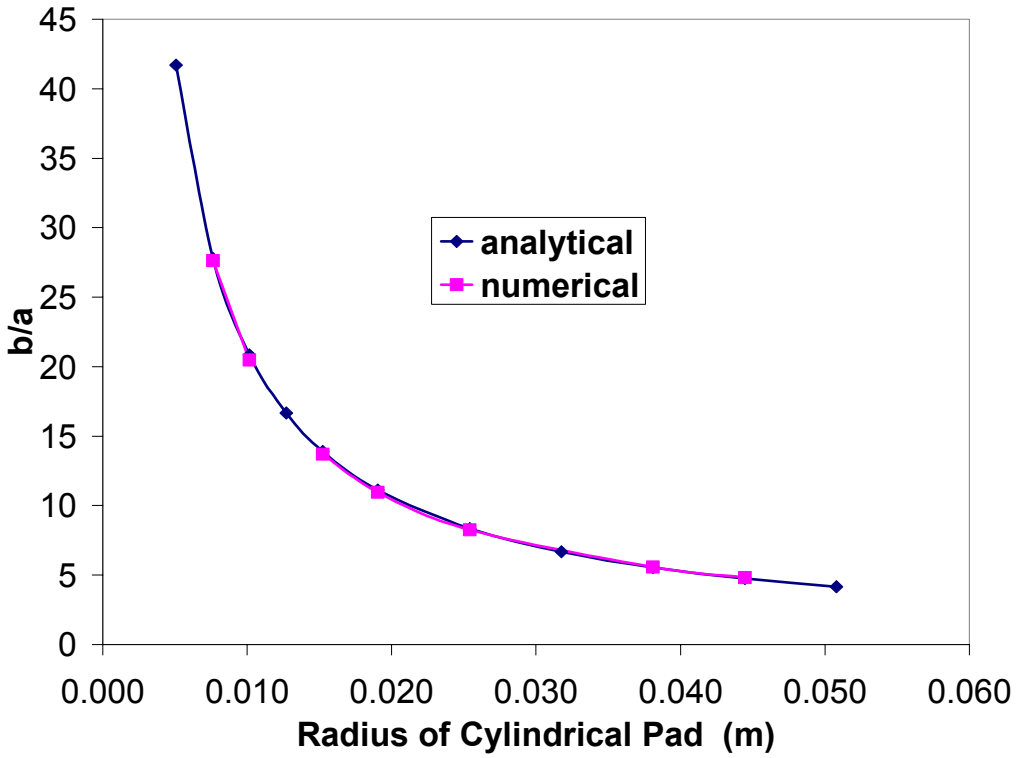

Figure 3.8 Ratio of Specimen Width, b, to Contact Semi-Width, a, for Validation of Half Space Assumption

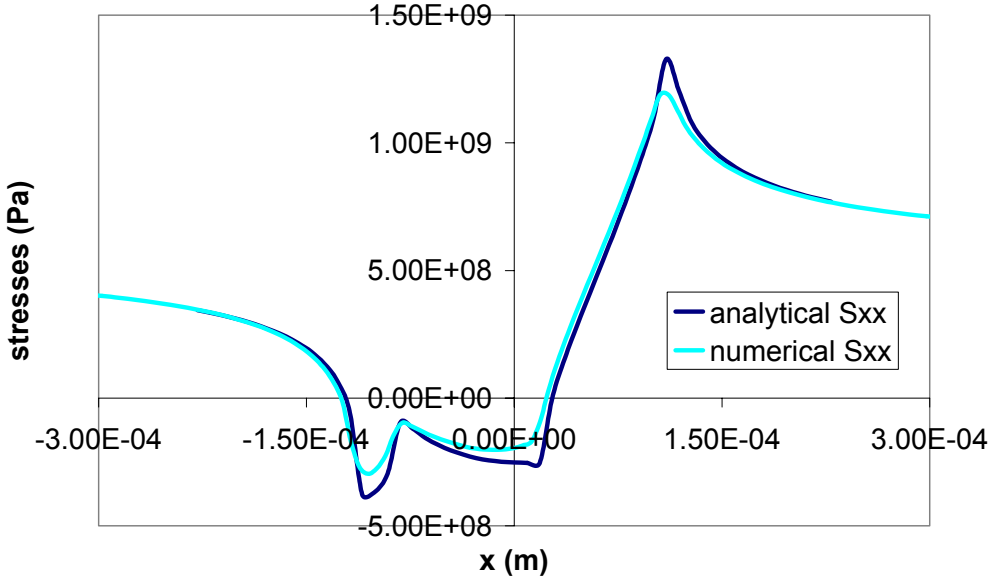

Figure 3.9 Analytically and Numerically Generated Sxx Stress Distribution Curves Along the Contact Area of the 7.62 mm Pad Radius Test Maximum Loading Case

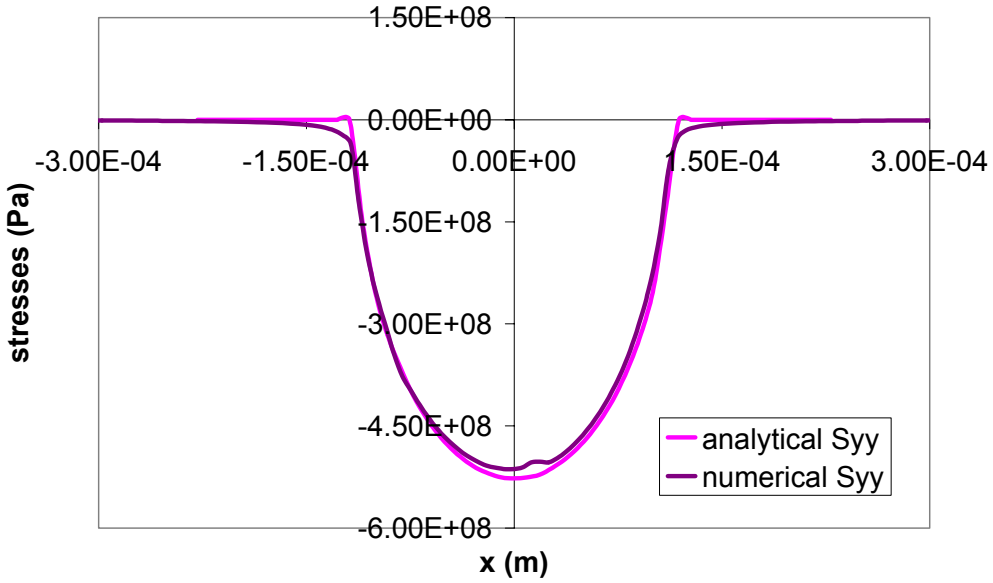

Figure 3.10 Analytically and Numerically Generated Syy Stress Distribution Curves Along the Contact Area of the 7.62 mm Pad Radius Test Maximum Loading Case

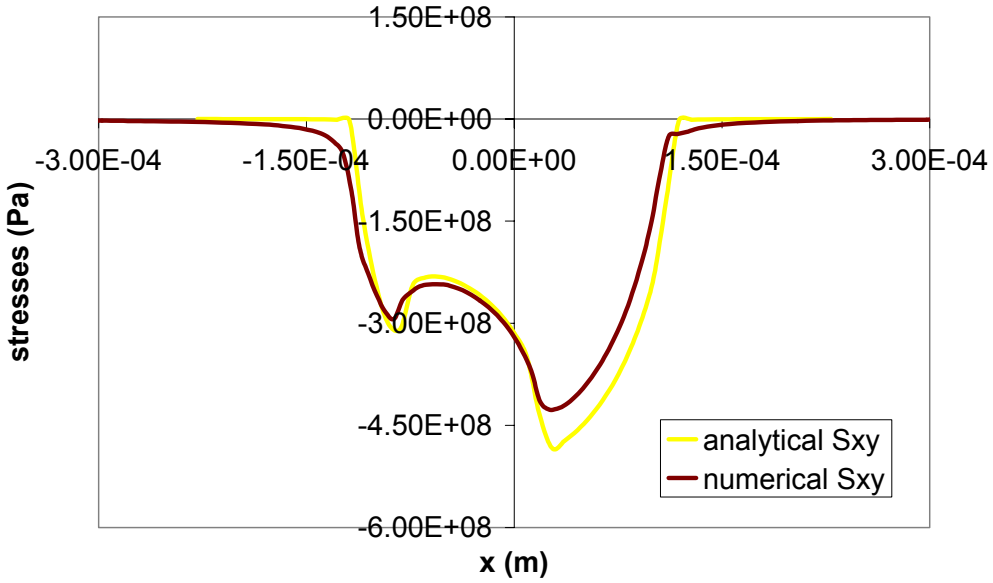

Figure 3.11 Analytically and Numerically Generated Sxy Stress Distribution Curves Along the Contact Area of the 7.62 mm Pad Radius Test Maximum Loading Case

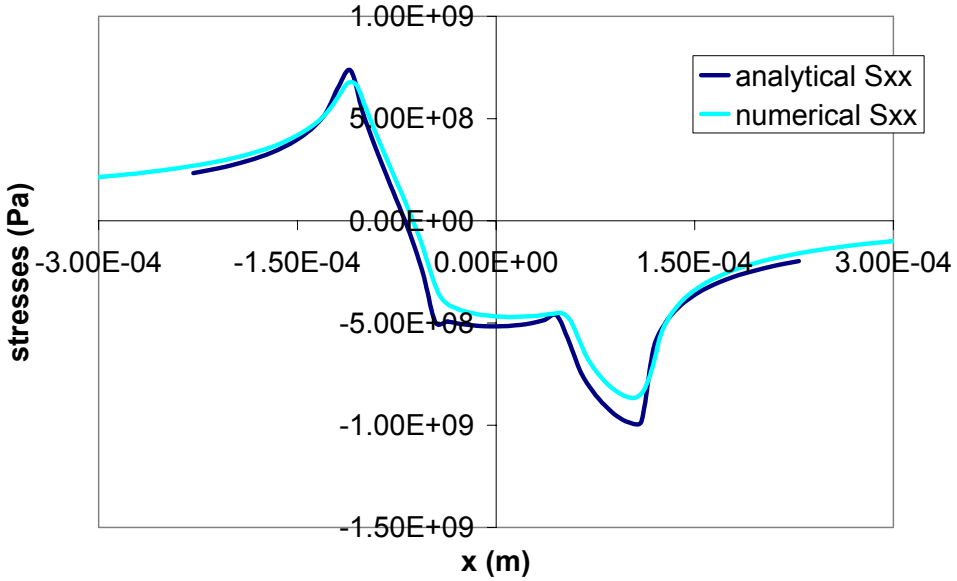

Figure 3.12 Analytically and Numerically Generated Sxx Stress Distribution Curves Along the Contact Area of the 7.62 mm Pad Radius Test Minimum Loading Case

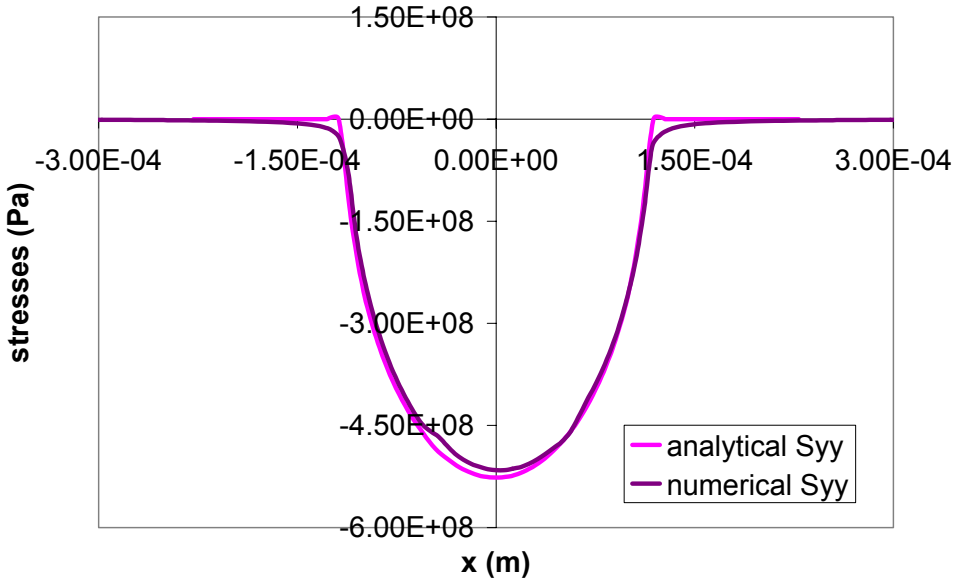

Figure 3.13 Analytically and Numerically Generated Syy Stress Distribution Curves Along the Contact Area of the 7.62 mm Pad Radius Test Minimum Loading Case

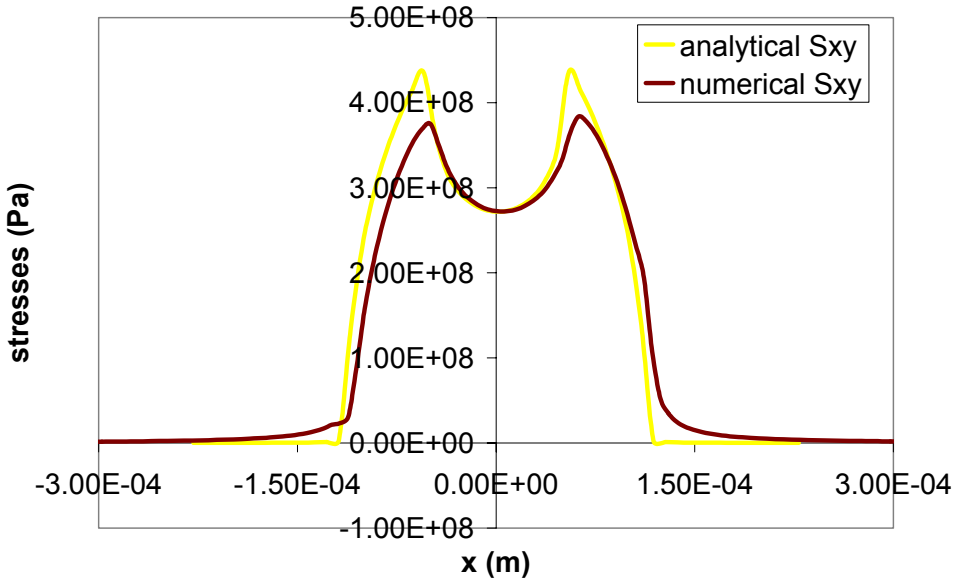

Figure 3.14 Analytically and Numerically Generated Sxy Stress Distribution Curves Along the Contact Area of the 7.62 mm Pad Radius Test Minimum Loading Case

Table 3.1 Program of Experimental Tests

Radius (m)	P(N)	$2a_{theo}$ (m)	$p_{0,theo}$ (Pa)	$\sigma_{N,max}$ (Pa)	$\sigma_{N,min}$ (Pa)	$\Delta\sigma_{N,max}$ (Pa)	Span (m)
5.08E-02	4.00E+03	1.52E-03	5.27E+08	5.50E+08	1.80E+07	5.32E+08	1.32E-03
4.45E-02	3.50E+03	1.33E-03	5.27E+08	5.50E+08	1.80E+07	5.32E+08	9.14E-04
3.81E-02	3.00E+03	1.14E-03	5.27E+08	5.50E+08	1.80E+07	5.32E+08	6.99E-04
3.18E-02	2.50E+03	9.52E-04	5.27E+08	5.50E+08	1.80E+07	5.32E+08	5.08E-04
2.54E-02	2.00E+03	7.62E-04	5.27E+08	5.50E+08	1.80E+07	5.32E+08	3.30E-04
1.91E-02	1.50E+03	5.71E-04	5.27E+08	5.50E+08	1.80E+07	5.32E+08	1.65E-04
1.52E-02	1.20E+03	4.57E-04	5.27E+08	5.50E+08	1.80E+07	5.32E+08	1.02E-04
1.52E-02	1.20E+03	4.57E-04	5.27E+08	5.50E+08	1.80E+07	5.32E+08	1.27E-05
1.27E-02	1.00E+03	3.81E-04	5.27E+08	5.50E+08	1.80E+07	5.32E+08	0.00E+00
1.02E-02	8.01E+02	3.05E-04	5.27E+08	5.50E+08	1.80E+07	5.32E+08	0.00E+00
7.62E-03	6.01E+02	2.29E-04	5.27E+08	5.50E+08	1.80E+07	5.32E+08	0.00E+00
5.08E-03	4.00E+02	1.52E-04	5.27E+08	5.50E+08	1.80E+07	5.32E+08	0.00E+00

Table 3.2 Summary of FEA Input

R(in)	R(m)	P(N)	Q_{max} (N)	Q_{min} (N)	σ_{max} (MPa)	σ_{min} (MPa)	$\Delta\sigma_{N,max}$ (MPa)
2.00E+00	5.08E-02	4.00E+03	3.35E+03	-3.33E+03	5.50E+02	1.80E+01	5.32E+02
1.75E+00	4.45E-02	3.50E+03	2.82E+03	-2.59E+03	5.50E+02	1.80E+01	5.32E+02
1.50E+00	3.81E-02	3.00E+03	2.40E+03	-2.19E+03	5.50E+02	1.80E+01	5.32E+02
1.25E+00	3.18E-02	2.50E+03	2.05E+03	-1.83E+03	5.50E+02	1.80E+01	5.32E+02
1.00E+00	2.54E-02	2.00E+03	1.69E+03	-1.46E+03	5.50E+02	1.80E+01	5.32E+02
7.50E-01	1.91E-02	1.50E+03	1.31E+03	-1.14E+03	5.50E+02	1.80E+01	5.32E+02
.6a d=.004	1.52E-02	1.20E+03	1.13E+03	-9.59E+02	5.50E+02	1.80E+01	5.32E+02
.6b d=.0005	1.52E-02	1.20E+03	1.00E+03	-7.27E+02	5.50E+02	1.80E+01	5.32E+02
5.00E-01	1.27E-02	1.00E+03	9.43E+02	-7.81E+02	5.50E+02	1.80E+01	5.32E+02
4.00E-01	1.02E-02	8.01E+02	7.29E+02	-6.73E+02	5.50E+02	1.80E+01	5.32E+02
3.00E-01	7.62E-03	6.01E+02	4.48E+02	-4.51E+02	5.50E+02	1.80E+01	5.32E+02
2.00E-01	5.08E-03	4.00E+02	7.65E+01	-6.44E+01	5.50E+02	1.80E+01	5.32E+02

Chapter IV: Results and Discussion

Results and discussion will begin with the output data of the experiments and finite element simulations. Following this, critical plane based fatigue predictive criteria will be applied to the output of the finite element analysis and the "Ruiz" program. Iyer's explanation and Nowell and Hill's explanation of the effects of changing contact semi-width will be evaluated. There will be parallels drawn between the opinions of Jin et al. and the findings in this study. Finally the new ideas brought forth by this study will be presented.

4.1 Output of Experimental Tests:

Eleven experimental tests were performed for the purposes of this study and a twelfth test's data, from a previous [16] study was used. Table 4.1, at the end of this chapter, summarizes the results. The values of shear traction were determined from the experimental output as described in Appendix A.1. The numbers of cycles until failure were also recorded. Test numbers 10, 11, and 12, on the Table 4.1, all experienced infinite fatigue life. Also the test data from Jin showed that test number 1 experienced infinite fatigue life.

4.1.1 Shear Tractions:

Figure 4.1 shows how the value of shear traction changed as contact semi-width changed. The relationship was approximately linearly positive.

Figure 4.2 illustrates the ratio of Q/P versus contact width. Two different sets of data points are plotted: the chosen steady state value of Q/P and the ratio of the absolute maximum value of Q to P throughout the test. The steady state values of Q/P were input into the finite element analysis. These values of Q and Q/P for each test are presented in Table 4.1.

4.1.2 Fatigue Life: Figure 4.3 is a plot of the number of cycles until failure for all of the tests used in this study. The arrows are attached to four of the data points to show that they lasted longer than 300,000 cycles. The values of cycles until failure are listed in Table 4.1.

4.2 Output of Finite Element Tests:

As was described in the previous chapter, finite element analysis was used to simulate many of the experimental tests. Table 3.2 lists the input values used in the various FEA models. Figures 3.9 to 3.14 are typical examples of the stress distributions produced by the numerical analysis. The finite element program's outputs are described much more deeply in the appendices A.8. to A.11.

Even though no clear explanation of changes in life with varying contact semi-width was attained solely from looking closely at the different stress and displacement distributions, a good understanding of what was probably occurring on a local level was achieved. Many trends were identified in appendices A.8. to A.11. for fretting tests that keep constant p_0, Q/P, $\sigma_{N,max}$, and $\sigma_{N,min}$ while varying other parameters. The base of understanding of what was happening in the experimental tests was established and a search for an explanation of the effects of contact width on fatigue life and critical contact semi-width could begin.

4.3 Critical Plane Based Predictive Criteria Evaluated:

Namjoshi et al. recently claimed that fretting fatigue crack initiation is a function of the shear stress on the critical plane and that fretting fatigue life is related to the normal stress on the critical plane [23]. It was decided to evaluate several of the critical plane based fatigue predictive parameters for the tests conducted in this study. In general

the value of the parameters is inversely proportional to the fatigue life of the specimen. So significant increases in the parameters' values would be expected for the tests that experienced lives of over 300,000 cycles compared to the tests that failed in less than 100,000 cycles. Would the parameters' values change for the tests that experienced infinite fatigue life?

Usually these predictive parameters are used to forecast fatigue life, crack location, and crack angle, but for this study the hope was to use them just to show changes in life. Furthermore, it was a hoped in this study that some of the predictive fretting fatigue parameters would work in showing a significant change in value around the critical contact semi-width.

These critical plane based predictive parameters could be used to isolate the important variables. Different parameters emphasize the importance of different fretting fatigue variables in their prediction. If a predictive parameter, that had slip amplitude, bulk normal stress, and shear traction as its key influences, showed a dramatic change about the contact semi-width, while a parameter that focused on shear stress range showed no effect, then it could be logically assumed that variables or a variable in the former parameter had a greater effect on change in specimen longevity than variables in the latter parameter.

4.3.1 Namjoshi Program: In this work, a program written by Namjoshi was used to evaluate five critical plane based fatigue predictive parameters: Findley, Smith-Watson -Topper, Shear Stress Range, Effective Shear Stress Range, and Modified Shear Stress Range [24]. The relevant details of these parameters were discussed in the chapter on background research. The output stresses of the specimen surface layer in the vicinity

of contact had to be brought from the FEA output data file in both maximum and minimum loading cases for each run on the "parameters program." The output data from the ABAQUS finite element program was specifically ordered in an array, which included the x and y locations of nodes and their corresponding stresses calculated for the xx, yy, and xy directions along the specimen surface. This information was then processed by the program, which calculated the parameters in steps of 0.1^{o} at angles ranging from $-90^{o} \le \theta \le 90^{o}$ and then output the parameter values along the length of the specimen surface at the critical plane.

4.3.2 Parameter Values: The results of using these parameters did not seem to help in identifying a critical contact semi-width. Instead there were no great changes in parameter values for the pad radii above or below the critical contact width found in the experimental tests. Tables 4.2 and 4.3 list the maximum values of these parameters as determined from FEA output and "Ruiz" program output. Each parameter was examined over the complete surface of the contact region and compared to the same parameter distributions for the other tests.

The Namjoshi program gave the option to calculate the Smith-Watson-Topper parameter in two different ways. Both cases were run for the data in this study. The maximum values of the SWT parameter are graphically plotted against contact semi-width in Figure 4.4. SWT stays relatively constant for all of the tests, both with infinite and finite fatigue lives.

The maximum values of the other parameters examined, Shear Stress Range, Effective Shear Stress, Modified Shear Stress Range, and Smith-Watson-Topper are plotted versus radius in the appendices A.12. Remembering that 1,000,000+ cycle life

was generated in the tests with pad radii of 0.01016 m, 0.00762 m, and 0.00508 m and 300,000+ cycle life was observed in the 0.0508 m pads test, there seemed no significant change in any of the critical plane based fatigue parameter values from those critical plane values determined for all the other tests, which lasted below 80,000 cycles. Running the analytical solution program's output through the Namjoshi parameters program duplicated these findings, except that the analytical parameter values seemed to be marginally higher. This meant that the five critical plane based fatigue predictive parameters failed to predict changes in life with changes in the contact semi-width!

4.3.3 Correlation with Q/P: Given that Q/P, p_0, and $\Delta\sigma_N$ were held constant, what was the cause of the slight variances of parameter values versus contact width? It was noticed that a possible cause of the trends noted in the different parameters was that, despite efforts to keep the ratio of Q/P constant, it was not held exactly constant in the experimental testing. Even though the input from the parameters program came from the finite element output and did not come from the experimental tests, the input to the finite element program came from the experimental testing results. Therefore, it is reasonable to guess that trends in the parameters were influenced by variations in the Q/P ratio. Comparing the values of Q/P that were input into the finite element program, as shown in Figure 4.2, to the various critical plane predictive parameter values, a common trend can be found. Therefore variance in the predictive parameters was probably more a result of imperfect test conditions than any influence of the critical contact semi-width.

4.4 Iyer's Explanation:

As is consistent with his view on the causes of fretting fatigue, Iyer attributed changes in life with changes in contact width to variances in the local mechanistic

parameters. More specifically, he thought that decreasing local tensile stress concentrations caused the increases in life. Tests with lower local stress concentrations would have greater longevity. The FEA shows that as contact semi-width decreases, the local tensile stress concentration also decreases while the remote stresses stay constant. This occurs because of differences in tensile stress concentrations generated exclusively by the normal load [14].

By looking closely at the step 1 output, the effects of the cylindrical contact independent of applied bulk stresses, can be examined. In order to investigate these issues, stress distribution data for the different finite element tests with only normal load being applied was closely examined. These stresses, as well as the entire step 1 output for all of the different radii processed through finite element analysis, are thoroughly discussed in the Appendices.

4.4.1 P-only Tensile Stress Concentrations: In hope of confirming the Iyer's explanation, stress distributions in the x-direction were looked at from the pressure load only finite element analysis. The tensile stress concentrations Iyer noted can be seen to indeed exist at the edges of the contact area. The peaks of these tensile stress concentrations lie exactly on the edges of the contact zones. For example the edge of the step 1 contact zone for the 0.0508 m radius fretting pads case was $x = \pm .75*10^{-3}$ m. The peak tensile stress of $222.115*10^{6}$ Pa was located at $-.75*10^{-3}$ m and $222.115*10^{6}$ Pa at $.75*10^{-3}$ m. Their peaks represent the maximum values of σ_{xx}, or maximum tensile stress values, along the substrate surface. The sharpness of these tensile stress peaks dulled for the smaller radii pads tested. Figure 4.5 shows the trend of how the σ_{xx} distributions

changed with the different tests. It is important to note that in each case where the load is changing, the radius of the cylinder is also changing.

The tensile stress concentration is a function of normal load and not radius [14]. Therefore it does not matter that the pad radius is changing for the different normal loads. The ratio of P to maximum σ_{xx}, generated solely from normal loading, remained almost constant, at a slope of 383.52 N/Pa, for nine the different values of normal force tested.

4.4.2 Iyer's Explanation of the Critical Contact Semi-width: According to this explanation, these changes in P-only tensile stress concentration translate to the combined loading case and are the source of differences in local stress concentrations.

Iyer made the claim, presumably starting with a very small contact semi-width, if one were to increase the contact semi-width (by changing the radius) continuously while holding the peak contact pressure and maximum, nominal bulk stresses fixed, there will be a particular contact semi-width for which the maximum, local bulk stress exceeds the yield stress. For all contact semi-widths smaller than this 'critical' value, the local, maximum bulk stress will be less than the yield stress. [14]

This quote from Iyer is an explanation of the critical contact semi-width based on the local mechanistic parameters. The hypothetical test he describes directly matches the test set-up that was attempted in this study.

4.4.3 Local Principal Stresses: The question arises as to which "local, maximum bulk stress" was being described. It was not clear in Iyer's published paper. However, by definition the principal stresses are the premier stresses experienced at a point. It would seem logical to look at the principal stresses along the substrate surface for changes in local stress concentration that correlate to differences in contact semi-widths.

The S1 principal stress distributions along the contact areas of the various pad radii tests were analyzed. It is significant to note that the maximum value of this principal stress is attained just on the inside of the contact zone at the trailing edge. There is a clear trend that the S1 principal stresses increase as pad radius increases. For the numerical analysis of experimental tests actually conducted in this study, excluding Jin's data, tests with principal S1 stresses above $1.325*10^9$ Pa all failed with short fretting lives and those tests below this stress level lasted longer than 1000000 cycles. According to the finite element analysis, there is a definite trend that local, maximum bulk stress increases with radius. If Iyer's explanation was correct, then the critical local stress for fretting crack initiation had to be about $1.325*10^9$ Pa. These principal stress values are shown on table 4.4.

4.4.4 Problem's with Iyer's Case: Iyer's explanation seemed possibly correct except for two things. First, Titanium alloy, Ti-6Al-4V, has a yield strength of 930 MPa and ultimate tensile strength of 978 MPa. These numbers did not match with the findings of the principal stress analysis. The yield stress was not the border between infinite and finite life tests. Secondly, the data received from the test conducted by Jin seemed to directly contradict this explanation.

4.4.5 Jin's Anomaly: Jin ran a test with 0.0508 m radius pads and at a steady state Q/P ratio of .83, using independent pad displacement. It had a life of 300000+ cycles [16]. Jin's test was conducted on the same servohydraulic test machine used in this study, with the same fretting fixture. His specimen was from the same batch as the specimens used in this study, and it was under Jin's close scrutiny that the first few tests in this study were set up properly. If Jin's data is correct, it stands in direct opposition to

Iyer's explanation of the critical contact semi-width, because the maximum, local bulk stress should have exceeded the material yield and lead to early failure.

Jin's test was conducted for the purposes of his study on the phenomenon of "gross slip." It is his contention that the .0508m radius pad test had infinite life because it experienced fretting wear conditions induced by gross slip [16]. It seems that Iyer's approach did not include the effects of gross slip.

There are several possible explanations of this inconsistency with Jin's test results. The reason that Jin's test had infinite life could be totally separate from the phenomenon that leads to infinite life below the critical contact semi-width. Either the data from this study or Jin's data could be bad. Both data could be bad. Or the reason for infinite life in the .0508m could be the same reason that led to infinite life in the tests of the .01016m and smaller radii pads.

4.5 Relation to Gross Slip:

Triggered by the search for an explanation of Jin's anomalous test data, the study of changes in life with changes in contact semi-width took a new turn. From his work, Jin concluded that the reason that his specimen had infinite fatigue life was because it was experiencing gross slipping. When gross slipping occurs, fretting wear prevents crack initiation by wearing away newly formed cracks before they have time to propagate [16]. Could the specimens experiencing infinite fatigue life below the critical contact semi-width be in gross slip?

4.5.1 Slip, Stick-Slip, Gross Slip: There are three conditions in fretting that will be looked for in tests of this study: slip (also called global sliding condition), stick-slip, and gross slip. Typically, when fretting fatigue tests start they are experiencing the slip

condition. This is before a stick zone has formed. The pads and substrate are relatively free to slip against each other without sticking. After a time, tests either go to the slip-stick condition and fail due to fretting fatigue or they go to the gross slip condition, which is dominated by fretting wear. The slip amplitude of tests in stick-slip is much smaller than those in gross slip, because the stick zone prevents free sliding.

4.5.2 Interpreting Fretting Condition from Q vs δ Loops: The hysteresis loops generated when plotting Q versus slip displacement for a cycle are typically used to classify the fretting condition being experienced [34]. The Q versus δ hysteresis loops for the tests using 0.00508 m, 0.00762 m, 0.01016 m, 0.01905 m, 0.4445 m, and 0.0508 m radius fretting pads are shown at the end of this chapter. Also presented at the end of each hysteresis loop series is the corresponding Q versus cycle curve for that test. These curves can be found in Figures 4.6 to 4.41.

4.5.2.1 Slip: Slip conditions were experienced during the earliest cycles of all tests. When tests were in this condition, the Q versus displacement curves formed almost a rectangular box. In an early cycle, such as the second, fifth, third, tenth cycle, etcetera, Q quickly goes from negative to positive without much corresponding change in displacement relative to the total displacement experienced in that cycle. After the rapid change in Q, a period of either positive or negative sliding displacement follows as Q is at its minimum or maximum value. The substrate and pad slide with respect to each other. When Q shifts polarity and then the substrate and pad slide in the opposite direction. This state is known as slip. Q is free to change direction quickly as the bulk stresses changes, because there is only slipping taking place. Figures 4.6, 4.12, 4.17, 4.30, and 4.37 are examples of tests in slip.

4.5.2.2 Transition from Slip to Stick-Slip: After a number of cycles the substrate and pads start "welding" together in the center of the contact. The hysteresis curves start to change shape. The range of displacement becomes less as the change in Q increases, hence the loops become taller and thinner. This rise in Q can be seen in Q versus cycle curves, Figures 4.11, 4.16, 4.22, 4.29, 4.36, and 4.41, to be present in the early cycles of the curves. Q and the displacements are beginning to change simultaneously. The components are not as free to slide with respect to each other as they originally were. This transition from long flat rectangular hysteresis loops to taller rectangles with thinner widths continues until the shapes are no longer rectangles. This is the transition from slip to stick-slip.

4.5.2.3 Stick-Slip: After a few thousand cycles into tests, the shear traction and displacement no longer changed independently of each other. What was once a rectangle has become a diamond-shaped loop that is so narrow that it appears to be diagonal line. These narrow pointed loops represent a situation in which displacement only changes when Q is changing. No large sliding is taking place. Part of the contact area of both the pad and the substrate are physically stuck together in the stick zone. This state is known as stick-slip. It is significant to note that all of the samples that fractured in under 100000 cycles eventually experienced stick-slip fretting, which is illustrated by the narrow loops in Figures 4.25, 4.28, 4.34, 4.35, and possibly 4.38.

4.5.3 Fretting Fatigue Stick-Slip: The majority of tests conducted for this study, such as tests using 0.0381 m, 0.03175 m, 0.0254 m, 0.01905 m, 0.01524 m, and 0.0127 m pad radii, had Q versus δ loop transitions that looked very much like those of the test using 0.04445 m radius pads. The 0.04445 m radius test's hysteresis loops show the

classic transition from slip to stick-slip, which is characteristic of fretting fatigue. The loops start with a rectangular shape, become diamond-shaped, and eventually form diagonal lines (closed loop) [15]. The Q versus cycle curve, as shown in Figure 4.36, increases for the first 5000, and then levels off. The flat portion of this curve represents steady state fretting fatigue in the stick-slip condition.

Some differences in the tests that failed in less than 100000 cycles were that the magnitudes of Q and δ and the number of cycles for transition from slip to stick-slip changed for each test. The 0.01270 m radius pad test, for example, did not have the long, narrow loops of stick-slip until right before fracture. The general trend was that the tests with smaller pad radii took longer to transition from slip to stick-slip.

4.5.4 Mixed Fretting: Many of the tests in this study showed signs of "mixed fretting," especially within the first 10000 cycles of their respective tests. Mixed fretting is when the fretting conditions switch back and forth between slip and stick-slip regimes. This is illustrated on the Q versus δ loops when the loops are starting to thin, reaching stick-slip conditions, but then suddenly get wide again for a while and then once again continue to narrow once again and eventually reach stick-slip. Specimens experiencing mixed fretting can bounce back and forth between slip and stick-slip several times.

An example of mixed fretting can be seen in the 0.01905 m radii pad test: figures 4.23 to 4.29. The Q versus δ loops narrow from cycle 500 to cycle 700 and from cycle 700 to 2000, where the loops appear as if in stick-slip. But cycle 5000 shows a loop, which has clearly returned to the slip regime. By cycle 15000 the loop has narrowed once again. The sample fractures after 70000 cycles in stick-slip.

4.5.5 Gross Slip: The Q versus δ loop transitions were different for the four tests with pad radii of 0.0508 m, 0.01016 m, 0.00762 m, and 0.00508 m. These four tests all started in slip but never fully transitioned to the stick-slip regime. They all share similar Q versus δ loop features.

4.5.5.1 0.0508 m Pad Radius Test: It is important to reiterate the fact that the 0.0508 m fretting pad test data was from a previous study on "gross-slip" by Jin [16]. In that study the test was previously classified as experiencing gross slip. Figures 4.37 to 4.40 show four Q versus δ loops from the 0.0508 m pad test. The loop at cycle 2 shows a typical shape for an early Q versus δ loop in the slip regime. The loops through cycle 70000 continue to transition from the slip toward the stick-slip regime. However stick-slip is never fully attained or held until fretting fatigue fracture. By cycle 100000 the Q versus δ loop is wider and less like a loop in the stick-slip condition. By the 120000th cycle the loops have completely changed shape. The long flat rectangle is indicative of the gross-slip condition. There is a large amount of sliding for little change in Q. In this test, the Q versus cycle curve never leveled off to steady state. The absence of a clear steady state is a trait common to all 4 tests with infinite fatigue life. In Jin's study, tests that reached this gross slip condition had lives significantly longer typical fretting fatigue lives.

The first piece of evidence, supporting that the tests with fretting pad radii smaller than 0.0127 m were experiencing gross-slip, like Jin's test was, comes with examination of the shear traction versus displacement hysteresis loops. Figures 4.6 to 4.10, 4.12 to 4.15, and 4.17 to 4.21, show the Q versus δ curves for the three tests, conducted by this study, that had significant increases in life.

4.5.5.2 0.01016 m Pad Radius Test: In the .01016 m radius test, the loops narrow from cycles 2 to 50, 50 to 1500, and 1500 to 12000. However, the hysteresis loop at around 12000 cycles was the thinnest. After this the loops begin to widen and shorten. The slipping displacements continue to increase and the shear traction decreases until 1000000 cycles when the test was ended. The hysteresis loop for the 1000000^{th} cycle is shown on Figure 4.21. Its shape is somewhat long and rectangular. This is much different than the slip-stick hysteresis loops of the test that failed in fretting fatigue. It is a hysteresis loop of a test in gross slip.

4.5.5.3 0.00762 m Pad Radius Test: The hysteresis loops in the 0.00762 m test case are still different from the typical fretting fatigue tests. This time the loops narrow from the 2^{nd} to the 2000^{th} cycle as shown in figures 4.12 and 4.13. But after the 2000^{th} cycle they remain pretty much the same shape for around 100000 cycles. The narrowest loop is not as narrow as hysteresis loops were in the 0.01016 m pad radius test. After the 100000^{th} cycle the loops start to widen and shorten. The millionth cycle loop is longer and shorter than the 1000000^{th} cycle loop from the 0.01016 m radius test. This short and wide loop is also representative of the gross slip condition.

4.5.5.4 0.00508 m Pad Radius Test: In the 0.00508 m pad radii test, the Q versus δ hysteresis loops seemed to never even narrow toward the stick-slip condition. Instead, the 10^{th} cycle rectangular shaped loop has a greater Q range and displacement range than even the 2^{nd} cycle loop. Over time the rectangular height did shorten. The slip displacement first shortened and then became longer towards the 1000000^{th} cycle. This test's millionth cycle hysteresis loop was shorter in height and longer in width than the previous gross slip tests' geometry. Its shape resembled the 150000^{th} cycle's loop from

the 0.0508 m test run by Jin. Compare Figure 4.40 to Figures 4.10, 4.15, and 4.21. The latter three tests were clearly not experiencing stick-slip conditions, but were very likely in gross slip, like Jin's test.

4.5.6 Interpreting the Fretting Condition from Q vs N Curves: There was a strong relationship between the Q versus δ hysteresis loops and the Q versus N curves, which are a plot of the maximum value of shear traction for each cycle. The maximum value of Q on the hysteresis loops is the same Q used in the Q/P ratios and is plotted in the Q versus N. Therefore the "height" of the hysteresis loops changed as the magnitude of Q changed on the Q versus N curves.

Events such as mixed fretting, the transition from slip to stick-slip, and even gross slip can be reasonably well identified by inspecting the Q vs N curves. The curve for the first few cycles starts in the slip condition. The part of the curve, before the Q levels off, represents the transition stage. The stick-slip condition is when the curve levels off to long flat plateaus. When the Q versus N curve has a positive slope the hysteresis loops tend to be transitioning from slip to stick slip.

For example, compare the Q vs N curve of Figure 4.36 to the hysteresis loops of Figures 4.30 to 4.35. The hysteresis loops are narrowing in width and increasing in height from 0 to about 5000 cycles. After about 5000 cycles the curve flattens out and a steady state, stick-slip condition has been reached. Checking with Figures 4.30 to 4.35, it can be seen that the hysteresis loop at cycle 7000 is narrow and does not change shape much from the hysteresis loop at 70000.

The hysteresis loops widen if the Q versus N curve slope is negative in slope, such as in the case when a test goes from near stick-slip to gross slip. The tests that

resulted in infinite life all had Q vs N curves that never leveled off and Q vs δ loops that never fully closed. They may have had positive Q vs cycle slopes for the first portion of the tests, but at some point during the test, the Q vs N slope became negative and stayed negative long enough for the magnitude of Q to decrease significantly. The test with 0.0508 m pads and tests with radii below 0.0127 m all had the Q vs N curve trends that correlated with infinite life and gross slip.

4.5.7 The Breakthrough: It is the contention of this study that the tests with pad radii smaller than 0.0127 m experienced gross slip conditions. Gross slipping, and the resulting fretting wear, could be the reason that there is such a dramatic change in life between tests about the critical contact semi-width! This study is the first to make the connection between gross slipping and the critical contact semi-width. Tests above the critical contact semi-width (with the exception of the 0.508 m pad radius test) all failed experiencing the stick-slip condition, while tests below the critical contact semi-width and Jin's test all experienced gross slipping and infinite fatigue life. The four gross slip tests experienced over 10 times the longevity of even the longest running tests that were considered to fail in the slip-stick regime.

4.5.8 Comments on Iyer's Solution to the Critical Contact Semi-width: As a result of the gross slip analysis it seemed likely that the effect of the critical contact semi-width can not be predicted by the divide between local stresses above and below yield stress, as proposed by Iyer, but instead correlated with the fretting condition and slip amplitude.

Iyer's explanation of fretting fatigue still might be valuable for analysis of the tests with pad radii from 0.0127 m to 0.04445 m. The trends he described seem to hold

true for the tests that failed under normal fretting fatigue. However his solution broke down when it came to the effects of gross slipping. His explanation of the critical contact semi-width holds merit, but it doesn't extend to Jin's findings.

Iyer's local mechanistic parameters analysis can possibly be used to help explain why the life of pad radii failing under stick-slip decreased with increasing contact semi-width. He noted that an increase in normal load, P, results in an increased local, maximum stress range, $\Delta\sigma_{L,max}$ for the same values of pad radius and nominal bulk stress range. The general trend of a decrease in fretting fatigue life found with increasing P could have been because of increases of $\Delta\sigma_{L,max}$.

4.5.9 Comments Nowell/Hill's Solution to the Critical Contact Semi-width: Nowell and Hill had their own opinions as to the relationship of changes in the contact semi-width with changes in fatigue life and the nature of the critical contact semi-width effect. In their opinion, the two possibilities for the "size effect" in fretting fatigue were that either fretting fatigue cracks did not initiate at smaller contact widths or that they did initiate, but their growth was somehow halted [28]. The critical contact semi-width phenomenon could stem from either crack initiation or growth. They did not consider the possibility that the reason cracks could not grow or initiate was independent of contact size, as was shown by the Jin test.

4.5.10 Comments on Bramhall's Solution to the Critical Contact Semi-width [28]: Their predecessor Bramhall suggested the crack arrest solution (crack growth approach). He asserted the idea that "if the contact stress field is not sufficiently extensive to propagate an embryo crack to a length at which it can grow under the bulk stress alone then crack arrest will take place and the specimen will not fail." However,

when Nowell and Hill examined the sections of the different specimens they found no evidence to support this idea. There were no embryo cracks in the specimens with the contact widths below the critical value, but there were many micro-cracks in the specimens with the larger contact widths. Furthermore for some of the unfailed specimens that underwent fretting with smaller contact widths, they moved the fretting contact location and ran a second test on the same specimens. They did not fail where the first fretting pads had been located. This was probably because cracks never initiated in that original location. Therefore, Nowell and Hill thought that cracks at smaller contact widths did not initiate.

4.5.11 This Study's Solution to the Critical Contact Semi-Width: The reason for the critical contact semi-width was not that cracks could not grow or that cracks could not initiate. But because gross slipping was taking place in the tests with infinite fatigue life, fretting wear was rubbing away newly initiated cracks forming on the surface before they had a chance to grow. Every time a crack would start to form, the surface was wiped clean by the wearing of the pads. This did not occur in tests with a stick zone because the pads and specimen were not wearing where they were stuck together.

4.6 Slip Amplitude:

The question then becomes, why did some tests go into gross slip while others fail in stick-slip? The answer to this lies in the analysis of the slip amplitudes between pads and substrate.

4.6.1 Slip Amplitude from FEA: Slip amplitudes can be determined, based on the finite element data, through analysis of the relative nodal displacements on the surfaces of the pads and specimens. It can be seen, from the u_1 displacement

distributions, that some of the nodes that are directly "touching" between the pad and substrate in the normal load only case, move relative to each other in the maximum and minimum loading conditions cases. Other nodes stay touching in all cases. The former described nodes are said to be slipping and the latter described nodes are sticking. By looking at the difference in u_1 displacement of the pad and specimen surfaces in the contact region, their displacement relative to each other is what is known as "slip range." Remember that the "slip amplitude" is half of the slip range.

In the fretting cases run by the finite element model, all contact regions have both "stick" and "slip" zones. Both of these type zones are found in the contact region. In every case in this study, one stick zone is found in the middle of two slip zones. Figure 4.42 shows the relative slip amplitude between the .0254 m test case's pad and substrate surfaces for both maximum loading and minimum loading conditions. Several trends can be noticed. The non-zero ranges of the curves represent the slip zones while the somewhat flat middle regions are the stick zones. The relative displacement of points along the surface of the pad and substrate is essentially zero in the stick zones. But there is sliding in the slip zones, the magnitude of which is shown by the amplitude of the curve.

It can also be noted from Figure 4.42 that the stick and slip zones of the two different loading conditions shift. The positive x slip zone is much larger in the maximum loading case than it is in the minimum loading case and the opposite is true for the negative x-side slip zones. The stick zones shift such that only part of the stick zone is always stick. The other part of the stick zone changes between slip and stick depending upon the specific loading conditions. The reason for this shifting of slip and

stick is two-fold. The first explanation is illustrated in Figure 4.43. Points A and C are "touching" and B and D are "touching" in the pressure load only cases. However when the step 2 conditions are applied the pad rolls and the contact zone shifts. The last point on the fretting pad that is always in contact with the substrate on either side constitutes of the borders of the slip zone. Point A is at the edge of the contact zone in the minimum loading case and Point B is at the other edge of the contact zones in the maximum loading case. The nodes in between A and B and their corresponding nodes on the substrate surface between C and D are the nodes whose displacements were looked at for slip amplitude determination. The second reason for the shifting and size changing of the slip and stick zones is primarily due to the Q force being experienced at that specific loading condition.

The total slip amplitude of a point is the sum of its slip amplitudes for both the minimum and maximum loading cases. It can be generally noted, for tests in this study, that as the contact semi-width increased the slip amplitude also increased, not to say that the two were directly related. In all cases the maximum slip amplitude was located on the edge of the slip zone closest to the end of the specimen on which the bulk stress was applied, also known as the trailing edge. As can be seen on Figure 4.44 the magnitude of this maximum slip range, calculated from the finite element data, increased with contact semi-width. The trend from the finite element data was almost linear.

4.6.2 Slip Amplitude from Experimental Data: The FEA slip amplitude analysis could be compared to the actual experimental data. Whereas the heights of the Q vs δ hysteresis loops correlate well with the Q vs N curves, the width of the Q vs δ loops is representative of the slipping experienced between the pads and specimen. As was

established, the thin Q versus δ hysteresis loops are representative of when the experimental test was in the stick-slip regime. The difference in the x-coordinates of the extreme tips of these narrow stick-slip loops is slip range, because the x-axis is the displacement. For cases in which the stick-slip condition was never reached, the slip amplitude at the occurrence of the maximum value of Q/P during the respective test was considered. Therefore, the experimental slip amplitudes could be measured and compared to the finite element amplitudes.

The finite element model was different than the experimental tests. Clearly the experimental tests that ran for infinite fretting life were not experiencing much sticking for the latter parts of their tests, but because of the way the finite element program was set up (and the high value of μ selected) the cycles simulated by FEA all showed sticking. This is the reason for the difference in slip amplitude versus contact width trends between FEA and the experimental analysis, which will be discussed next. The finite element model showed no sign of difference in slip amplitude from the linear trend for tests that, in the real world experiments, went into gross slip.

4.6.3 The Critical Slip Amplitude: A plot of maximum experimental slip amplitude versus 2a is shown in Figure 4.45. This plot is significant, because for the first time there seems a relationship that includes a difference on both sides of the pad radii spectrum. The anomalous data from Jin's experiment can be included! The smallest maximum slip amplitude of all tests in this study occurred for the 0.0254 m radii pads and it was $2.4*10^{-5}$ m. There is an increase in slip amplitude for all pad radii larger or smaller than 0.0254 m. The maximum slip amplitude of specimens that lasted for infinite fretting fatigue life was greater than 5.4*10-5 m in all cases! All tests that failed in less

than 100000 cycles had smaller maximum slip amplitudes. It is the finding of this study, that there is not a contact width that is critical, but instead there is some critical maximum slip range that correlates to a certain contact semi-width when independent displacement is not applied. Slip amplitudes above the critical slip amplitude lead to gross slipping and infinite fretting life. Figure 4.46 shows the slip amplitude versus fretting fatigue life. All cases where maximum slip was above the critical slip amplitude had infinite life, while all cases below the critical slip amplitude failed in less than 80000 cycles.

In his experiments on gross slip, Jin found that "a minimum fretting fatigue life was observed at a relative slip range of 50 to 60 μm … when the relative slip range was greater than 80 μm, the gross sliding occurred and the specimen did not fail" [15]. His numbers are slightly different. But as Wittkowsky noted, it is difficult to measure the relative displacement between contact surfaces. There are often substantial differences between the measured relative displacements of different sources. True relative displacements can vary significantly from reported values [34]. For example the finite element values of slip are about an order of magnitude different from the experimental values for slip. The important thing to take from this study is not the exact number value of the critical slip amplitude, but the idea that there is one.

Even though it might not have been specifically identified or understood as such, previous researchers have found this critical slip amplitude in their studies as well. Without the benefit of independent pad displacement Nowell and Hill might have mistakenly associated the slip amplitude effects with contact semi-width, since the two parameters are often linked proportionally together. Therefore they reported that there was a certain critical contact semi-width. In truth this a_{crit} probably correlated to the

critical slip range below which fretting fatigue did not occur. What Nowell and Hill missed was what Jin found with his tests on independent pad displacement. "At the very high relative slip amplitudes, the gross slip condition resulted where … it did not cause specimen failure."

4.6.4 Comments on Jin's Conclusions: Jin's conclusions from his study of gross slip entitled, "Effects of Independent Pad Displacement of Fretting Fatigue Behavior of Ti-6Al-4V," seem to relate well to the findings in this study and will be discussed:

Jin's first conclusion was that,

> The tangential force increased with increasing fretting fatigue cycles and was quickly stabilized in a few hundred cycles. The ratio of the tangential force to normal force [also known as the ratio Q/P] increased initially with the increase of the relative slip range, and then it remained constant when the relative slip range was greater than approximately 80 micrometers. [15]

It did take some time for the tests to stabilize, but the description of a few hundred cycles did not hold true for every test in this study. For many of the different tests it took between 2000-5000 cycles before stabilization took place. The general trend was that as contact semi-width decreased, the number of cycles until the tangential force stabilized increased. The tangential force never stabilized for tests that lasted for infinite fretting fatigue life.

Jin's second conclusion statement was that life was minimum at a specific slip range and that increasing and decreasing the slip range from that specific slip range led to increased fretting fatigue life [15]. In this study, as Q/P was held constant, there was a

certain minimum slip range, which occurred with the .0254m pad, for which increasing or decreasing the pad radius produced greater slip ranges. The .04445m pad radius test had a slip range of 45 μm and a life until failure of 40,500 cycles. The pad radius above it, .0508m, had infinite fretting fatigue life, and the pad radius below it, .0381 lasted for 46,000 cycles.

In Jin's third conclusion statement he said that, "the fretting contact condition was identified from the relationship between tangential force [Q] and relative slip range [δ]. The change in the contact condition [slip, stick-slip, gross slip] was identified by the change in the area inside the tangential force versus relative slip range hysteresis loop." It was found in this study that the narrow diagonal line shaped hysteresis loops corresponded to stick-slip, while the short but wide rectangular loops represented the occurrence of gross slipping.

Finally Jin noted that "at very high relative slip range, the gross slipping resulted in the excessive material removal from the specimen … this contact condition did not cause the fretting fatigue failure" [15]. This is the explanation of why cracks did not occur in the infinite fretting life tests that resulted in this study.

4.7 Ruiz Parameter:

The maximum slip amplitude is a key variable in the Ruiz Parameter, used in fretting fatigue prediction. The Ruiz Parameter is easy to calculate and has been the subject of a lot of debate in the fretting fatigue world. Instead of scientifically determined combinations of variables, the Ruiz Parameter is based more on empirical observations. There are many differing opinions as to its worth. Since the parameter's value is proportional to slip range, it seems as if it would compliment the findings of this

study. It was decided to determine and compare maximum Ruiz Parameters values for the different tests.

The first Ruiz Parameter (he created a second parameter which is just the product of the first Ruiz Parameter and the bulk stress) was the product of the shear force and slip range,

$$F_1 = \tau\delta \tag{16}$$

but for the purposes of this study it will be defined as

$$F_{1,\max} \approx Q_{\max}\delta_{\max} \tag{17}$$

It was determined in this work first from the finite element results and then from the experimental output data. Using the finite element data, the Ruiz parameter was assumed to be the product of maximum τ_{max} and the maximum slip amplitude. From the experimental data, the maximum Q value and corresponding slip amplitude were multiplied together.

This study was concerned with how the values of the Ruiz Parameter compared to the life of the different pad radii tests run. Figure 4.47 shows how the maximum values of the first Ruiz Parameter calculated from the finite element data compared to the different pad radii. The curve is almost linear and does not show any significant changes for tests that had infinite fretting life. Figure 4.48 somewhat correlates to test results, however, the plot is not perfect. The maximum Ruiz Parameter values for the smaller pad radii that lasted for infinite life are not larger than the .04445m pad radius test, which failed under fretting fatigue.

4.8 Modified Ruiz Parameter:

In light of all the findings of this study up to this point, the author empirically created a new parameter, based on the first Ruiz parameter. The idea behind it was simply to weigh the variables in the Ruiz Parameter differently. Since the variables in the Ruiz parameter were originally chosen based on observed trends, no problem was seen in changing their weighting based on the new observed trends. It was felt that, based on the newly realized significance of the slip amplitude, greater weight should be given to δmax. Therefore the modified Ruiz parameter became:

$$F_{\mathrm{mod}\,ified} = Q_{\max}\delta_{\max}^{2} \tag{18}$$

Not surprisingly this parameter did match up well with the data from the given tests as is illustrated in Figure 4.49. There seemed to be a significant parameter value difference in all those tests that experienced infinite fretting life from those that failed under fretting fatigue.

A table summarizing the slip ranges and Ruiz Parameter values from the FEA and experimental analysis is located at the end of this chapter.

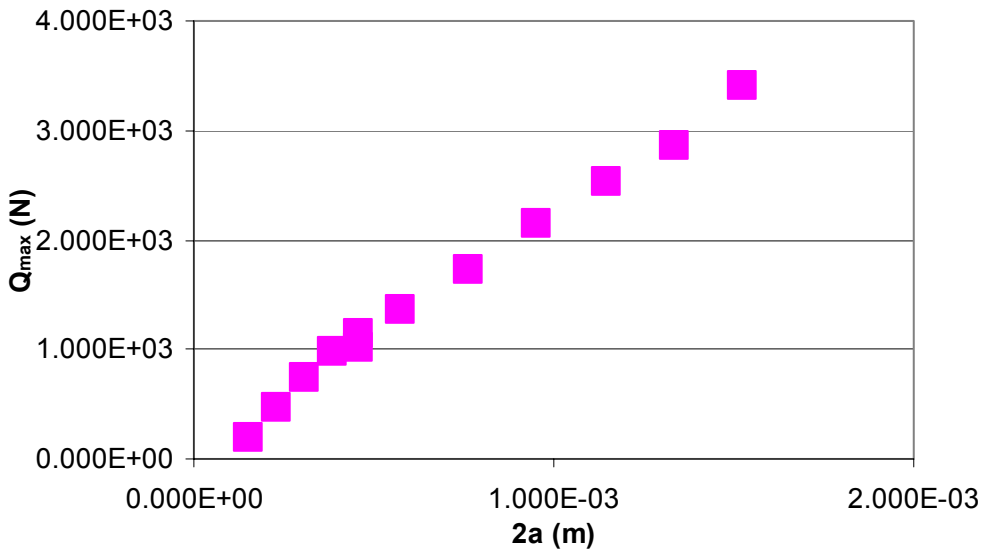

Figure 4.1 Maximum Experimentally Recorded Q/P Ratio Versus Contact Width

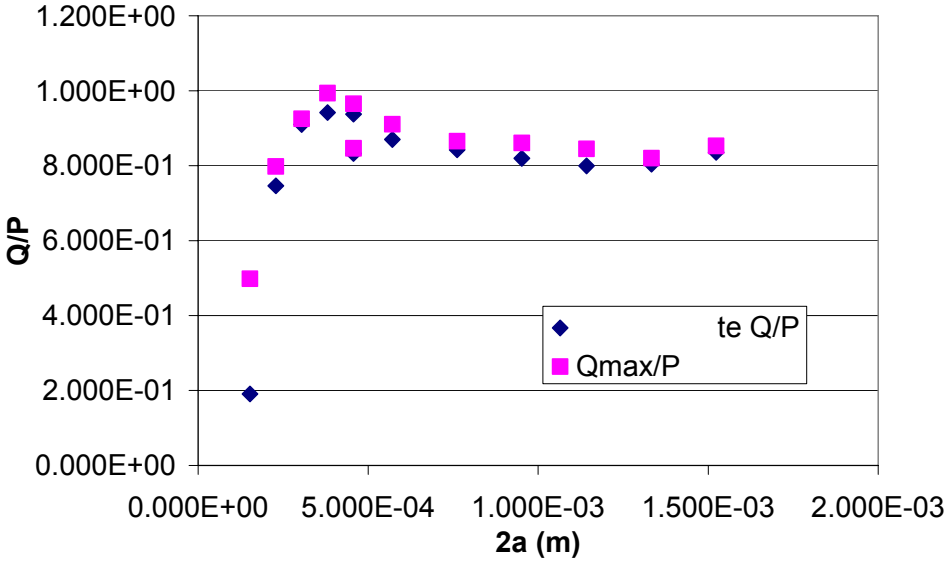

Figure 4.2 Experimentally Observed Steady State and Maximum Q/P Ratios Versus Contact Width

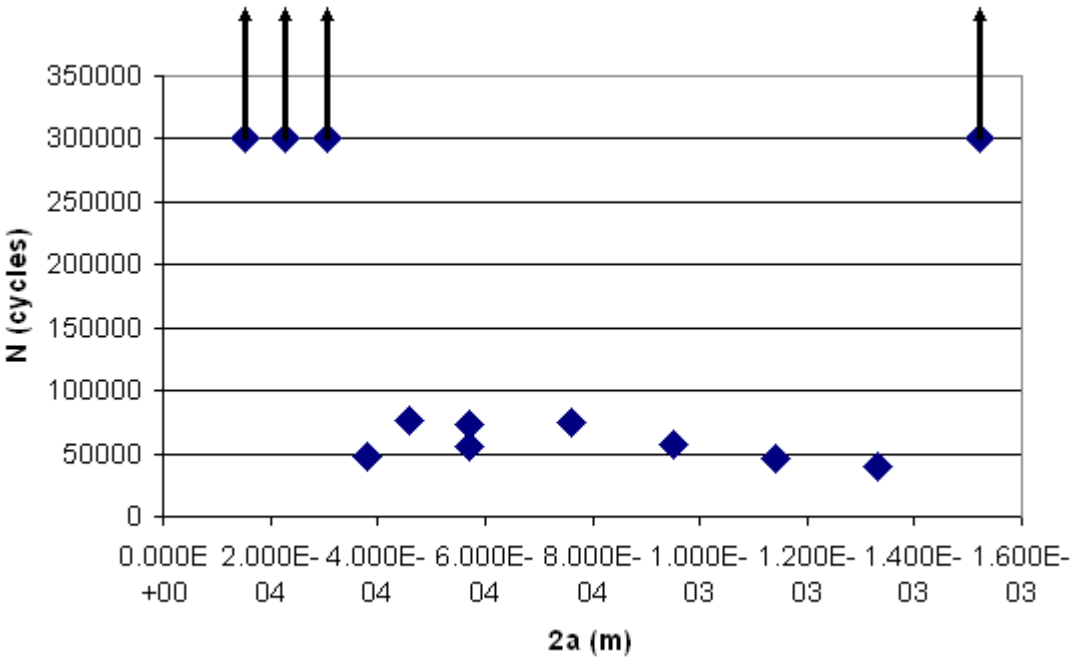

Figure 4.3 Fatigue Life Versus Contact Width

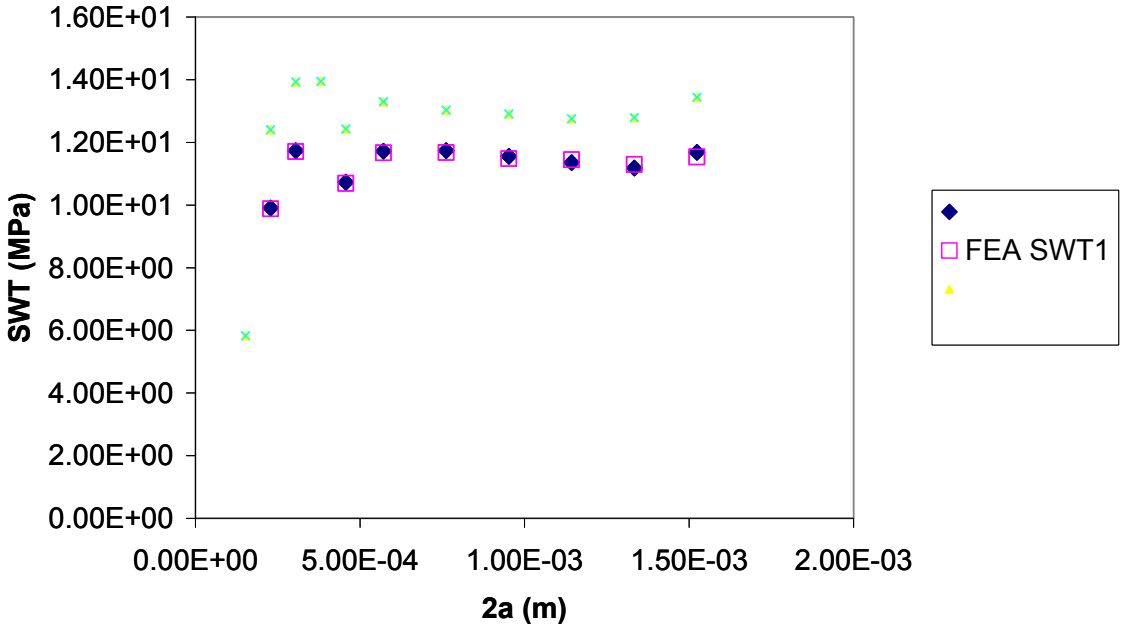

Figure 4.4 Smith-Watson-Topper Parameters Based upon FEA and "Ruiz" Outputs

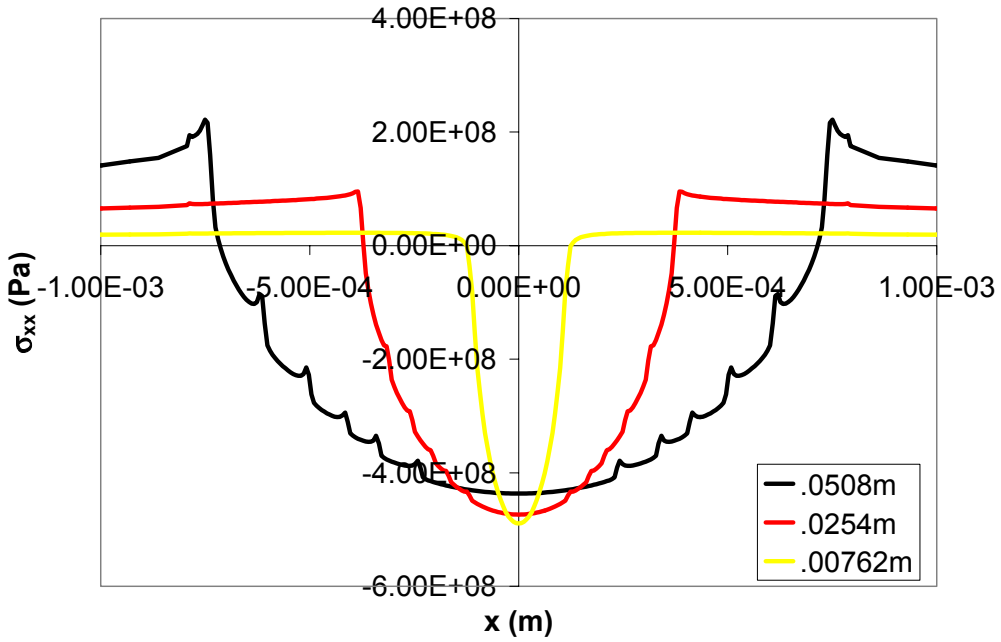

Figure 4.5 P-only Sxx Distributions of 3 Tests with Different Radii Fretting Pads.

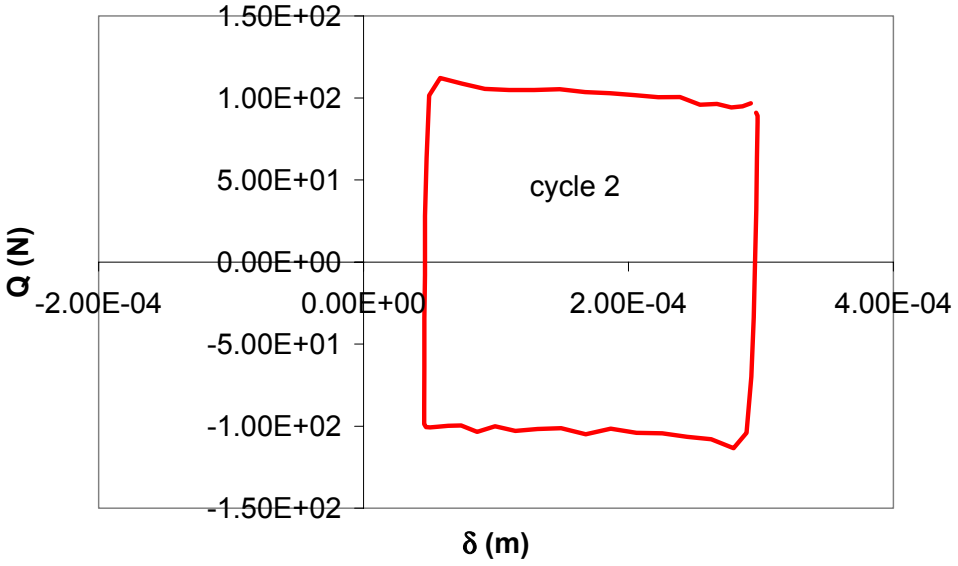

Figure 4.6 Hysteresis Loop for Test Using 5.08 mm Radius Fretting Pads: Cycle 2

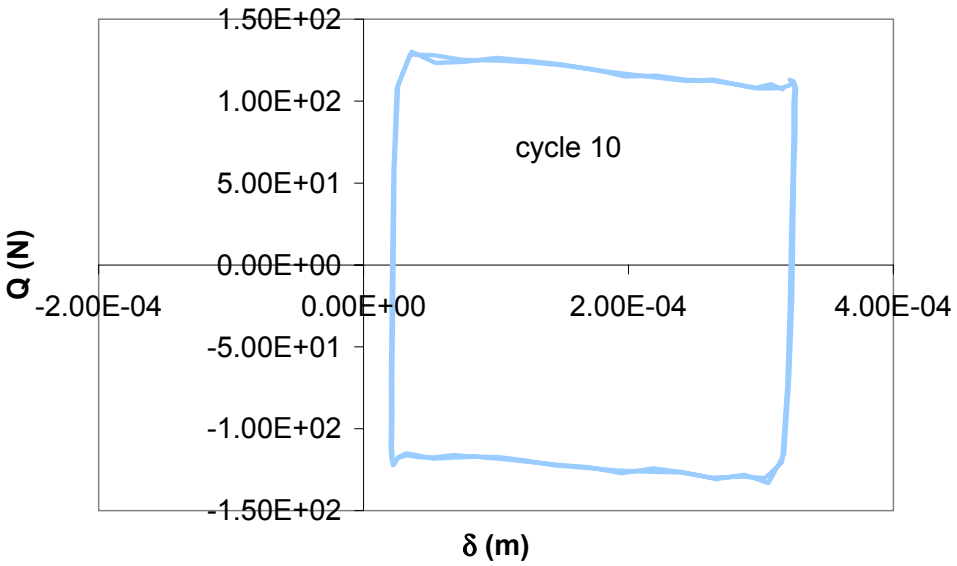

Figure 4.7 Hysteresis Loop for Test Using 5.08 mm Radius Fretting Pads: Cycle 10

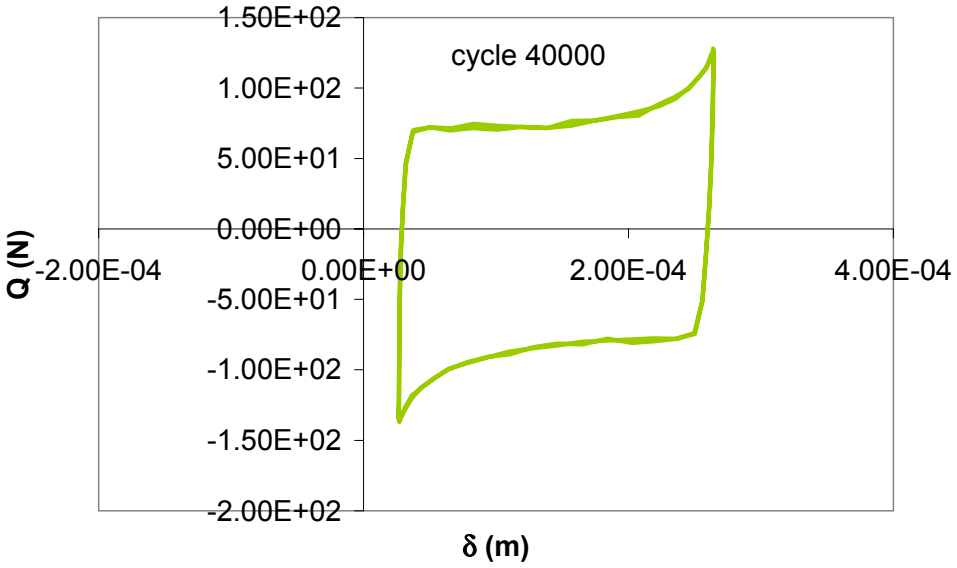

Figure 4.8 Hysteresis Loop for Test Using 5.08 mm Radius Fretting Pads: Cycle 40000

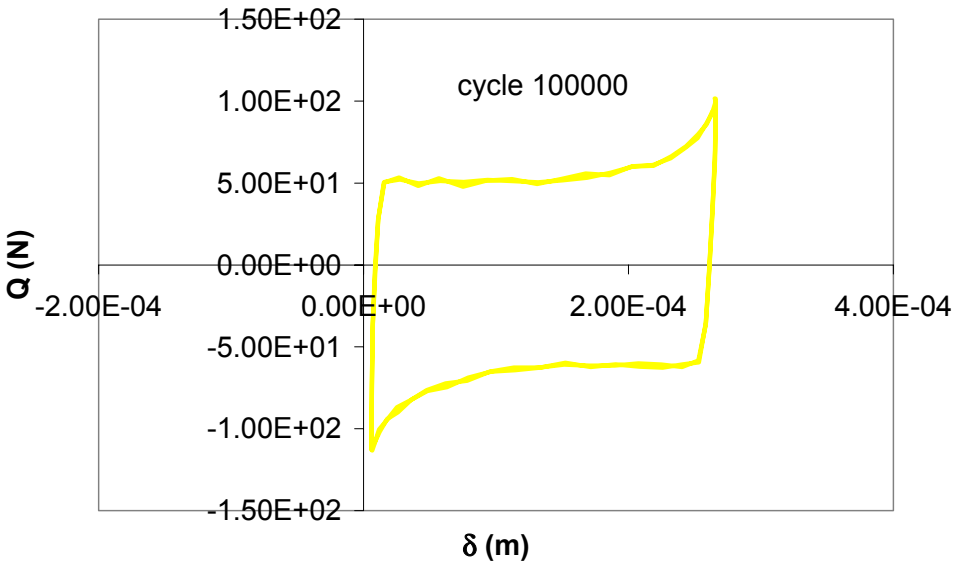

Figure 4.9 Hysteresis Loop for Test Using 5.08 mm Radius Fretting Pads: Cycle 100000

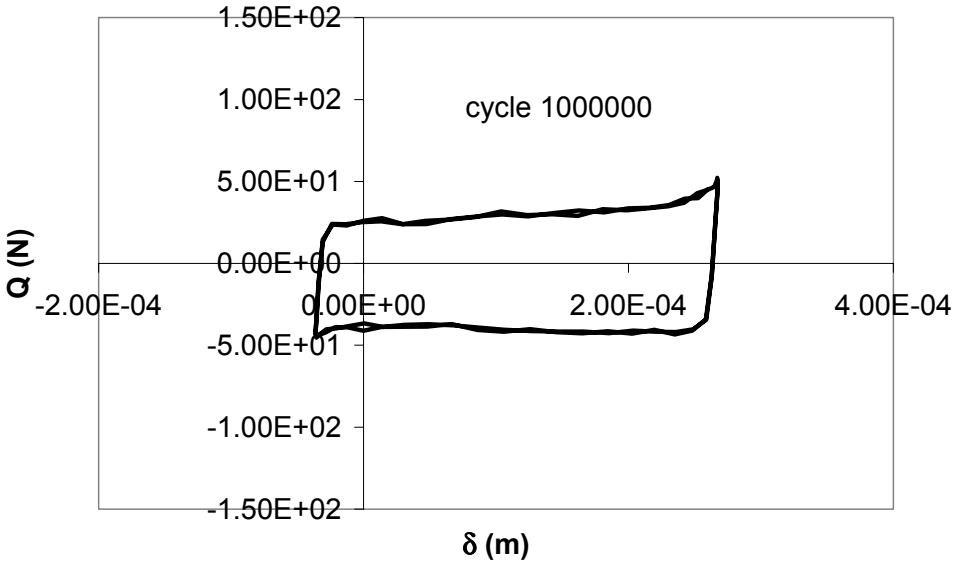

Figure 4.10 Hysteresis Loop for Test Using 5.08 mm Radius Fretting Pads: Cycle 1000000

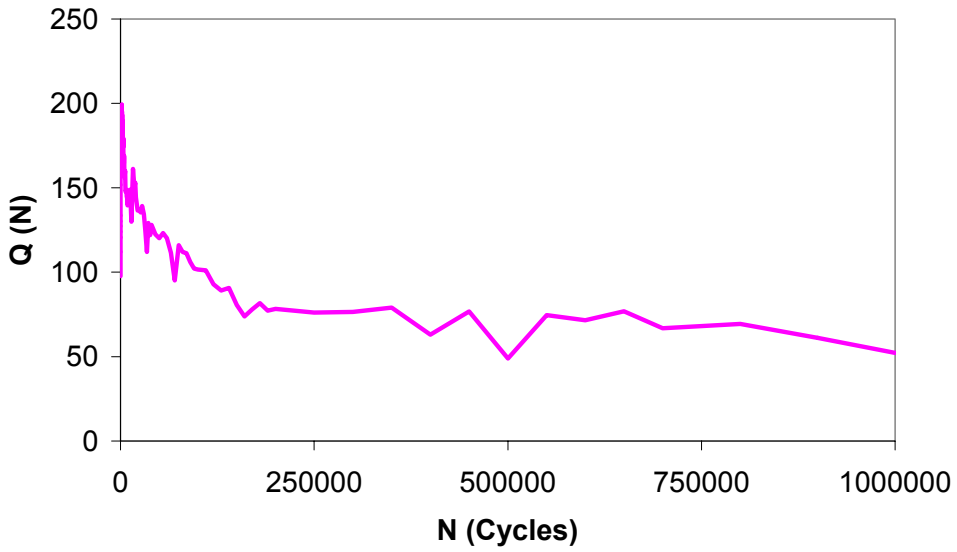

Figure 4.11 Q versus Cycle Curve for Test Using 5.08 mm Radius Fretting Pads

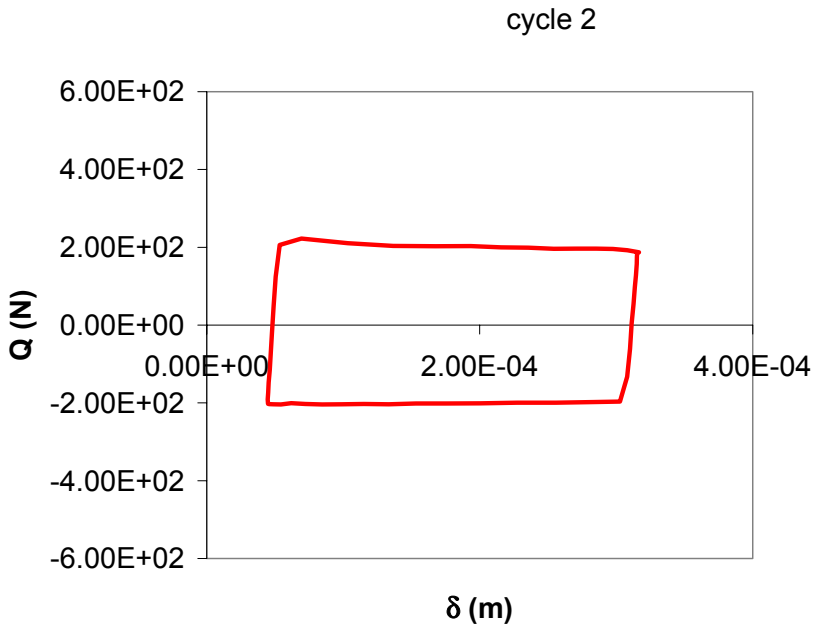

Figure 4.12 Hysteresis Loop for Test Using 7.62 mm Radius Fretting Pads: Cycle 2

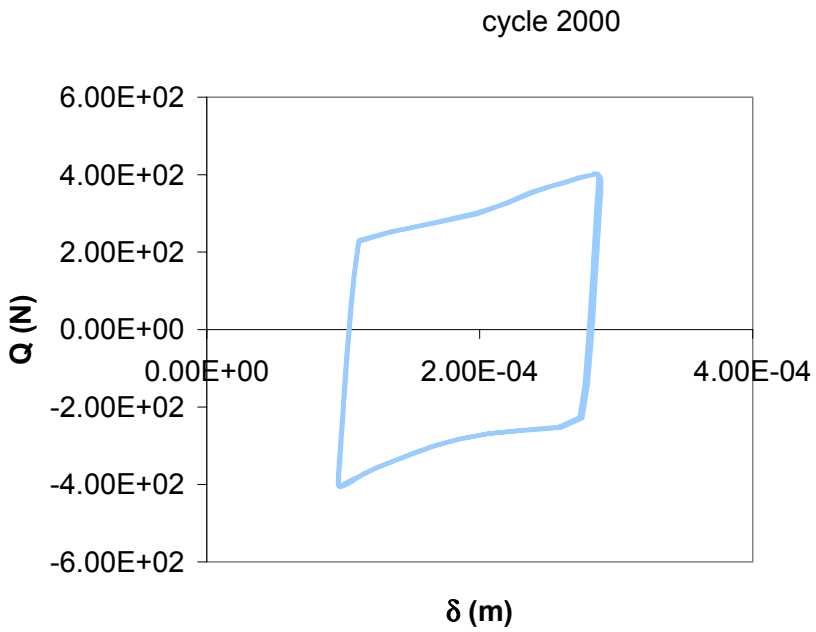

Figure 4.13 Hysteresis Loop for Test Using 7.62 mm Radius Fretting Pads: Cycle 2000

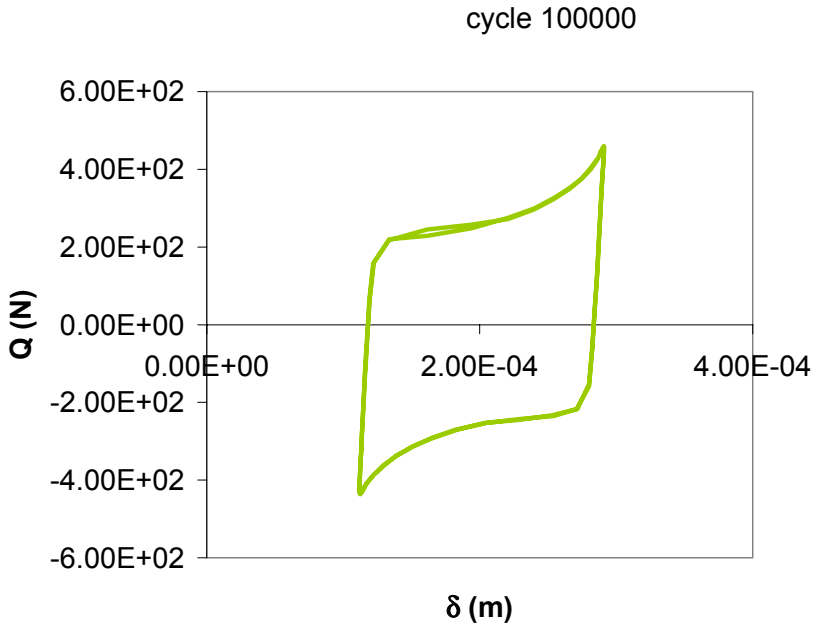

Figure 4.14 Hysteresis Loop for Test Using 7.62 mm Radius Fretting Pads: Cycle 100000

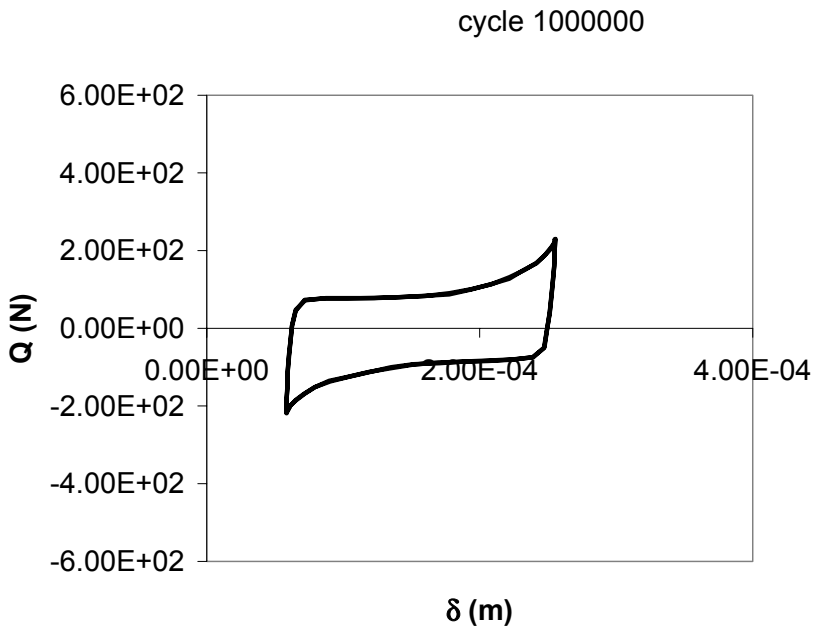

Figure 4.15 Hysteresis Loop for Test Using 7.62 mm Radius Fretting Pads: Cycle 1000000

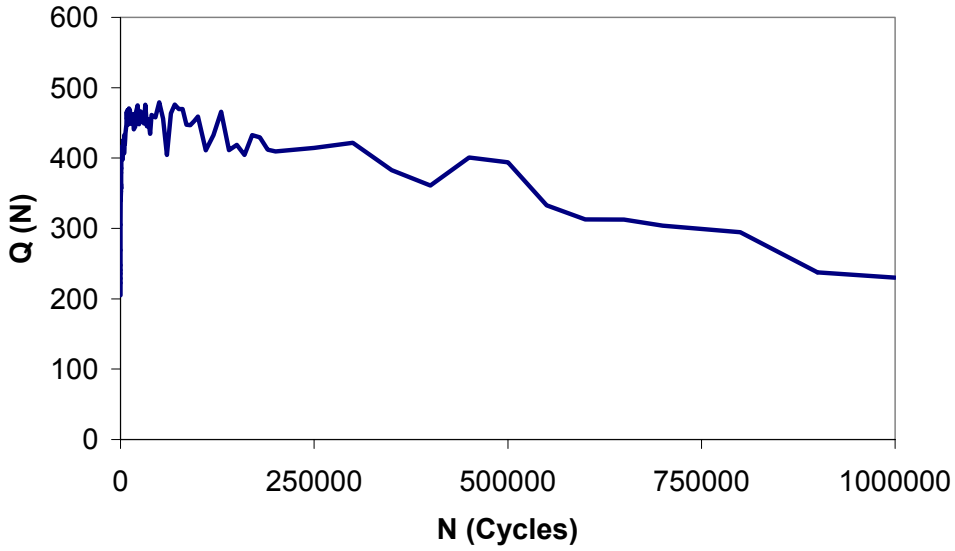

Figure 4.16 Q versus Cycle Curve for Test Using 7.62 mm Radius Fretting Pads

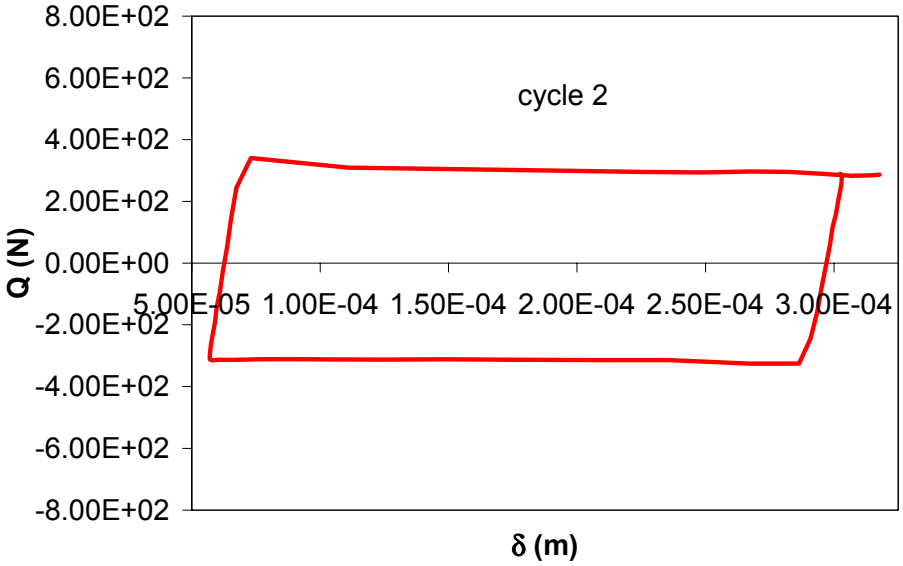

Figure 4.17 Hysteresis Loop for Test Using 10.16 mm Radius Fretting Pads: Cycle 2

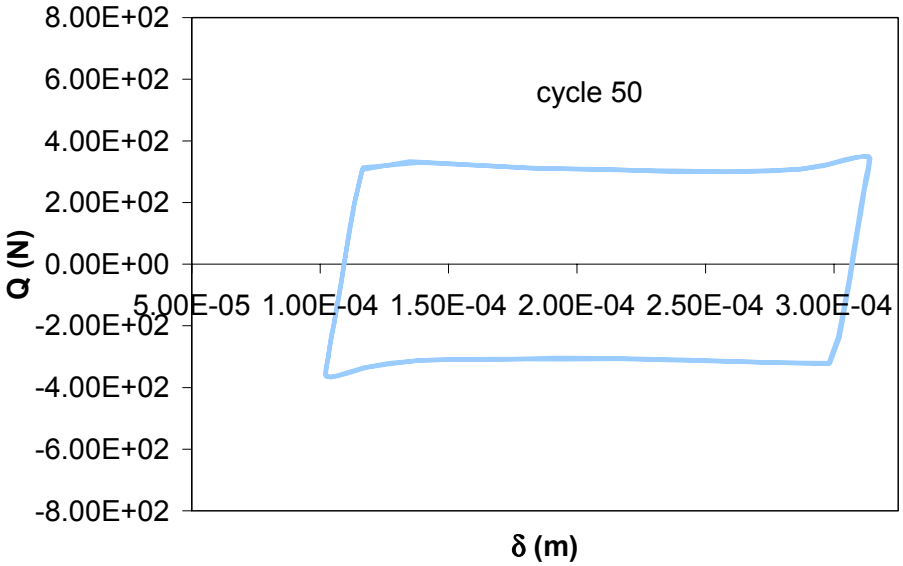

Figure 4.18 Hysteresis Loop for Test Using 10.16 mm Radius Fretting Pads: Cycle 50

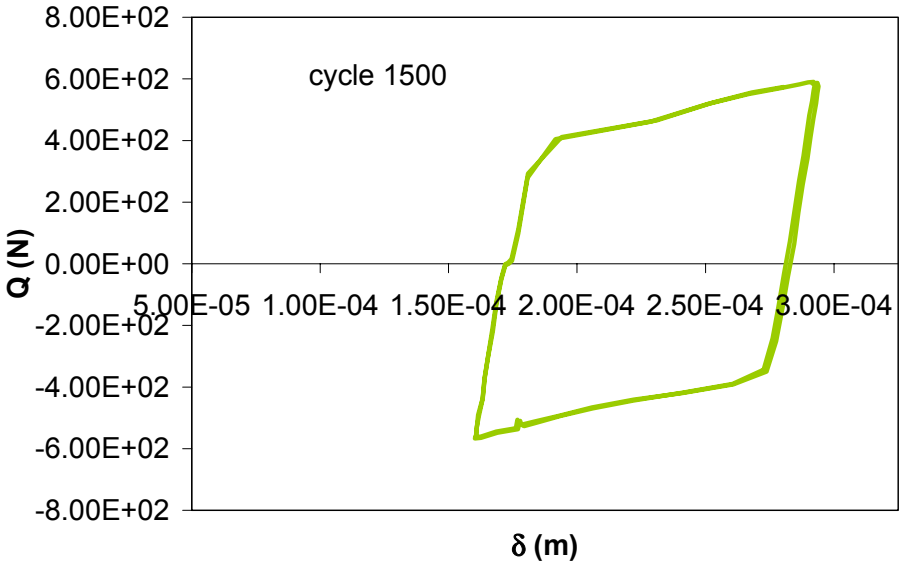

Figure 4.19 Hysteresis Loop for Test Using 10.16 mm Radius Fretting Pads: Cycle 1500

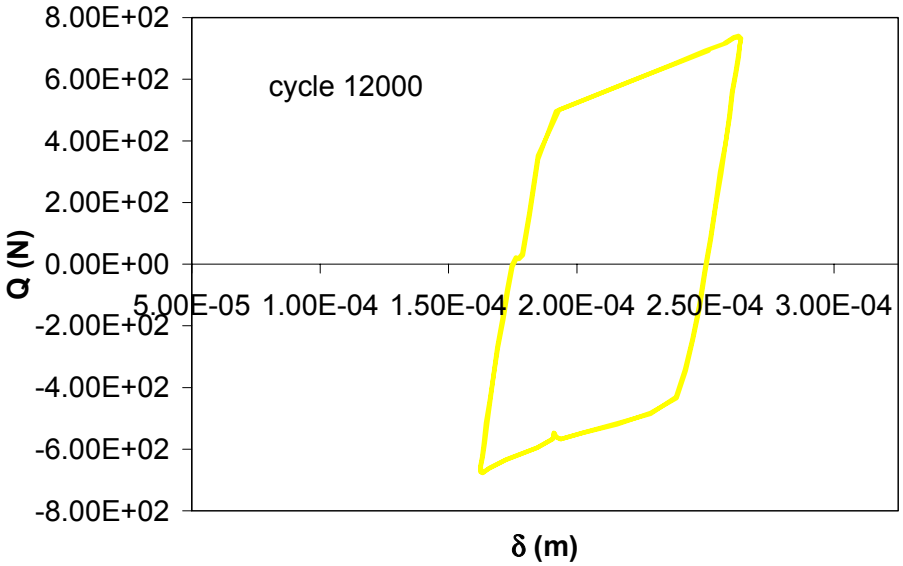

Figure 4.20 Hysteresis Loop for Test Using 10.16 mm Radius Fretting Pads: Cycle 12000

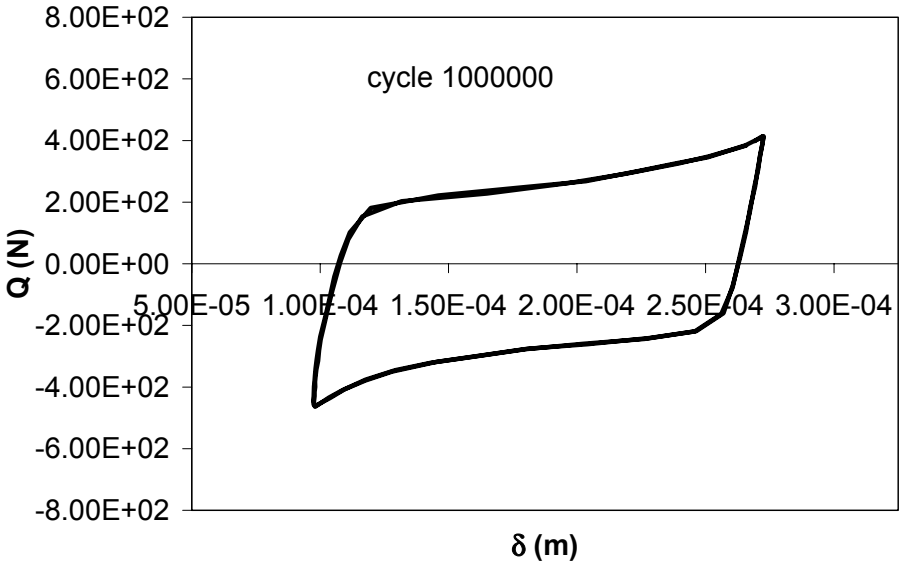

Figure 4.21 Hysteresis Loop for Test Using 10.16 mm Radius Fretting Pads: Cycle 1000000

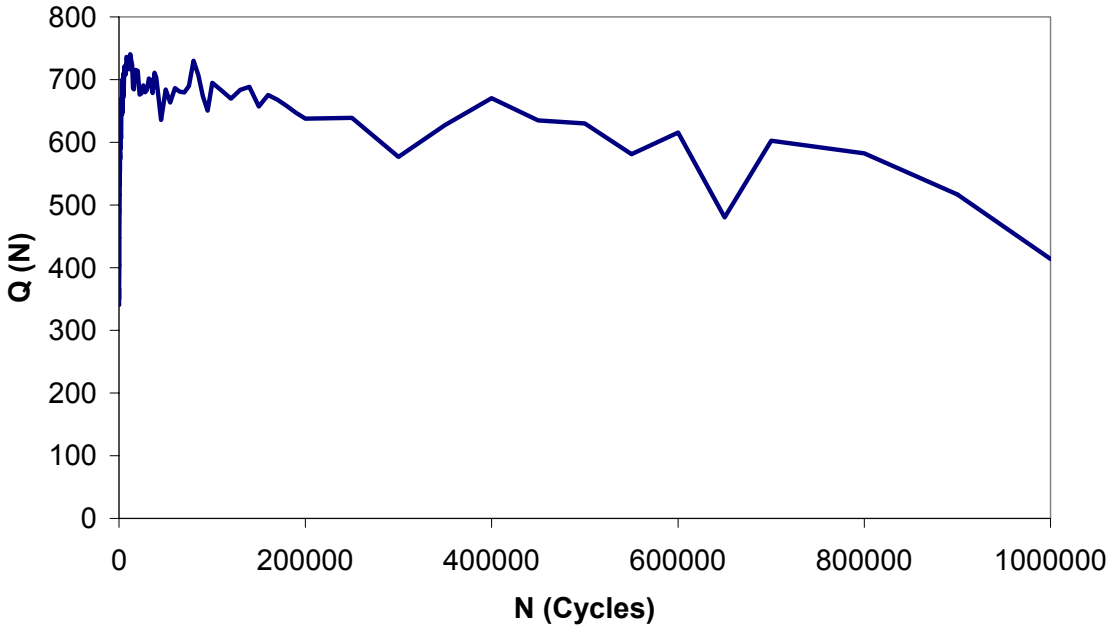

Figure 4.22 Q versus Cycle Curve for Test Using 10.16 mm Radius Fretting Pads

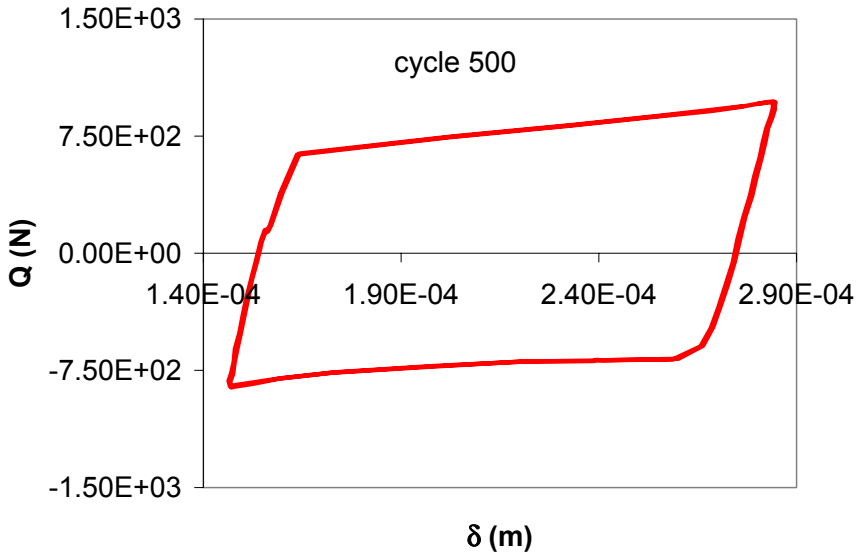

Figure 4.23 Hysteresis Loop for Test Using 19.05 mm Radius Fretting Pads: Cycle 500

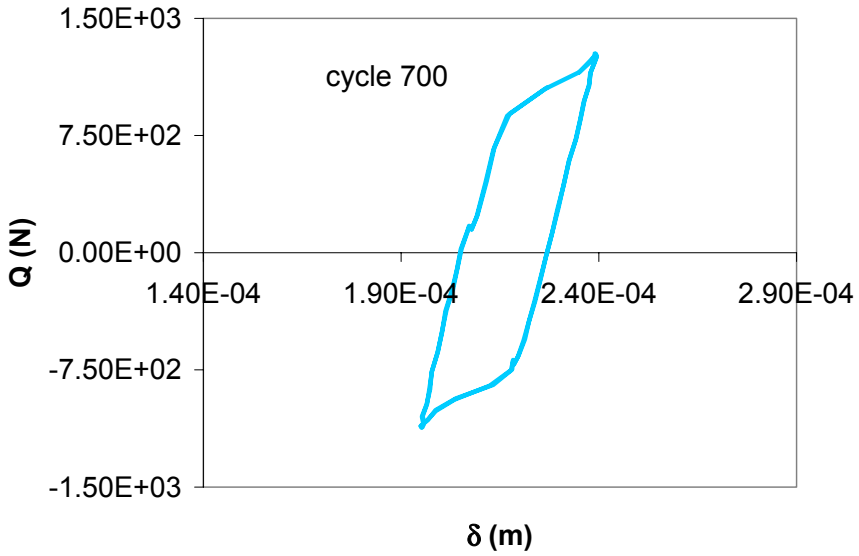

Figure 4.24 Hysteresis Loop for Test Using 19.05 mm Radius Fretting Pads: Cycle 700

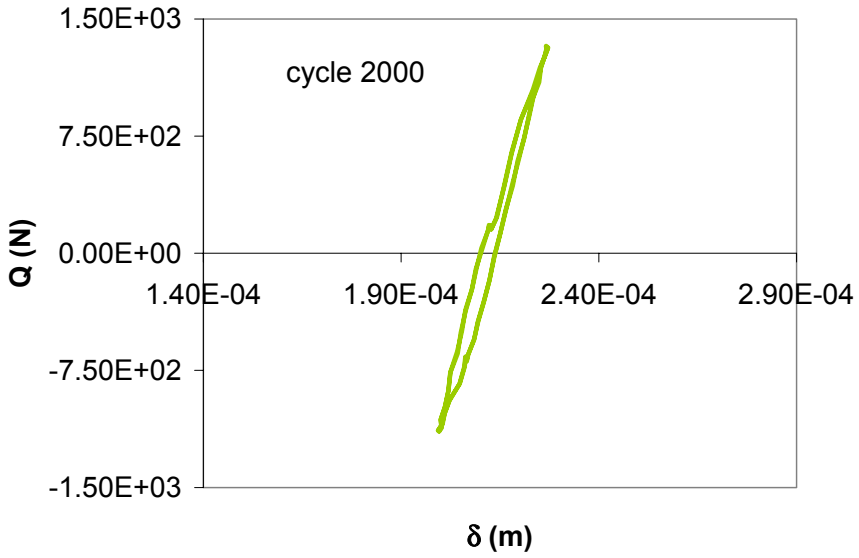

Figure 4.25 Hysteresis Loop for Test Using 19.05 mm Radius Fretting Pads: Cycle 2000

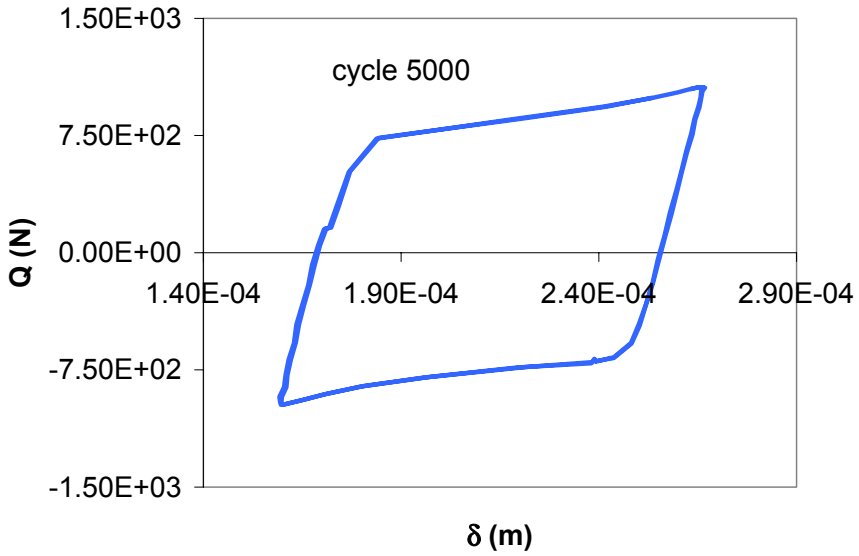

Figure 4.26 Hysteresis Loop for Test Using 19.05 mm Radius Fretting Pads: Cycle 5000

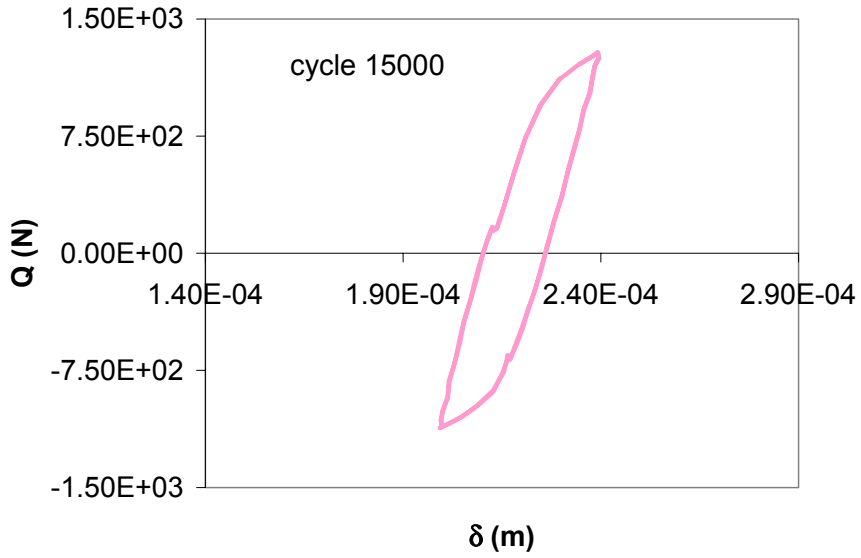

Figure 4.27 Hysteresis Loop for Test Using 19.05 mm Radius Fretting Pads: Cycle 15000

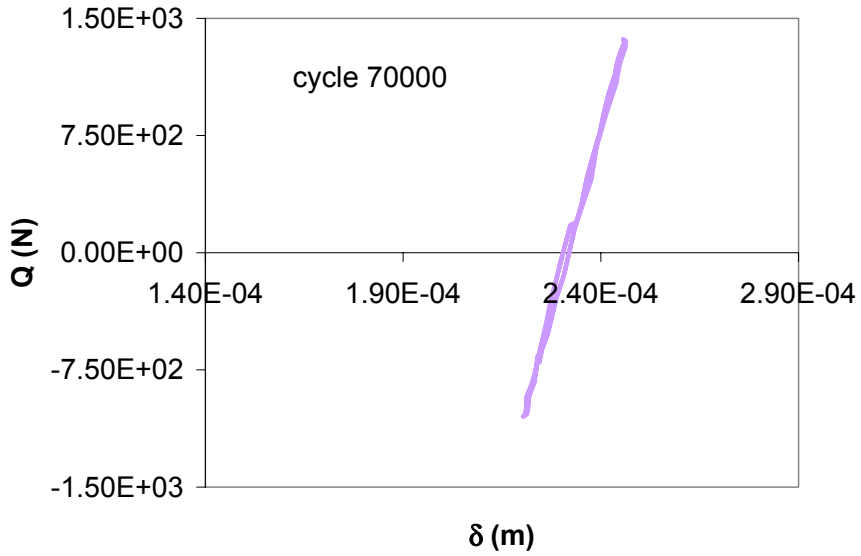

Figure 4.28 Hysteresis Loop for Test Using 19.05 mm Radius Fretting Pads: Cycle 70000

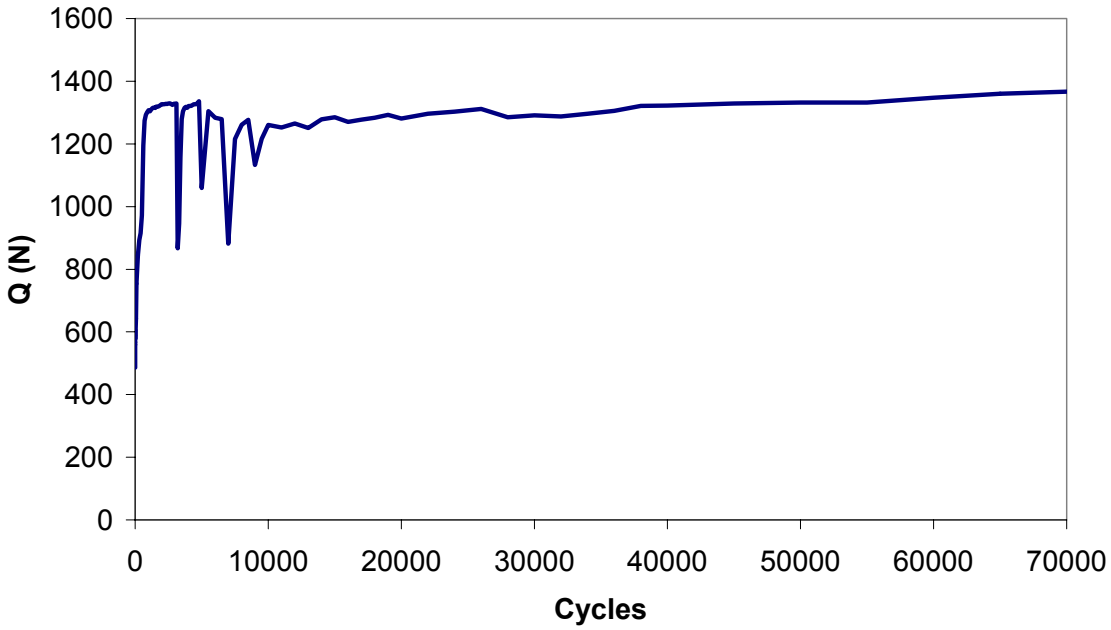

Figure 4.29 Q versus Cycle Curve for Test Using 19.05 mm Radius Fretting Pads

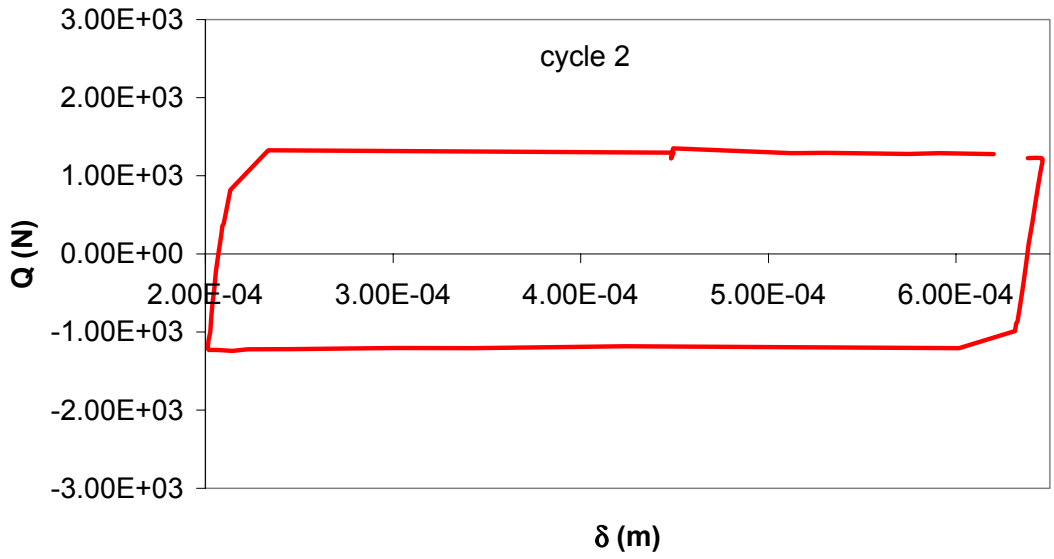

Figure 4.30 Hysteresis Loop for Test Using 44.45 mm Radius Fretting Pads: Cycle 2

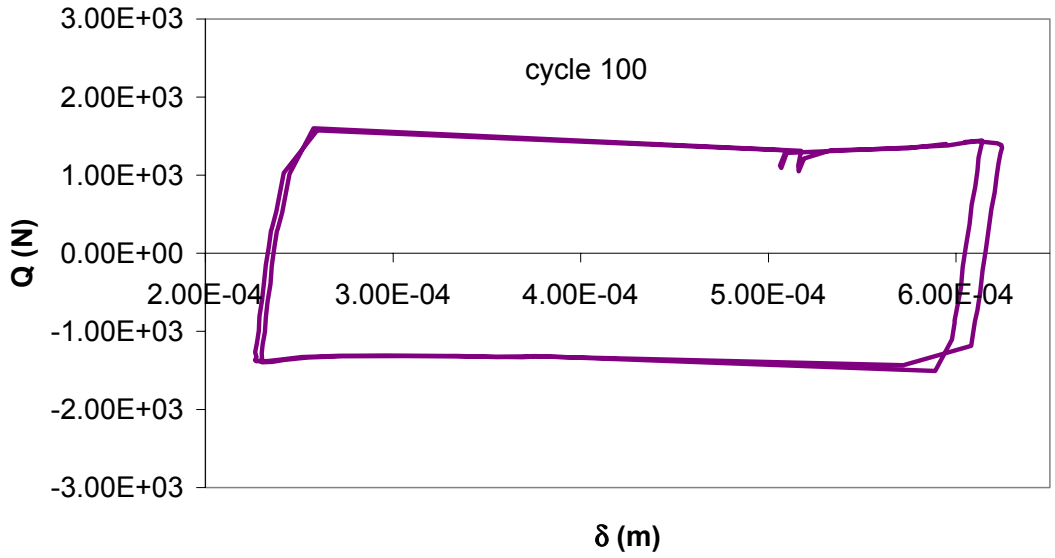

Figure 4.31 Hysteresis Loop for Test Using 44.45 mm Radius Fretting Pads: Cycle 100

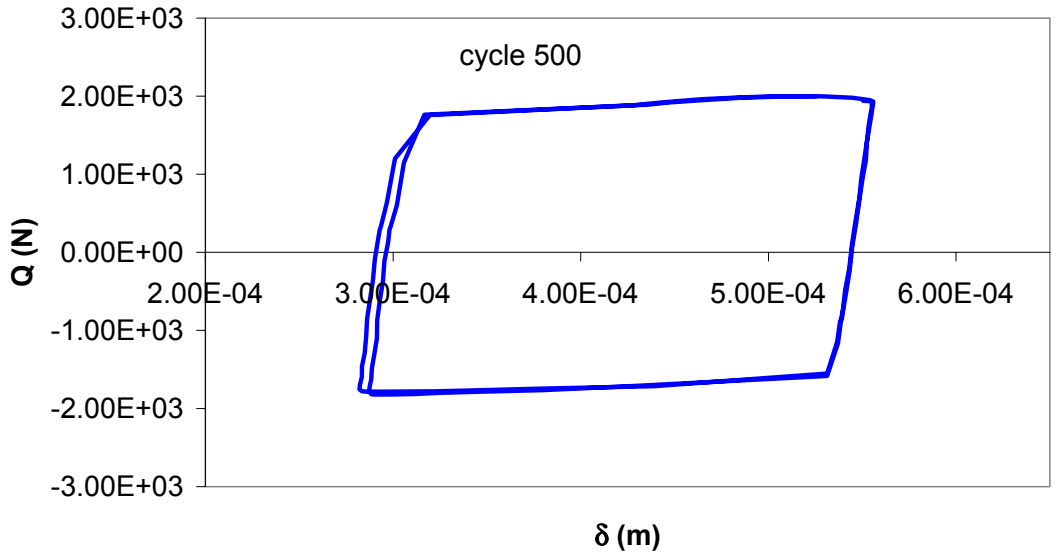

Figure 4.32 Hysteresis Loop for Test Using 44.45 mm Radius Fretting Pads: Cycle 500

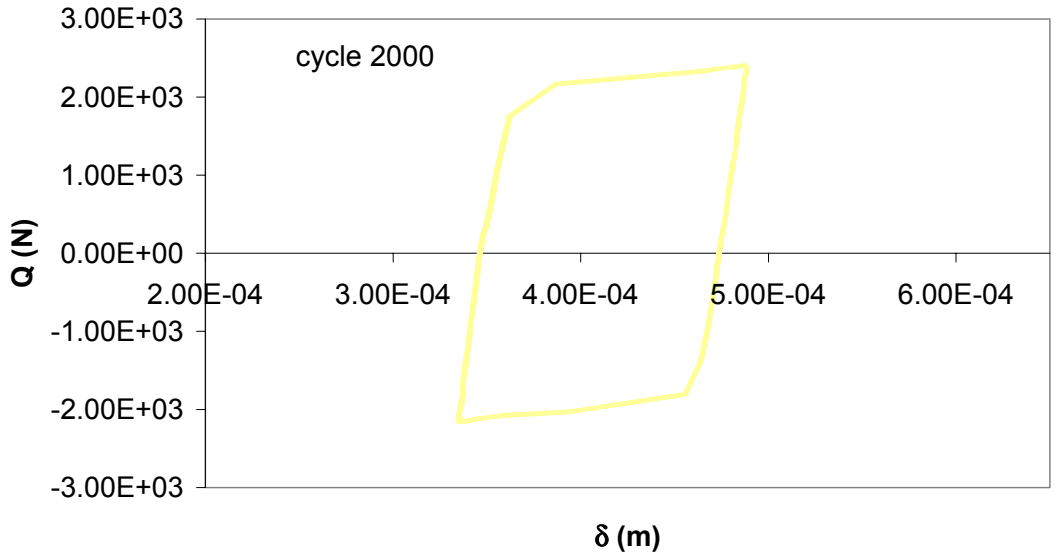

Figure 4.33 Hysteresis Loop for Test Using 44.45 mm Radius Fretting Pads: Cycle 2000

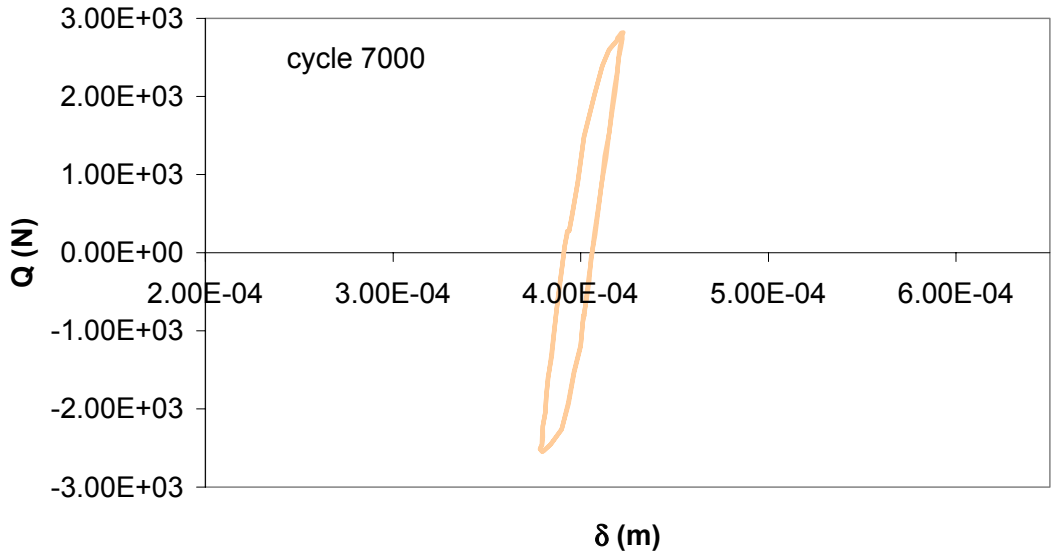

Figure 4.34 Hysteresis Loop for Test Using 44.45 mm Radius Fretting Pads: Cycle 7000

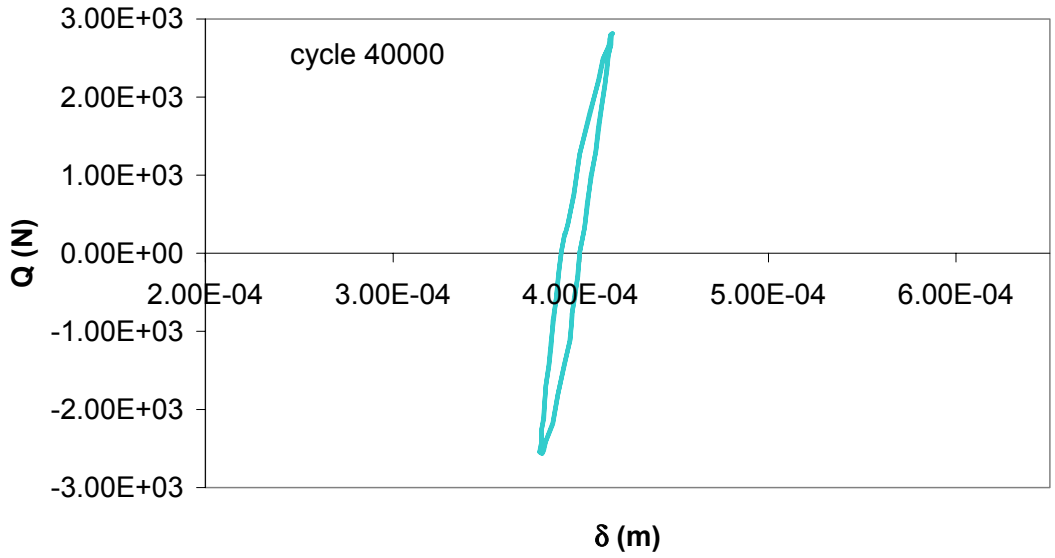

Figure 4.35 Hysteresis Loop for Test Using 44.45 mm Radius Fretting Pads: Cycle 40000

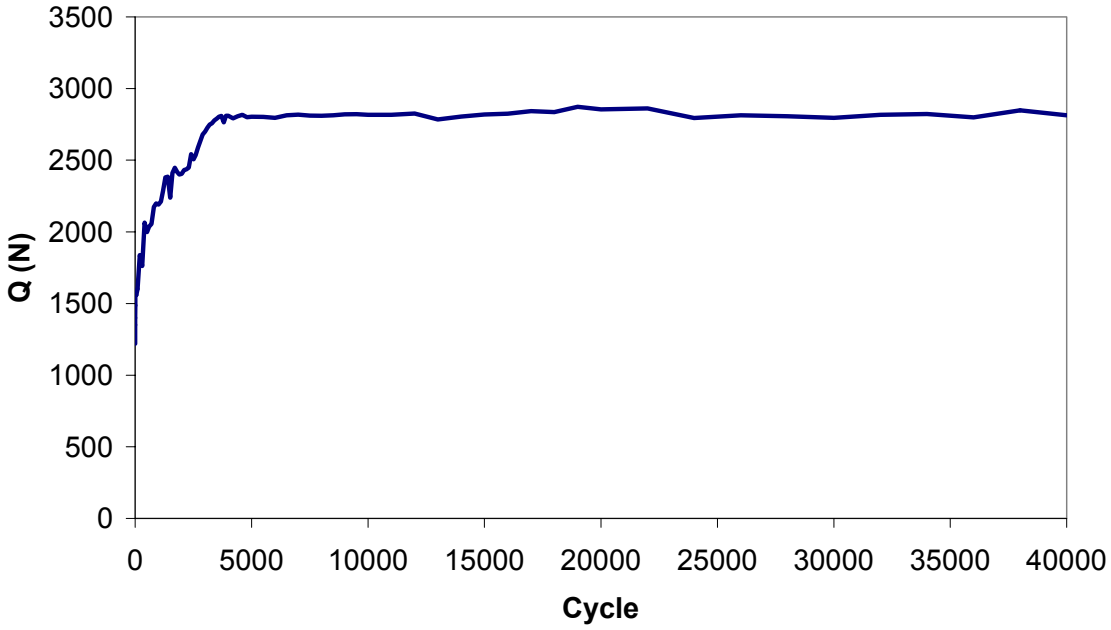

Figure 4.36 Q versus Cycle Curve for Test Using 44.45 mm Radius Fretting Pads

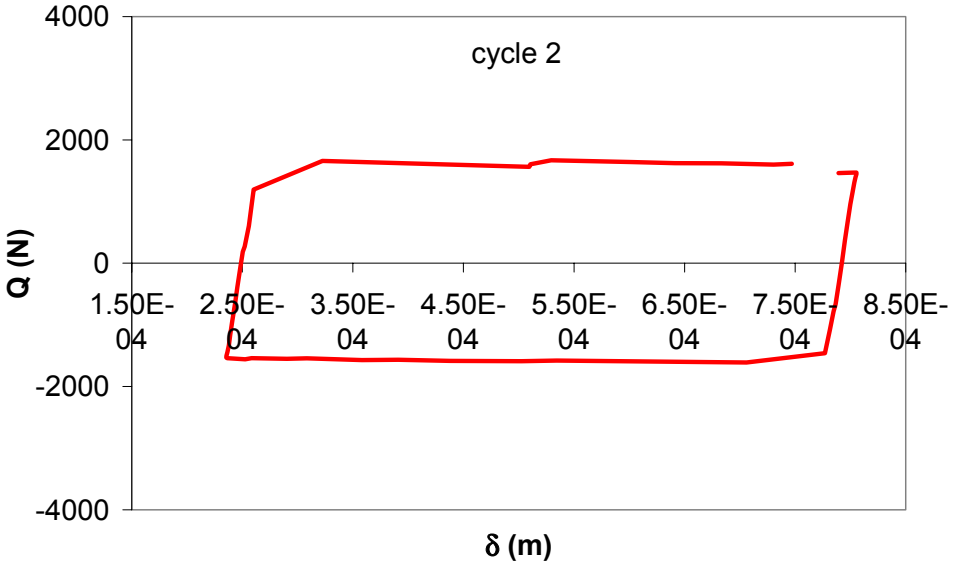

Figure 4.37 Hysteresis Loop for Test Using 50.8 mm Radius Fretting Pads: Cycle 2

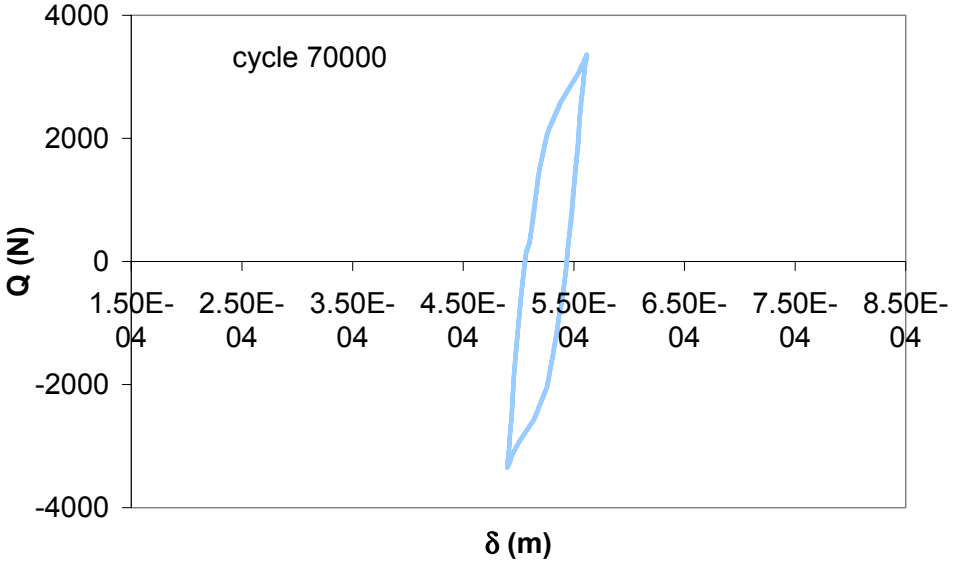

Figure 4.38 Hysteresis Loop for Test Using 50.8 mm Radius Fretting Pads: Cycle 70000

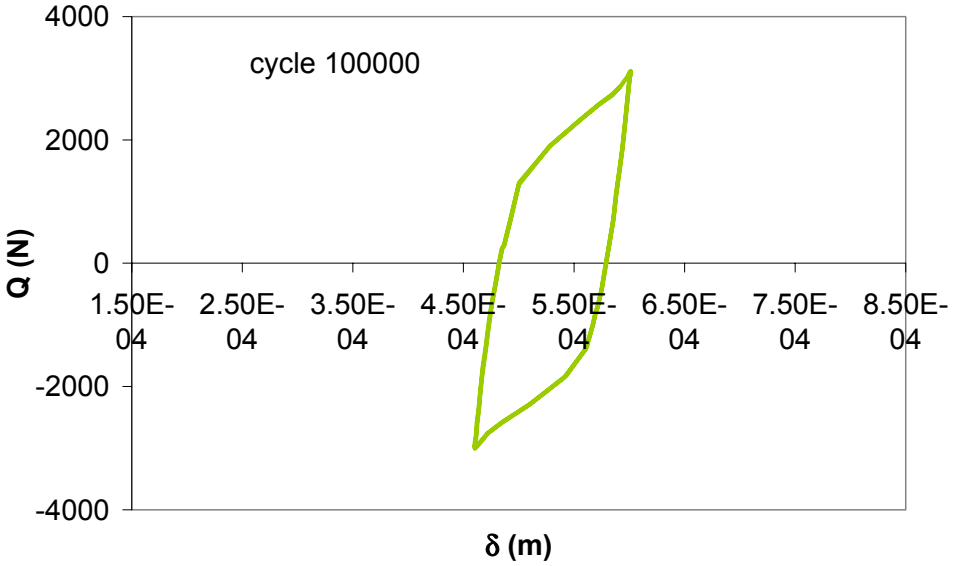

Figure 4.39 Hysteresis Loop for Test Using 50.8 mm Radius Fretting Pads: Cycle 100000

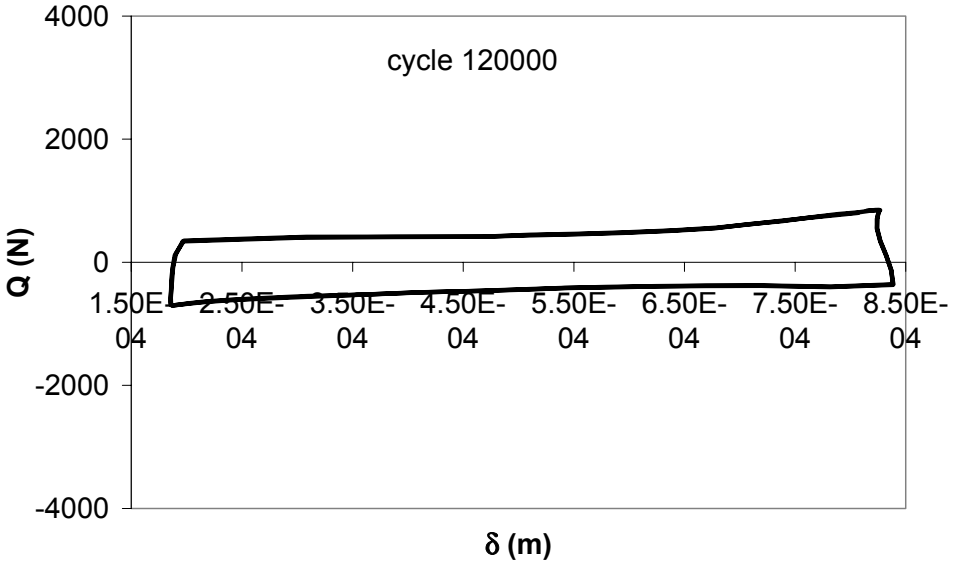

Figure 4.40 Hysteresis Loop for Test Using 50.8 mm Radius Fretting Pads: Cycle 120000

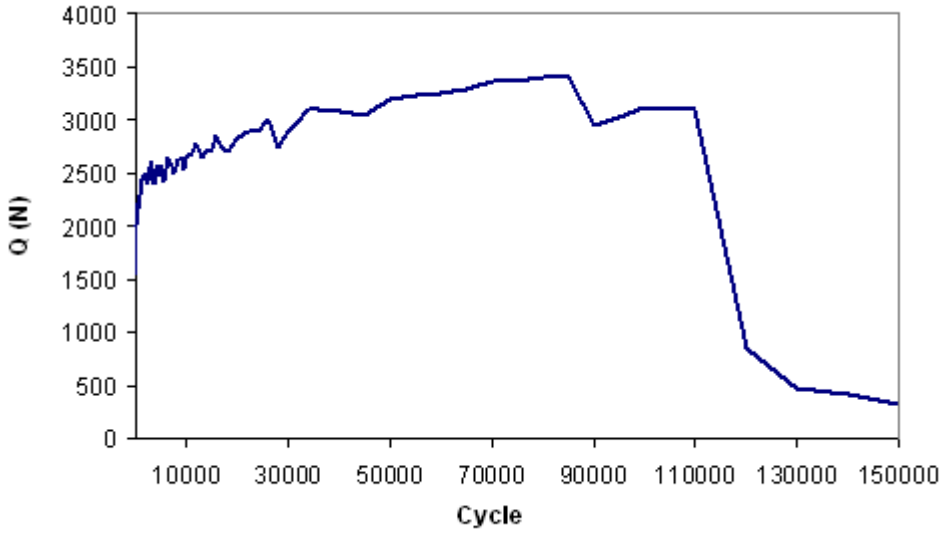

Figure 4.41 Q versus Cycle Curve for Test Using 50.8 mm Radius Fretting Pads

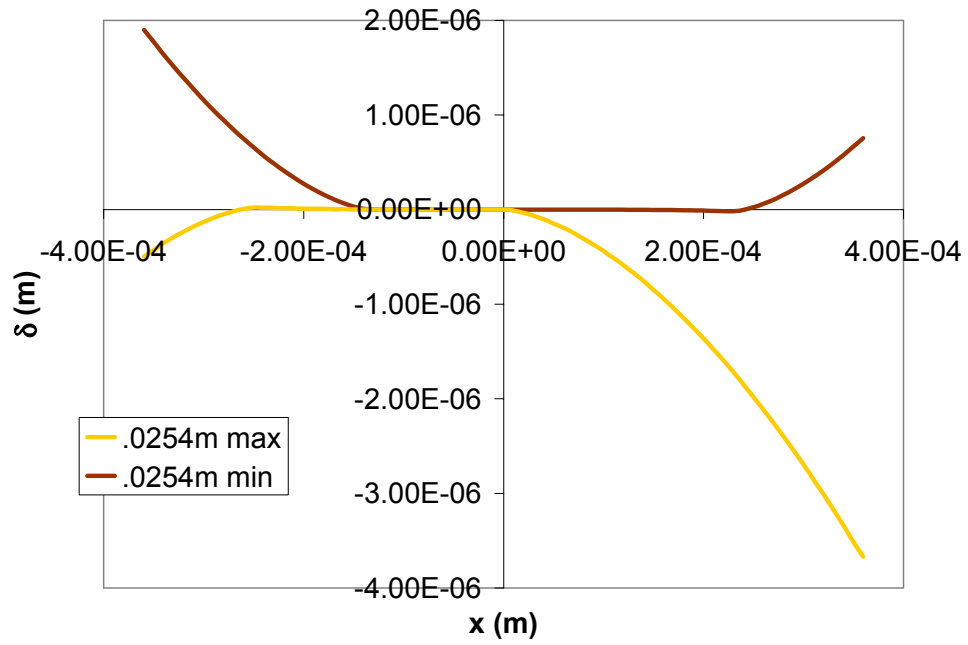

Figure 4.42 Slip Amplitude of Points in the Contact Region of the 25.4 mm Pad Radius Test Case For Minimum and Maximum Combined Loading Conditions

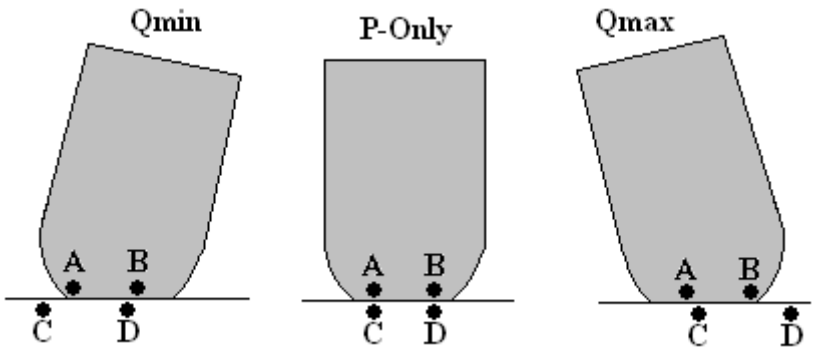

Figure 4.43 Three Loading Conditions Illustrating Slip Between Pad and Substrate

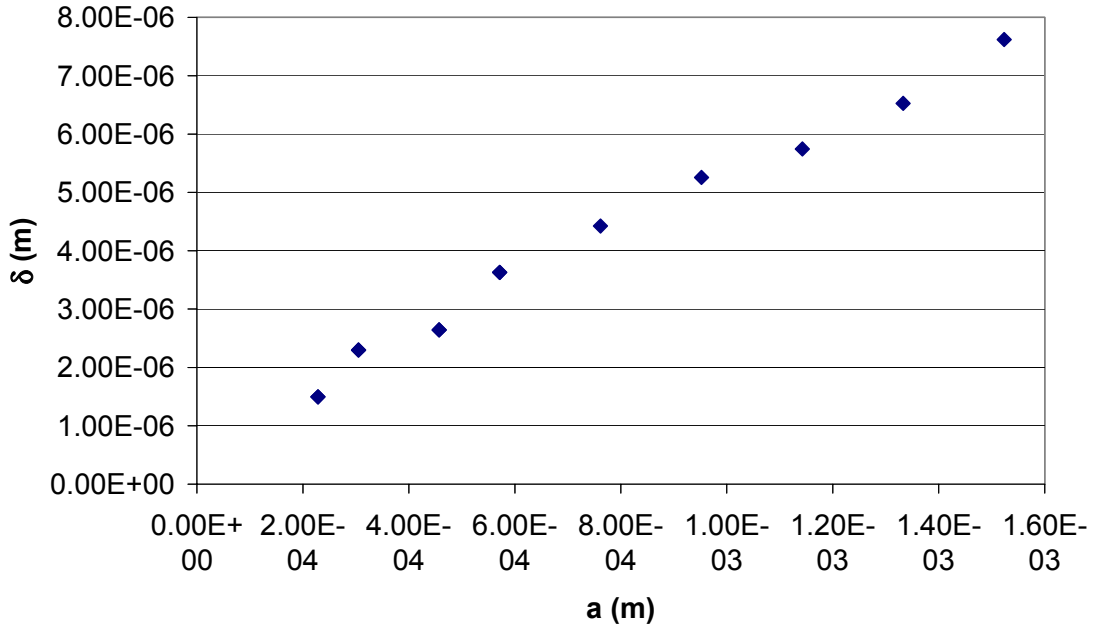

Figure 4.44 Maximum Slip Range for 9 Different Radii Tests from FEA Analysis

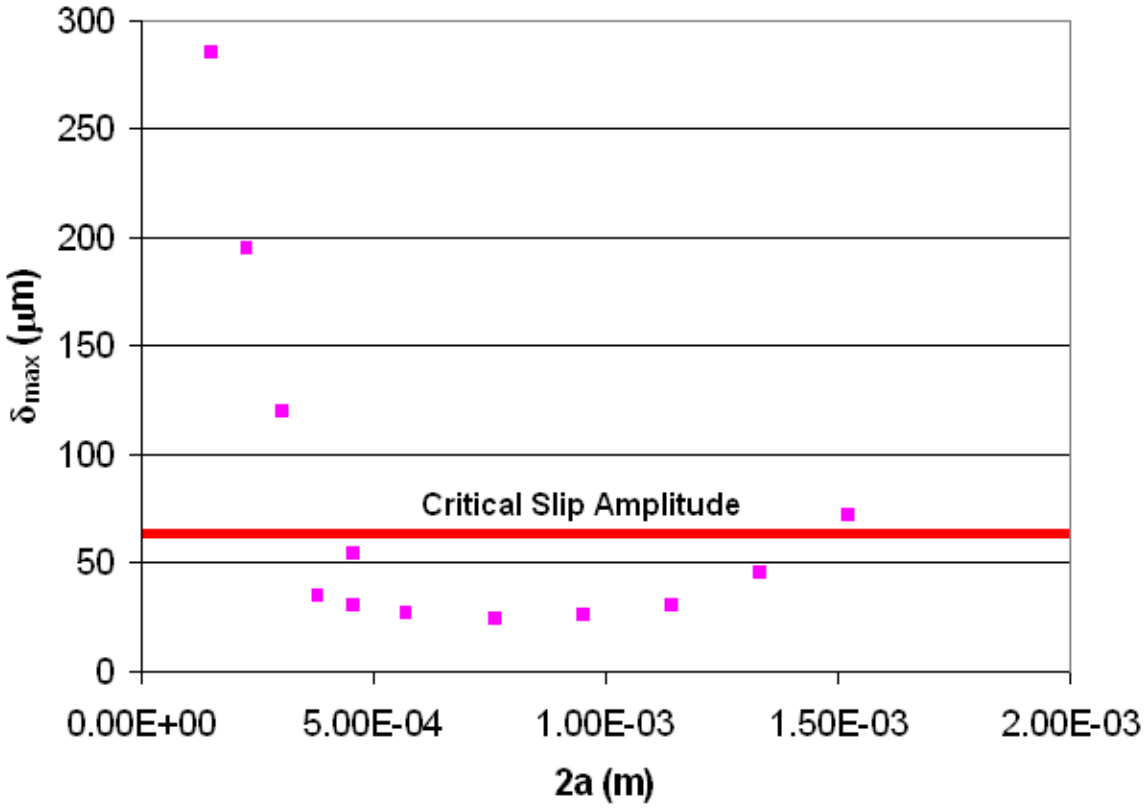

Figure 4.45 Maximum Slip Range for 12 Different Radii Tests from Experimental Analysis

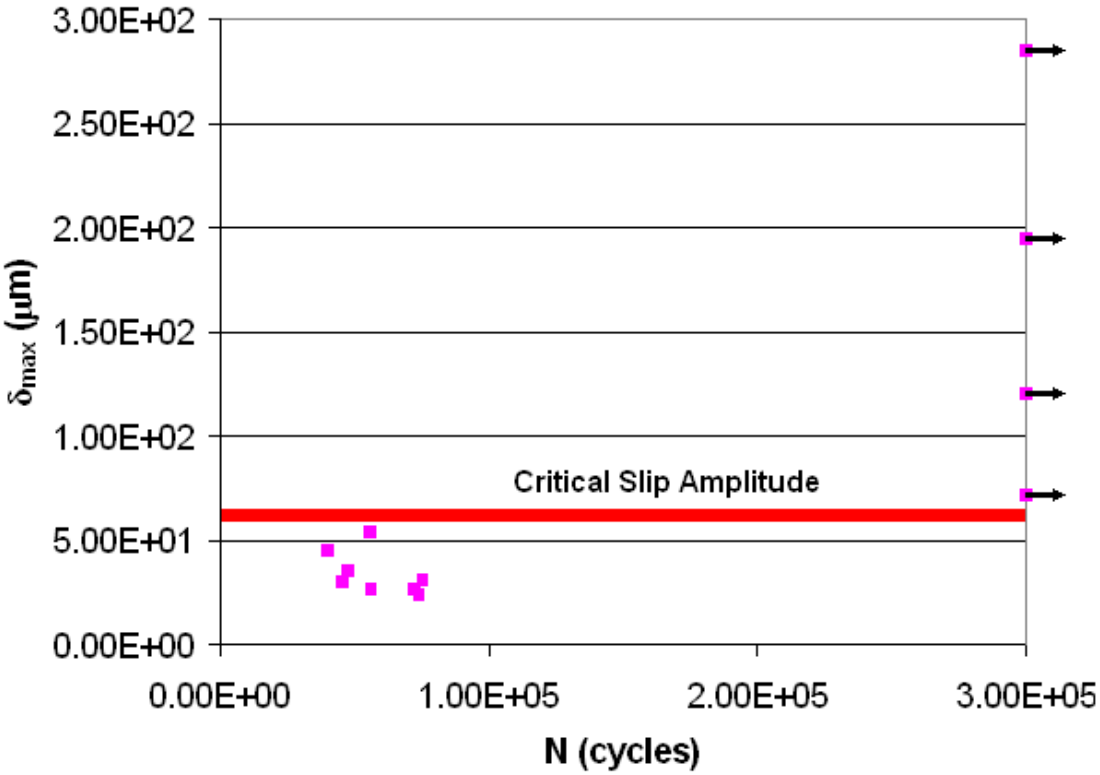

Figure 4.46 Maximum Slip Range Versus Life to Failure from Experimental Analysis

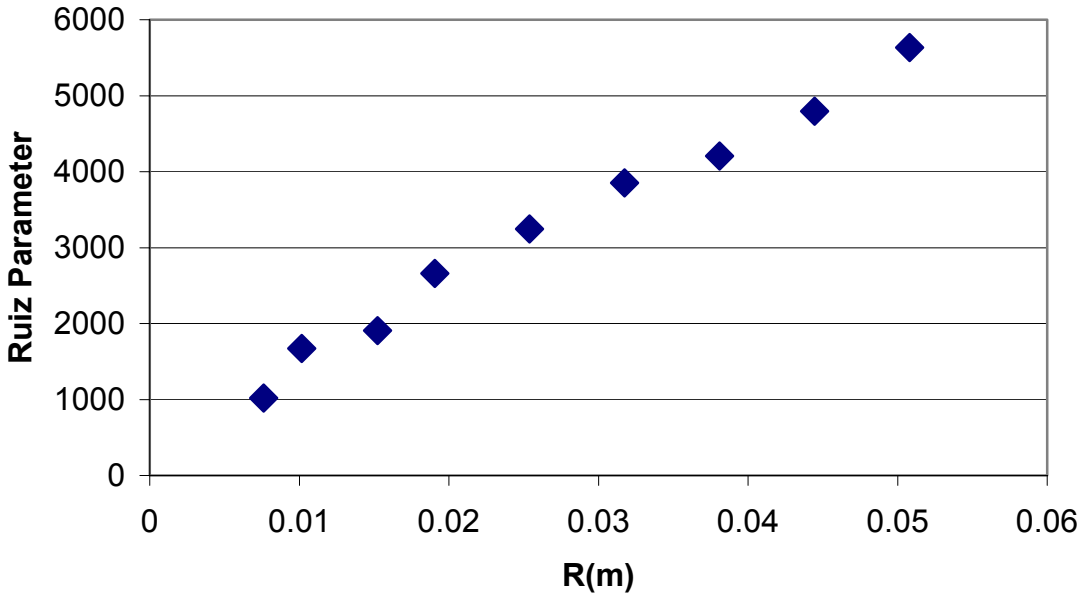

Figure 4.47 Maximum Values of the F1 Ruiz Parameter, $\delta\tau$, for the Different Radii Analyzed by Finite Element Method

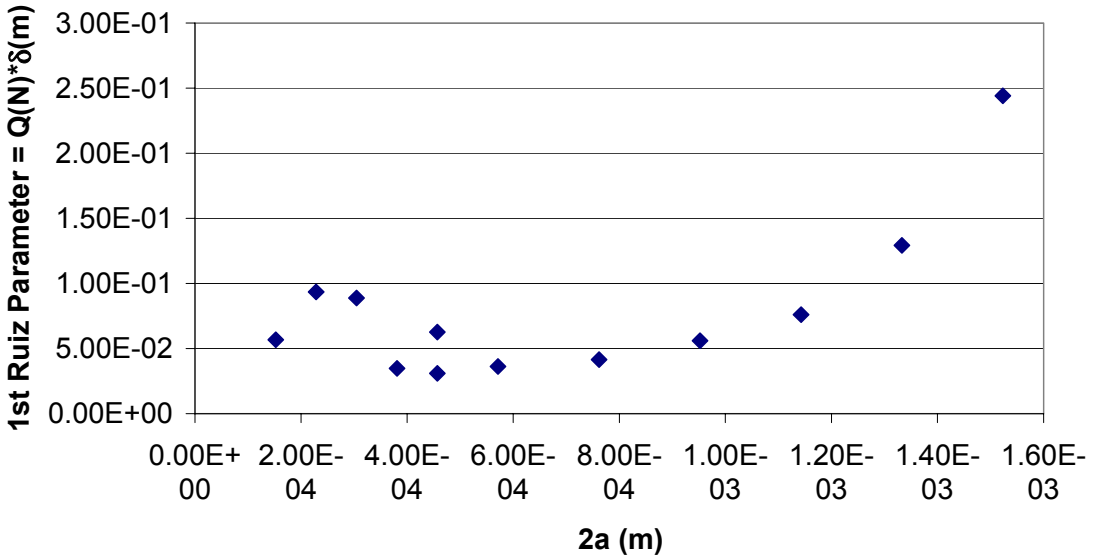

Figure 4.48 Maximum Values of F_1 Ruiz Parameter, with max δ and max Q (Both from the Experimental Test Output) Versus Contact Width

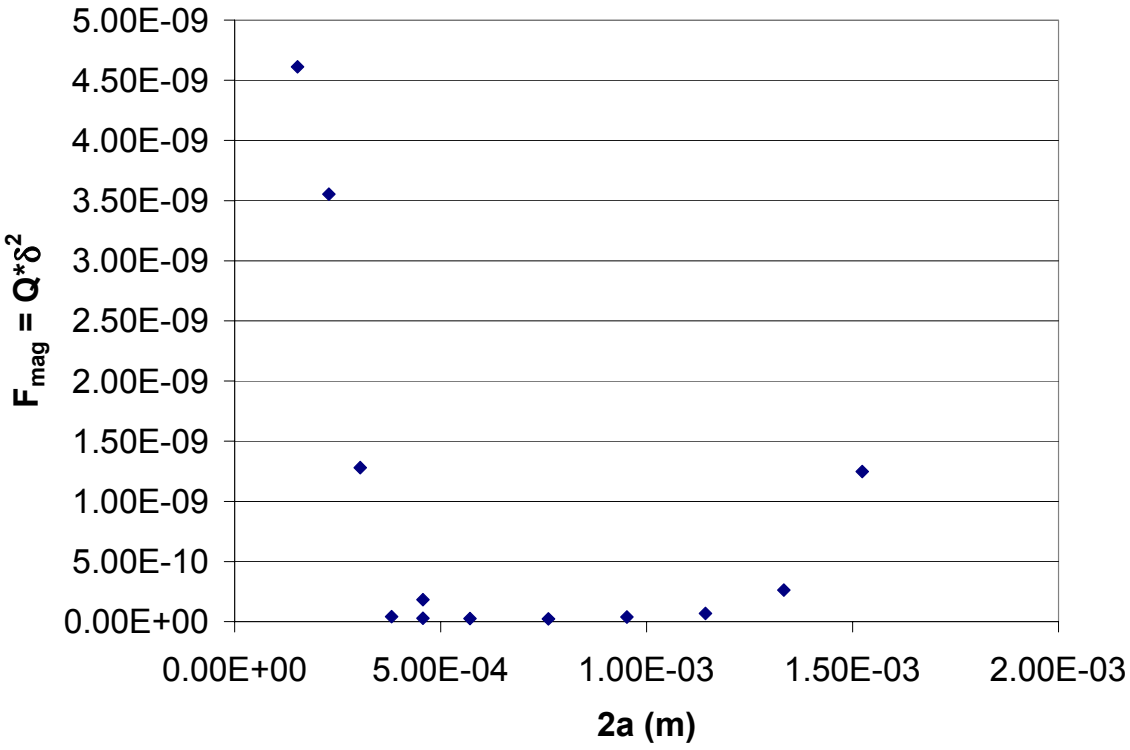

Figure 4.49 Maximum Values of Modified Ruiz Parameter Versus Contact Width

Table 4.1 Table of Experimental Results

	Radius (m)	$2a_{theo}$ (m)	P(N)	Q_{max}(N)	Q/P	N_f (cycles)
1	5.080E-02	1.523E-03	4.003E+03	3.345E+03	8.355E-01	300000+
2	4.445E-02	1.333E-03	3.503E+03	2.816E+03	8.039E-01	40500
3	3.810E-02	1.143E-03	3.003E+03	2.400E+03	7.993E-01	46000
4	3.175E-02	9.521E-04	2.502E+03	2.050E+03	8.193E-01	56500
5	2.540E-02	7.617E-04	2.002E+03	1.687E+03	8.426E-01	74200
6	1.905E-02	5.713E-04	1.501E+03	1.306E+03	8.698E-01	72800
7	1.524E-02	4.570E-04	1.201E+03	1.126E+03	9.374E-01	56200
8	1.524E-02	4.570E-04	1.201E+03	9.998E+02	8.324E-01	75600
9	1.270E-02	3.809E-04	1.001E+03	9.426E+02	9.418E-01	48000
10	1.016E-02	3.047E-04	8.007E+02	7.287E+02	9.101E-01	300000+
11	7.620E-03	2.285E-04	6.005E+02	4.479E+02	7.459E-01	300000+
12	5.080E-03	1.523E-04	4.003E+02	7.646E+01	1.910E-01	300000+

Table 4.2 Summary of Maximum Critical Plane Based Fatigue Predictive Parameters Determined From FEA Output

FEA:								
R (m)	$2a_{theo}$ (m)	SWT2 (MPa)	SWT1 (MPa)	SSR (MPa)	teff (MPa)	MSSR	(MPa)	N (cycles)
5.08E-03	1.52E-04							1.00E+06
7.62E-03	2.29E-04	9.90E+00	9.88E+00	1.05E+03	8.21E+02	4.04E+01	7.96E+02	1.00E+06
1.02E-02	3.05E-04	1.17E+01	1.17E+01	1.12E+03	8.73E+02	4.06E+01	8.56E+02	1.00E+06
1.27E-02	3.81E-04							4.80E+04
1.52E-02	4.57E-04	1.07E+01	1.07E+01	1.02E+03	8.36E+02	3.67E+01	8.14E+02	7.56E+04
1.91E-02	5.71E-04	1.17E+01	1.17E+01	1.08E+03	8.62E+02	4.16E+01	8.49E+02	7.28E+04
2.54E-02	7.62E-04	1.17E+01	1.17E+01	1.04E+03	8.48E+02	4.23E+01	8.46E+02	7.42E+04
3.18E-02	9.52E-04	1.16E+01	1.15E+01	1.02E+03	8.36E+02	4.21E+01	8.41E+02	5.65E+04
3.81E-02	1.14E-03	1.14E+01	1.15E+01	1.00E+03	8.23E+02	4.17E+01	8.38E+02	4.60E+04
4.45E-02	1.33E-03	1.12E+01	1.13E+01	9.71E+02	8.11E+02	4.26E+01	8.33E+02	4.05E+04
5.08E-02	1.52E-03	1.17E+01	1.15E+01	1.00E+03	8.21E+02	3.43E+01	8.50E+02	3.00E+05
	Short N- Avg	1.14E+01	1.14E+01	1.02E+03	8.36E+02	4.12E+01	8.37E+02	
	Long N- Avg	1.11E+01	1.10E+01	1.06E+03	8.38E+02	3.85E+01	8.34E+02	
	Cum Avg	1.13E+01	1.13E+01	1.03E+03	8.37E+02	4.03E+01	8.36E+02	

Table 4.3 Summary of Maximum Critical Plane Based Fatigue Predictive Parameters Determined From "Ruiz" Program Output

Ruiz:								
R (m)	$2a_{theo}$ (m)	SWT2 (MPa)	SWT1 (MPa)	SSR (MPa)	teff (MPa)	MSSR	F (MPa)	N (cycles)
5.08E-03	1.52E-04	5.83E+00	5.83E+00	7.62E+02	6.53E+02	3.31E+01	6.02E+02	1.00E+06
7.62E-03	2.29E-04	1.24E+01	1.24E+01	1.18E+03	9.10E+02	4.16E+01	8.66E+02	1.00E+06
1.02E-02	3.05E-04	1.39E+01	1.39E+01	1.24E+03	9.50E+02	4.29E+01	9.16E+02	1.00E+06
1.27E-02	3.81E-04	1.39E+01	1.39E+01	1.22E+03	9.48E+02	4.31E+01	9.14E+02	4.80E+04
1.52E-02	4.57E-04	1.24E+01	1.24E+01	1.14E+03	9.06E+02	4.21E+01	8.64E+02	7.56E+04
1.91E-02	5.71E-04	1.33E+01	1.33E+01	1.20E+03	9.33E+02	4.25E+01	8.94E+02	7.28E+04
2.54E-02	7.62E-04	1.30E+01	1.30E+01	1.19E+03	9.25E+02	4.24E+01	8.85E+02	7.42E+04
3.18E-02	9.52E-04	1.29E+01	1.29E+01	1.18E+03	9.23E+02	4.22E+01	8.82E+02	5.65E+04
3.81E-02	1.14E-03	1.28E+01	1.28E+01	1.18E+03	9.19E+02	4.21E+01	8.77E+02	4.60E+04
4.45E-02	1.33E-03	1.28E+01	1.28E+01	1.18E+03	9.20E+02	4.21E+01	8.78E+02	4.05E+04
5.08E-02	1.52E-03	1.34E+01	1.34E+01	1.22E+03	9.39E+02	4.24E+01	9.00E+02	3.00E+05
	Short N- Avg	1.30E+01	1.30E+01	1.18E+03	9.25E+02	4.24E+01	8.85E+02	
	Long N- Avg	1.14E+01	1.14E+01	1.10E+03	8.63E+02	4.00E+01	8.21E+02	
	Cum Avg	1.24E+01	1.24E+01	1.15E+03	9.02E+02	4.15E+01	8.62E+02	

Table 4.4 Maximum Principal and Maximum Shear Stress Values

R(m)	S_{1max} (Pa)	S_{2min} (Pa)	maxτ_{max} (Pa)
5.080E-02	1.387E+09	-8.679E+08	7.396E+08
4.445E-02	1.376E+09	-8.549E+08	7.346E+08
3.810E-02	1.369E+09	-8.468E+08	7.326E+08
3.175E-02	1.363E+09	-8.448E+08	7.333E+08
2.540E-02	1.359E+09	-8.435E+08	7.340E+08
1.905E-02	1.342E+09	-8.406E+08	7.335E+08
1.524E-02	1.306E+09	-8.199E+08	7.216E+08
1.016E-02	1.310E+09	-8.234E+08	7.271E+08
7.620E-03	1.194E+09	-7.603E+08	6.814E+08

Table 4.5 FEA and Experimental Slip Ranges and Ruiz Parameter Values

R (m)	$2a_{theo}$ (m)	δ_{exp} (m)	δ_{FEA} (m)	$Q\delta_{exp}$	max$\tau_{max}\delta_{FEA}$	$F_{modified}$	N_f (cycles)
5.08E-02	1.52E-03	7.15E-05	7.62E-06	2.44E-01	5.64E+03	1.25E-09	3.00E+05
4.45E-02	1.33E-03	4.50E-05	6.53E-06	1.29E-01	4.79E+03	2.62E-10	4.05E+04
3.81E-02	1.14E-03	3.00E-05	5.74E-06	7.61E-02	4.21E+03	6.85E-11	4.60E+04
3.18E-02	9.52E-04	2.60E-05	5.26E-06	5.60E-02	3.85E+03	3.78E-11	5.65E+04
2.54E-02	7.62E-04	2.40E-05	4.42E-06	4.16E-02	3.25E+03	2.39E-11	7.42E+04
1.91E-02	5.71E-04	2.65E-05	3.63E-06	3.62E-02	2.66E+03	2.54E-11	7.28E+04
1.52E-02	4.57E-04	5.40E-05		6.26E-02		1.83E-10	5.62E+04
1.52E-02	4.57E-04	3.05E-05	2.64E-06	3.10E-02	1.91E+03	2.88E-11	7.56E+04
1.27E-02	3.81E-04	3.50E-05		3.48E-02		4.26E-11	4.80E+04
1.02E-02	3.05E-04	1.20E-04	2.30E-06	8.89E-02	1.67E+03	1.28E-09	3.00E+05
7.62E-03	2.29E-04	1.95E-04	1.50E-06	9.35E-02	1.02E+03	3.55E-09	3.00E+05
5.08E-03	1.52E-04	2.85E-04		5.68E-02		4.61E-09	3.00E+05

Chapter V: Conclusion

The United States Air Force is interested in the subject of this study because fretting fatigue is a potential problem in turbine bearing propulsive engines at the dovetail joint where each turbine blade connects to the outer annulus wall. The turbine blades experience cyclic loading in the form of vibrations, which causes the two surfaces to rub and slip against each other. Failure of these parts cannot be predicted accurately by conventional plain fatigue analysis. Instead Air Force designers need to over-compensate for this danger in the form of thicker, less efficient blades. Secondly, because of the lack of understanding of fretting fatigue, engine maintenance crews need to spend extra money and effort looking for cracks that may or may not be propagating on the blades. If cracks are missed, the lives of Air Force pilots, crews, and aircrafts are at risk. With a better understanding of the failure mechanism, turbine design engineers could make a more efficient engine, pilots and crews will be safer with a reduced chance of in-flight engine damage, maintenance costs will be reduced, and detection and prediction will be made easier for repair crews. For example, if engineers could design turbines that could undergo fretting wear instead of fretting fatigue, longevity of the parts would increase. Through applying a better understanding of how changes in the contact semi-width effect the life of specimens, engineers could create fretting fatigue resistant components by purposely having them grossly slip and cause fretting wear.

Modified from the typical test setup, experiments in this study were performed on a machine capable of independent pad displacement. The use of analytical and numerical test simulations, as well as using the latest in predictive fretting parameters were employed in this study. Previous studies were all closely examined throughout the

analysis and discussion of the tests in this study. New findings and ideas with regard to the relationship between changes in life and corresponding changes in contact semi-width as well as fresh ideas on the nature of fretting fatigue and new topics of research were presented.

5.1 Predictive Parameters for Fretting Fatigue:

5.1.1 Critical Plane Based Fatigue Predictive Parameters:

1. The five critical plane based fatigue predictive parameters failed to show changes in value for changes in life with the variations in contact width.
2. The five critical plane based fatigue predictive parameters were not affected by changes in life with changes in fretting condition, such as stick-slip versus gross slip.
3. The five critical plane based fatigue predictive parameters were not effective in recognizing tests that experienced fretting wear as opposed to fretting fatigue.
4. A reason for this ineffectiveness is that the input into the Namjoshi program was from the finite element analysis, which assumed the presence of a stick zone for every test. The finite element model was not representative of the tests in gross slip.

5.1.2 Ruiz and Modified Ruiz Parameters:

1. The values of Ruiz and Modified Ruiz Parameters proved to correlate well with the fretting fatigue lives of the specimens (as shown in table

4.4 and Figure 4.49). This was a result of the heavy weight that they placed on the slip range.

2. A Modified Ruiz Parameter was proposed which correlated very well with the experimental output. All infinite life experimental tests had larger modified Ruiz parameter values than the tests that failed quickly due to fretting fatigue.

5.2 Local Mechanistic Parameters:

1. Iyer's explanation could not account for the case of infinite life in the 0.0508 m pad test. His explanation of the effects of contact semi-width on fatigue life was absent of any consideration of the fretting condition: gross slip or stick-slip.
2. Iyer's opinion on the importance of local mechanistic parameters seemed viable for the tests that failed in the stick-slip regime. Tests with greater local tensile stresses, as a result of the stresses generated solely from the normal loads, generally failed in fewer cycles than the tests with lower levels of P-only induced local stresses.

5.3 Gross Slip:

Jin's explanation of gross slip fits best with the results and analysis as a reason why some of the tests experience infinite fatigue lives while others did not.

1. The wide and short rectangular hysteresis loops showed that the four tests, experiencing infinite fatigue lives, were in gross slip.
2. The Q vs N curves never leveled off to a steady state for the tests in gross sliding.
3. Fretting wear induced by the gross sliding rubbed away newly initiating cracks [15] and increased the specimens' longevity by 10-fold.

5.4 Slip Amplitude:

Instead of a critical contact semi-width there was really a critical contact slip amplitude. The reason that contact semi-width was mistakenly thought to be critical was because without independent pad displacement, the two variables were linked in fretting tests. Independent pad displacement, as used in the 0.0508 m pad radius test, demonstrated that the infinite life, associated with contact widths smaller than the critical width, was not a function of the contact geometry.

5.5 Grand Implication of this Study's Finding on Fretting Fatigue:

A new criterion to design against fretting fatigue has been conceived. Designers of parts, such as turbine planes, should look into designing their components to slip more than the critical slip amplitude. This could increase the life of components that would normally fail under fretting fatigue by 1000% or more!

Chapter VI: Future Works/ Author's Ideas

This chapter in the thesis put forth ideas toward fretting fatigue and points out direction for future works and studies in the area of fretting fatigue. They are not drawn upon solely by the results from this study's 12 experiments. Instead they are more creations of imagination based upon the various readings and personal experiences of the author in dealing with fretting fatigue.

6.1 Constant Contact Semi-Width Tests:

Firstly, as was mentioned in the background, Bramhall realized that one could vary pad radius while keeping the peak contact pressure constant. Also one can vary pad radii and keep a constant contact semi-width. It might be valuable to run some tests with different pad radii but with a constant contact semi-width and look at how the slip amplitude and life vary. This can be tried with different amounts of independent pad displacement. Without applying independent pad displacement, would all tests have the same slip amplitude? Increasing the span would probably show the tests would induce gross slip and not fail. This would support the idea that there is a critical slip amplitude and not a critical contact semi-width.

6.2 Constant Slip Amplitude Tests:

It might also be interesting to see if this critical slip amplitude was constant for different radii pads. The amount of independent pad displacement necessary to induce specific slip amplitudes could be calibrated. If some tests, which failed in fretting fatigue under the stick-slip condition, had larger slip amplitudes than tests with infinite life and gross sliding, then there would be no critical slip amplitude.

6.3 Multiple FEA Simulations for a Single Experiment in Gross Slip:

Run several finite element tests for a single experimental test in gross slip. Pick several key points in the test, probably from the Q vs N curve. Change the input value of Q for those chosen points, just as Q changes in the actual test. Look for trends as to how the size of the slip and stick zones change throughout the test. Does it seem as if the stick zone size is going towards zero just before the Q vs δ loops indicate that the test has gone into gross slipping?

6.4 FEA Model of Slipping in Turbine Dovetail Joints:

Try finite element modeling the dovetail joint of a typical turbine blade and compare local mechanistic parameters to those found in the typical laboratory experimental fretting fatigue tests. Could the turbine blade geometry be changed to put the turbine blade in the gross slip regime as opposed to stick-slip?

6.5 Fretting Wear Turbine Blade:

Modifications to the turbine engine blade-disk interface could be conducive to fretting wear. Two possibilities for inducing fretting wear as opposed to fretting fatigue exist as a result of the findings in this study. The contact between components could be made loose enough, that gross slipping would naturally occur. Or gross slipping in tighter joints can be intentionally created through forced displacements. The concept is illustrated in Figure 6.1 Possibly once every rotation, or once every set number of rotations, the blades could be loaded such that the blade pressure face would grossly slip against the disk pressure face. This would rub out newly initiate cracks before they had a chance to propagate.

6.6 Variables Held Strictly as Constants in FEA Analysis:

The finite element results showed that p_0 was not truly held constant for each different test case. This was probably because the p_0 calculated for the different experimental test conditions was based on the analytical solutions, which had error because of the half-space assumption. Furthermore the Q/P ratios input into the finite element runs were not constant either. Instead they were based on the actual experimental output, which was not perfect. So it might be interesting to run some finite element tests in which p_0 and Q/P were strictly held constant in the finite element analysis. Then the true influence of the other variables can be measured via FEA. This test could be run rather quickly using the Analytical solution program and the results would be reasonably valid for the smaller radii, because they met the criteria for the half-space assumption.

6.7 Wear Idea:

This is an explanation of why some tests go into gross slip while others do not. Wear occurs in all of the tests as the pad rubs against the substrate. This wear removes layers of both the pad and substrate. The amount of wear that occurs is probably proportional to the amount of slipping and the shear traction felt by a particular area. The shear traction itself is probably strongly related to the pressure being felt at a particular area. Due to this wearing, the initial contact geometry changes. The pads are no longer quite so cylindrical and the substrate is no longer quite so flat. Figure 6.2 tries to illustrate this idea.

Looking at changes in the pad geometry caused by wear through Iyer's approach, it becomes intuitively obvious that the local mechanistic parameters will change throughout the test. Peak contact pressure seems very much dependent on geometry. If

the tip of the fretting pad is dulled, the peak stresses will be more evenly and distributed not be as great in magnitude.

If certain magnitudes of local mechanistic parameters are necessary in order to reach stick-slip conditions, then it is possible that after wear, the new geometries would no longer achieve the initial stress levels that they started with. For example, if all different radii had the same peak contact pressure, and a certain peak contact pressure was required to attain the stick-slip condition necessary for fretting fatigue, but different geometries wore at different rates, then it is conceivable that after time in test some geometries might have the required local mechanistic parameters to reach stick-slip, while others would not.

If this idea were correct, then the smaller radii tips might dull quicker than the larger radii tips. Logically there is less volume loss required for the smaller radii pads to significantly change tip geometry than with the larger radii pads.

If rate of wear is proportional to slip amplitude, then this idea seems to correlate well with the tests from this study. A suggestion for future work would be to change the geometry of the finite element mesh to simulate wear throughout a test. How would the local mechanistic parameters change? The amount of wear could be measured on the pads and substrates from this study to see if geometry changes really did occur and if they were significant. A study could be done on how the amount of wear was proportional to variables such as slip amplitude, initial peak contact pressure, normal load, pad radius, etc.

6.8 Stick Zone Correlation Idea:

The mechanism that causes fretting fatigue is not so much the result of slip amplitude, but instead is a result of the existence of a stick zone. The correlation between fretting fatigue and slip amplitude is because at larger slip amplitudes, a stick zone cannot form. This idea correlates well with the evidence from this study. In the tests that experienced gross slipping and infinite fretting fatigue life, there was no stick zone in the later cycles.

It is possible that it takes time for the stick zone to develop. This time seems proportional to the slip amplitude. A stick zone has formed by the time the Q values on the Q vs N curve have stabilized and the Q vs δ hysteresis loops are thin. It takes less time for shorter slip amplitudes to form stick zones, but as slip amplitude increases the time until stick zone formation increases until it can no longer form.

It is very likely that there is some amount of sticking when the hysteresis loops start to change geometry. But this sticking is not as strong as when the hysteresis loops narrow. This change in the stick zone can be compared to the drying of glue. Imagine glue in between the fretting pad and the substrate. In the beginning of the fretting test, the glue is wet and the pad and substrate are free to slip against each other. However as the test goes on, and if the magnitude of slipping between the two bodies is small enough, the glue starts to dry. The two bodies are not as free to slip. As time goes on the glue has completely hardened and part of the two bodies stick together. Or because the slip amplitude is too great, the bond of the glue breaks at some point in its hardening. Once it's bond is broken, the glue no longer effects the rubbing and the only ill effect of the rubbing is surface wear.

The tests that went into gross slip did not have stick zones when they were in their gross slipping phase. All tests without stick zones had infinite fretting life. The location in which these two bodies stick is the source of a fatal stress concentration, which eventually leads to crack initiation and the substrates failure.

6.9 Stick and Rip Idea:

But how does the stick zone lead to cracking? It was mentioned that the border between the slip and stick zones in the contact area could be the source of a stress concentration that leads to crack initiation.

The way that the fatal stress concentration forms at the border of the stick zone could have to do with the shifting of the stick zone. Remembering the analysis of slip amplitudes from the finite element output, it was observed that the stick zone shifted location between the two combined loading cases. This shift in location was attributed to the rolling of the fretting pad as Q and σ_N changed. If the substrate and pad are fused together when they are sticking, then it is conceivable that if that stick zone shifts, that pad could rip material from the substrate surface that was stuck. An illustration of this concept is given in Figure 6.4. Cracks could then initiate from sharp tears in the ripped surface. These cracks then propagate because of the applied bulk stress. Without fretting wear, the cracks are not rubbed away. If a stick zone never forms, then maybe this stick and ripping cannot occur and cracks are not initiated via this method. Or if the slip amplitude increases throughout the test, such as what seems to be occurring in the case of gross slip, it is very possible that small cracks that have initiated by stick and rip are rubbed out by sliding.

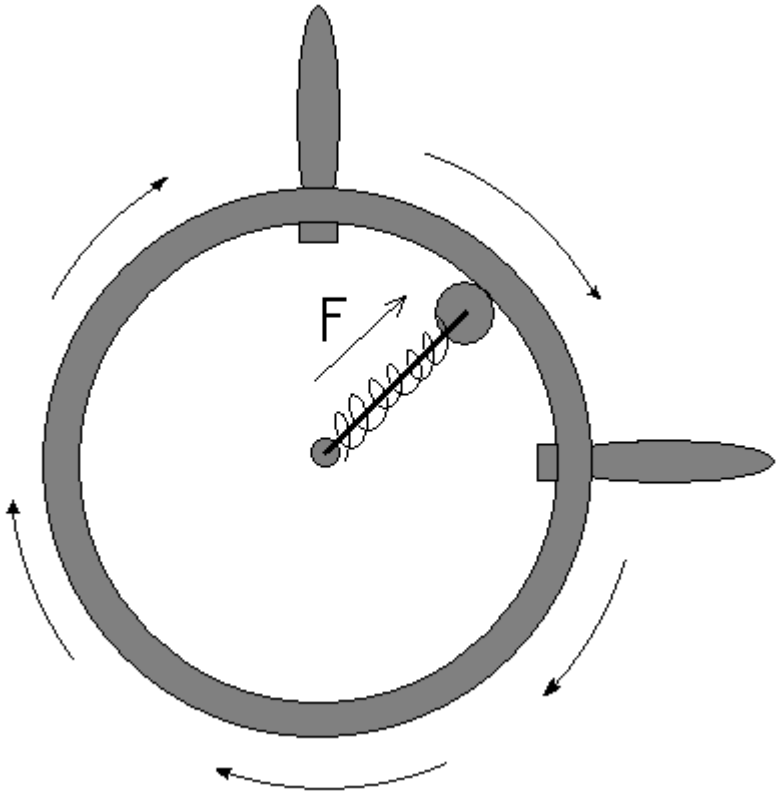

Figure 6.1 Induced Displacement in Turbine Concept Drawing

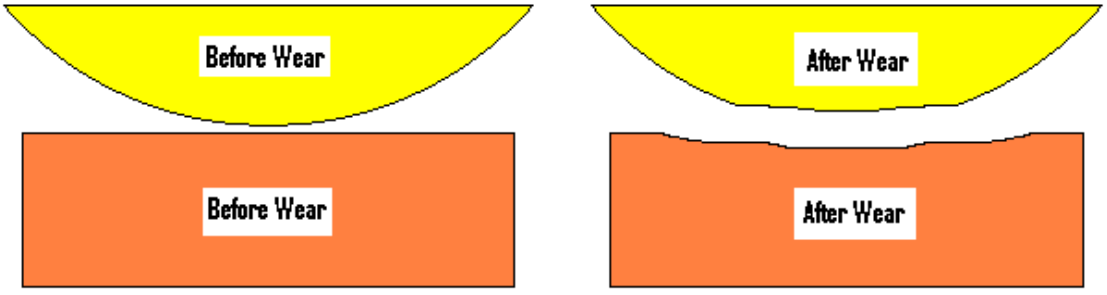

Figure 6.2 Ideal Cylinder-On-Flat Geometry Before Wear Versus After Wear

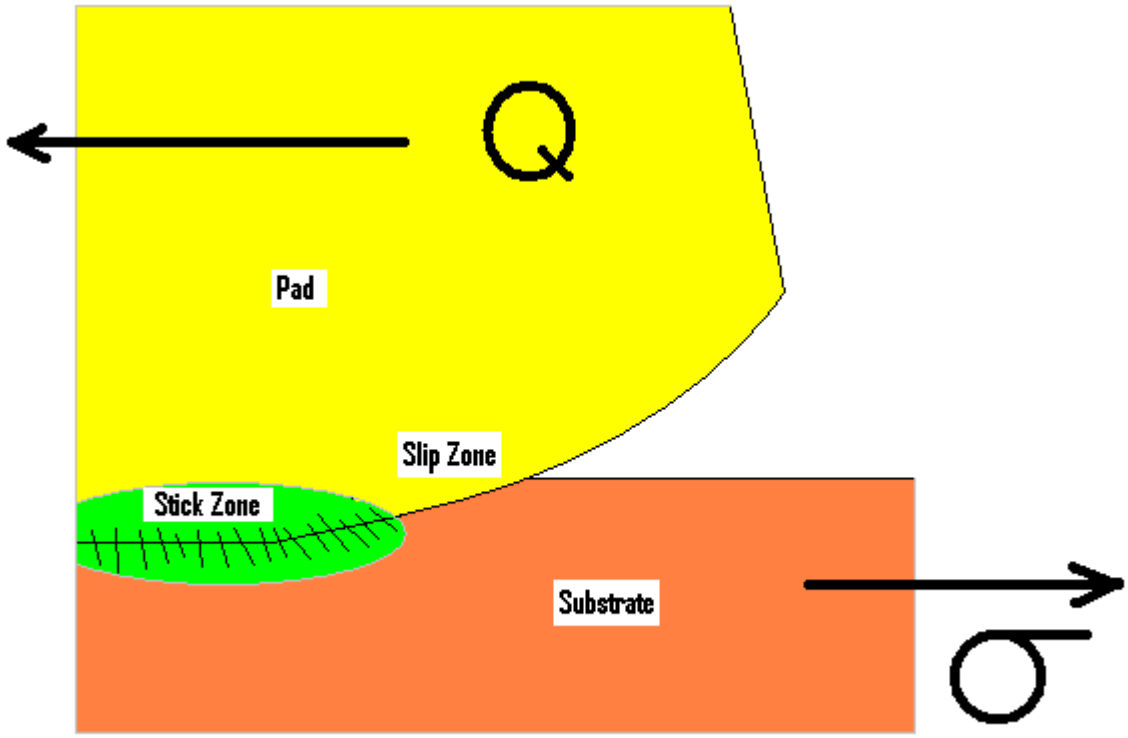

Figure 6.3 Stick Zone Illustration

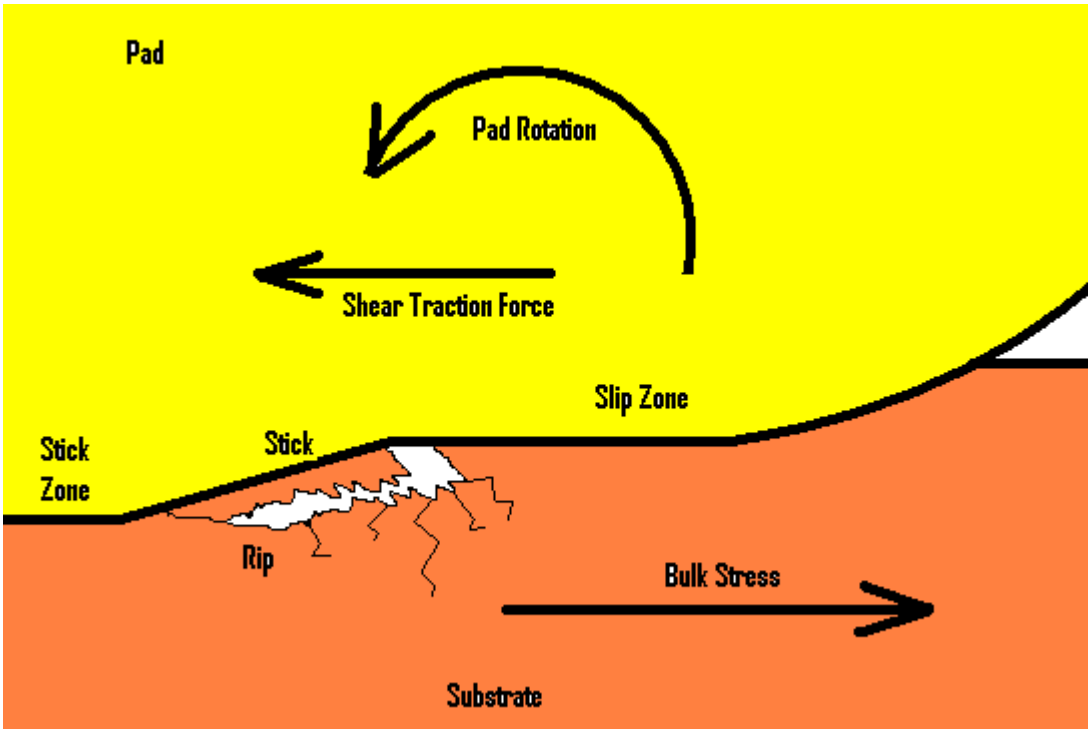

Figure 6.4 Illustration of the Stick and Rip Idea

APPENDICES:

The purpose of the appendices was to be helpful hint to future researchers following this work, to show the thought behind some of the analysis, and to preserve ideas that did not relate directly to the main report.

A1 Experimental Q/P Calibration and Test Diary

Even though Hill and Nowell had previously done similar fretting fatigue tests, maintaining a constant ratio of Q/P, their test setup was different. Calibrating the different radius pads and test conditions for a constant value of Q/P was necessary.

One of the intended conditions of this study was to keep the ratio of shear traction forces, Q, to normal loads, P, constant. This was not an easy task and had to be done by an iterative process. Whereas the peak contact pressure, P0, the contact semi-width, a, normal pressure, P, the bulk stresses and ranges, sN, could all be predicted fairly accurately using the analytical equations and by setting certain boundary conditions, there was no known way to predict value of the ratio of Q/P (with independent pad displacement included) without running a calibration test with certain known global boundary condition.

Q was adjusted using "independent pad displacement" or span control. The span was used to change the value of Q for a set value of normal pressure load, P in order to control the ration of Q to P. It was previously observed (Jin) that increasing the span caused Q to increase at a given radius. Also it was noticed that if no independent pad displacement was applied, as the pad radius increased but P was adjusted so that P_0 as held constant, the ratio of Q/P decreased. A third trend that was previously observed and was further observed in this study, was that the initial value of Q was not held constant.

Instead the value of Q had been previously observed, to increase and then by at most 2000 cycles level off to a steady value of Q that would remain for the duration of the test.

With the previously observed trends about the Q/P in mind, the task of calibration to a constant Q/P value for all radii tests began. It was decided to calibrate Q/P starting at the smallest radius without adding independent pad displacement. From a previous study (Jin), it was known that for a 4000 N pressure load on a 0.0508 m cylindrical radius, the Q/P ratio would produce a Q/P value of about 0.40. If the noticed trends were correct, then the smallest radius fretting pads, 0.00508 m, would produce the highest Q/P ratio without adding span. The Q/P value from the 0.00508 m calibration would then be the Q/P ratio all other radii would be calibrated to by adding an increasing amount of independent pad displacement as pad radius increased.

The first calibration test was for the 0.00508 m radius fretting pads, normal load was 400 N, σ_{max} was 550 MPa and σ_{min} 18 MPa. The normal load of 400 N was chosen so that the peak contact pressure would be 529.6 MPa, a constant throughout all radii calibrations and tests. The calibration was run for 2000 cycles at a frequency of 2 Hz. All tests and calibrations were run this frequency: 2 Hz. Strangely the Q/P ratio leveled off at about .33, way below expected. This value seemed odd because previous research had shown that, in cases of zero added span, the ratio of Q/P increased as radius decreased for a given constant peak contact pressure. Two more tests were run, with minor adjustment in procedure and checking of procedure by more experienced researchers. They showed similar results. Later it became understood that the Q/P was so low because of gross sliding.

Not understanding what the problem was with the 0.00508 m radius calibrations, but assuming that there was a problem, it was decided to move up to the next size pad radius, which was the .01016 m radii pads (0.00762 m and 0.0127 m radii pads were at a later time to the study), without adding span and try to find a maximum Q/P ratio. This time the Q/P ratio was in the range of what was expected, about 0.80. This value was taken to approximately be the maximum value of what Q/P would be for all the radii without added span. The next step was to calibrate the other radii pads and their respective normal loads to have a Q/P ratio of about 0.80.

If the amount of independent pad displacement necessary to increase the Q/P ratio to the given value increased as radius increased, then going to the largest radii pads, 0.0508 m, and calibrating for 0.80 Q/P, there would then be an upper bound as to the amount of span to add. The lower bound of course would be no independent pad displacement. Figure 4.41 shows how the Q versus cycle curves of the .0508m radii pads changed as span was changed. The value of span equal to 0.0011 m independent pad displacement per cycle was determined to produce a steady-state maximum Q/P ratio of about 0.76, which at the time seemed close enough to the 0.80 Q/P ratio to be considered close enough.

The steady-state maximum values of Q/P versus span were determined for the various radii tested in the initial calibrations. These test were all run to 2000 cycles and the steady-state maximum Q/P values were determined somewhat empirically by looking at the corresponding Q/P versus cycle charts. It can be noted that the relationship between change in Q/P and change in span seemed to be constant with respect to the

specific radius being looked at. Furthermore the slopes of these linear relationships seemed to decrease with increasing pad radius.

After calibrations were finished for 8 of the 9 different radii pads that were created for this study (0.00762 m and 0.0127 m radii pads came later), actual testing was ready to begin. The 0.00508 m radius pads were tabled at this time for possible use later depending upon the results of the 8 different radii tests.

It was arbitrarily decided to run the tests in descending pad radius order. Because data had already been collected for 2" radius pads at a Q/P ratio of .83 during a previous study (Jin), it was decided to go to the next largest radius and begin. Based on a hunch that the Q/P might continue to increase slightly beyond what was predicted for in the calibration testing, the Independent Pad Displacement was set for 0.000914 m, which was slightly less than the ideal span calibrated: about 0.000965 m. The 0.04445 m fretting pads were aligned perfectly using pressure paper. The test sample was inserted and 3500 N of normal load was applied through the fretting pads. A half-inch extensometer was attached and then "zeroed." The servohydraulic test machine was set to run cyclic sinusoidal nominal bulk stresses from the lower actuator and the span displacements were set to run under the control of the upper actuator. The TestStar II control system was set to record time, cycle, the two load cell values, and extensometer voltages during the preprogrammed desired cycles. Ochang Jin, a researcher with experience in fretting tests, checked the set-up. Everything looked okay, so the test was run. Figure 4.29 shows how the 0.04445 m pad radius test went. A steady-state maximum Q value was achieved after about 4000 cycles. The hunch to reduce the span proved to be a good. As can be seen from the figure, the maximum Q reached a steady-state value of about 2800 N for the

3500 N applied normal load. Therefore, the Q/P leveled off at the value of approximately 0.80. After only about 40000 cycles, the specimen failed. From the Q/P ratio perspective, test seemed to be successful for the purposes of the study. The magnitude of minimum and maximum Q values were almost equal, but the directions are different. This condition of shear traction load reversal was consistent in the other tests as well. It was generally the case that the minimum Q had a slightly lower magnitude of force than did the maximum Q.

The next three radius tests ran smoothly. The same procedure for set-up, based on the calibrations, was used. The 0.0381 m pad radius test was calibrated to a span of 0.000711 m but run at 0.000699 m. The 0.03175 m pad radius test was calibrated to a span of 0.000521 m, but run at a 0.000508 m span. The 0.0254 m pad radius test was calibrated for an independent pad displacement of 0.000356 m, but run at 0.00033 m. Despite the adjustments of span from the calibrated span, the ratio of steady-state maximum Q/P continued to increase. The steady-state maximum of Q/P was found to be about .84 for the 0.0381 m pad test, .85 for the 0.03175 m pad test, .86 for the 0.0254 m pad test. The Q/P ratio still increased for the 0.0254 m pad test even though the difference between the calibrated span and the span used in the test was greater than the last two tests. It was starting to look like something was wrong in the calibrations for Q/P. The figures show the Q versus cycle curves of these three tests. Steady-state maximum values of Q were achieved. It can also be noticed from these curves that the life of the specimen being tested was increasing as pad radius decreased. The 0.0381 m test specimen survived to approximately 46000 cycles, the 0.03175 m substrate failed at 56517 cycles and the 0.0254 m radius pads sample broke at 74222 cycles. Finally, the

amount of cycles until steady-state was greater in the 0.0254 m radius test than the 0.0381 m or 0.03175 m tests.

For the 0.01905 m radius fretting pads test, the span was cut considerably, from the calibrated value of 0.000203 m to 0.000165 m to try to compensate for this trend of Q/P increasing from the originally calibrated values. It did not help. The Q/P value for this test was approaching and even passed 0.90. The life for this test was shorter than the 0.0254 m radius tests. The 0.01905 m specimen failed at 72778 cycles. It was at this point that the decision was made to do more calibration testing before trying a test with the 0.01524 m pad radii.

Through background readings, especially the paper by Nowell and Hill, it was known that some previous studies had reported a critical contact semi-width below which the life to failure increased dramatically, as much as 10-fold. It was an original goal of this study to find the critical contact semi-width for the Titanium Alloy used, which had not been previously done before. Not having found such a dramatic change in life from the 0.04445 m, 0.0381 m, 0.03175 m, 0.0254 m, and 0.01905 m pad radii tested, it was decided to skip to the smallest radius calibrated.

A test was run on the 0.01016 m pad radii cylinders. There was a potential for danger in that if the calibration proved to be very wrong for this radius then it would not match with the previously recorded tests' data because Q/P could not be considered a constant. Fortunately this test ran for over 1000000 cycles and never broke. The Q versus cycle curve can be seen in the figure at the end of chapter 4. This probably meant that its contact semi-width was below the critical contact semi-width. Furthermore, even

though the Q value never really achieved a steady state, for the first 200000 cycles the Q/P ratio stayed mostly around 0.85, which was acceptable.

Now it was decided to go back and look at the 0.01524 m pad radii in a test. Would the 0.01524 m radius have a short or long life? When considering the what value of span to apply to this test, the trend that the tests were taking longer and longer to reach a steady state condition was considered and the thought occurred that a 2000 cycle calibration test was not long enough to get a good picture of what the steady state Q/P was going to be. The calibration length was bumped up to 5000 cycles. From calibration, it was decided that a span of 0.000102 m would produce the correct Q/P ratio.

The 0.01524 m pad radius test was run and there was still trouble. The Q versus cycle curve can be seen in at the end of this appendix. The Q/P Ratio was never very steady. It bounced around at about 0.94 or 0.95 Q/P. This was not an acceptable level of Q/P. So a second test was run. This time only a very minor amount of span, 1.27E-5 m, was applied. The life, between the first and second 0.01524 m pad radius tests, increased from 56,181 cycles to 75,645. Furthermore, the ratio of Q/P was down to about 0.81. The second test would suffice.

The 0.01524 m pad radius test did not last anywhere near 1000000 cycles. That led to the thought that the critical contact semi-width was probably generated by a pad radius between the 0.01016 m and 0.01524 m radii. An order was at this time placed for 0.0127 m and 0.00762 m radius fretting cylinders. The 0.0127 m radii pads would help to narrow down what the critical contact semi-width was and the 0.00762 m radii pads would probably lead to infinite life for its specimen, which would further support the thought that a critical contact semi-width was found.

Three more tests were run to help solidify the findings in this study. These tests were run with 0.0127 m, 0.00762 m, and 0.00508 m fretting pads.

The 0.0127 m pad test had a span value of 2.54E-6 m, which is the smallest nonzero span that the upper actuator could attain. A span of this small should really have had no effect. The Q versus cycle curve is shown at the end of this appendix. Amazingly the Q/P ratio keep increasing throughout the duration of this test such that by the end of the test, just before failure, the Ratio of Q/P was approximately 1! Interestingly, the 0.01016 m test never achieved a Q/P ratio as high as this test. Therefore this broke the rule that as radius decreased the ratio of Q/P increased.

Both the 0.00762 m and 0.00508 m pads were tested and their respective specimens each lasted over 1000000 cycles. As can be observed in figures of chapter 4, that both Q versus cycle curves initially increase to a peak value and then dropped off continuously. This same trend occurred in the 0.01016 m radius pads, but the difference was that as the pad radius decreased, the peak Q value was reached in less cycles and Q dropped at a faster rate to a lower level. The 0.00762 m pad radius test reached a Q/P value of .75 to .8 at cycles before about 150000. The 0.00508 m pad radius test hit its peak maximum Q value at around cycle 2000 and then decreased rapidly until about cycle 200000 at which point the steep slope relaxed but was still negative. The peak maximum Q/P value for the 0.00508 m test never was higher than 0.5 and it was only that high for a couple thousand cycles in the beginning of the million cycle test.

By the end of calibrations and testing it could be noted that original observed trends of how Q and Q/P reacted to different amounts of independent pad displacement were not very helpful. Increasing the span did cause Q to increase at a given radius for

the cases tested in this study. If no independent pad displacement was applied, as the pad radius increased but P was adjusted so that P_0 as held constant, the ratio of Q/P did not always decrease. The value of Q/P decreased as radius decreased for pad radii smaller than 0.0127 m. In each of these four tests the independent pad displacement was zero or negligible. While the initial value of Q was not held constant, it did not always level off to a steady state value quickly. Of the tests in this study, as the radius decreased, the amount of time until steady state was achieved seemed to increase. For the pad radii whose specimens did not break, the values of Q never leveled off.

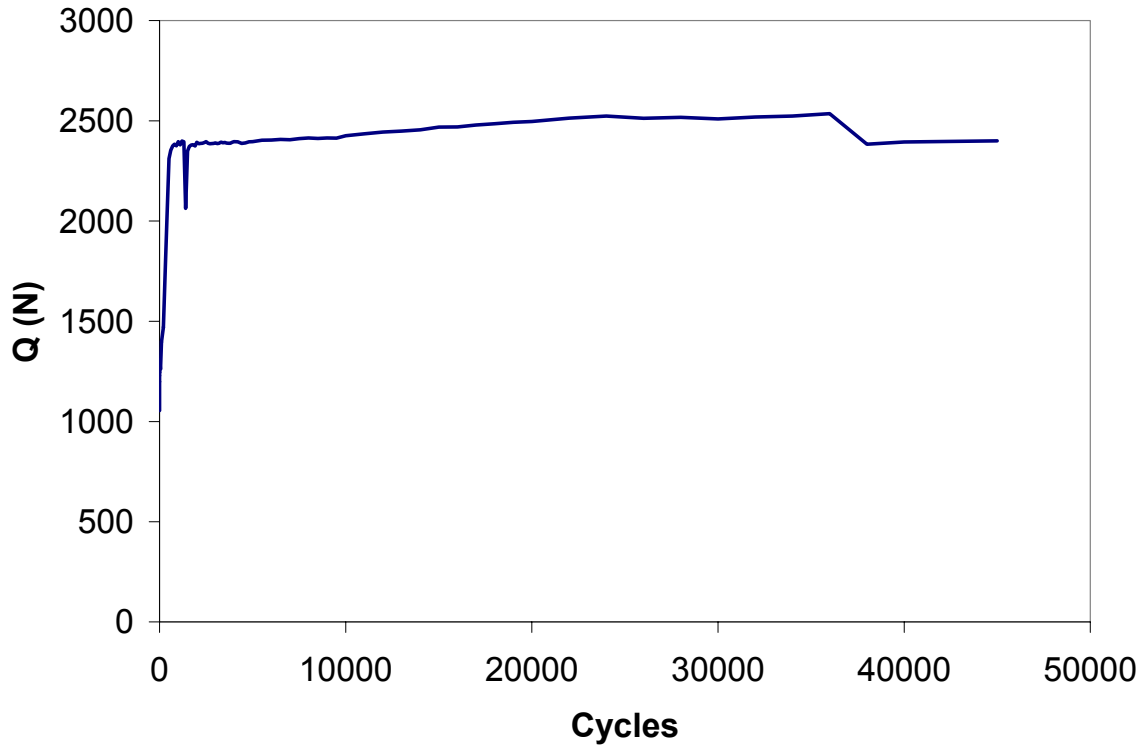

A1.1 Q vs Cycle Curve for Experimental Test Using Pad R=0.0381 m

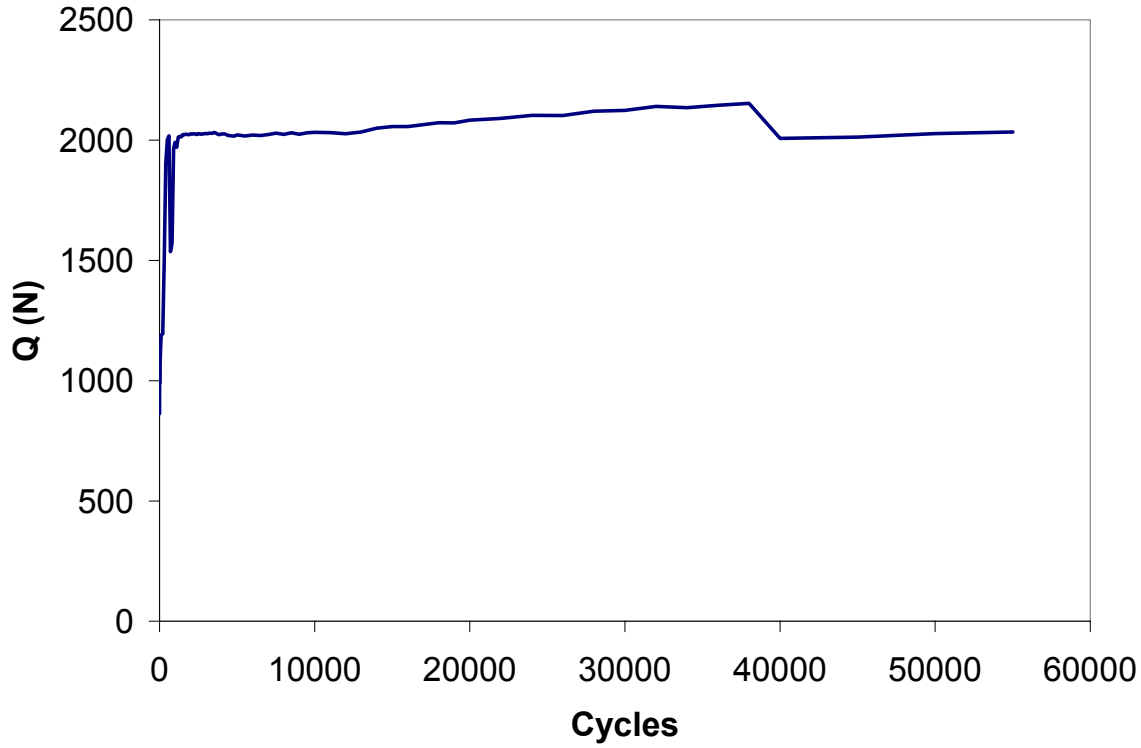

A1.2 Q vs Cycle Curve for Experimental Test Using Pad R=0.03175 m

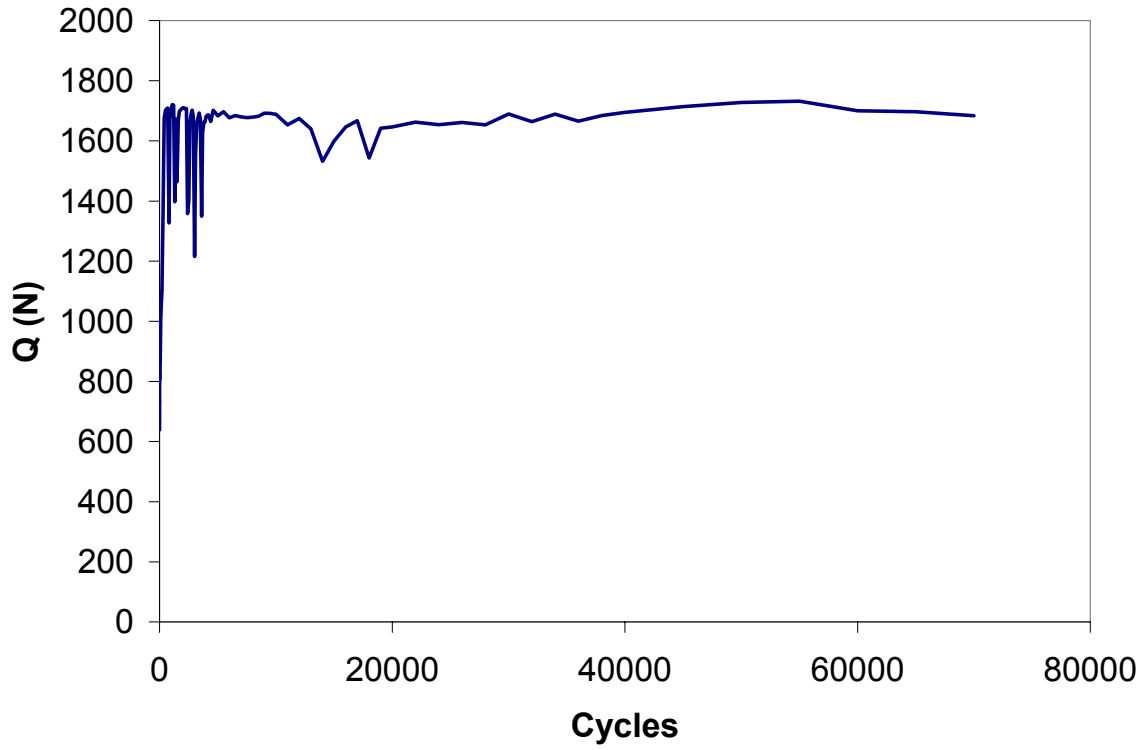

A1.3 Q vs Cycle Curve for Experimental Test Using Pad R=0.0254 m

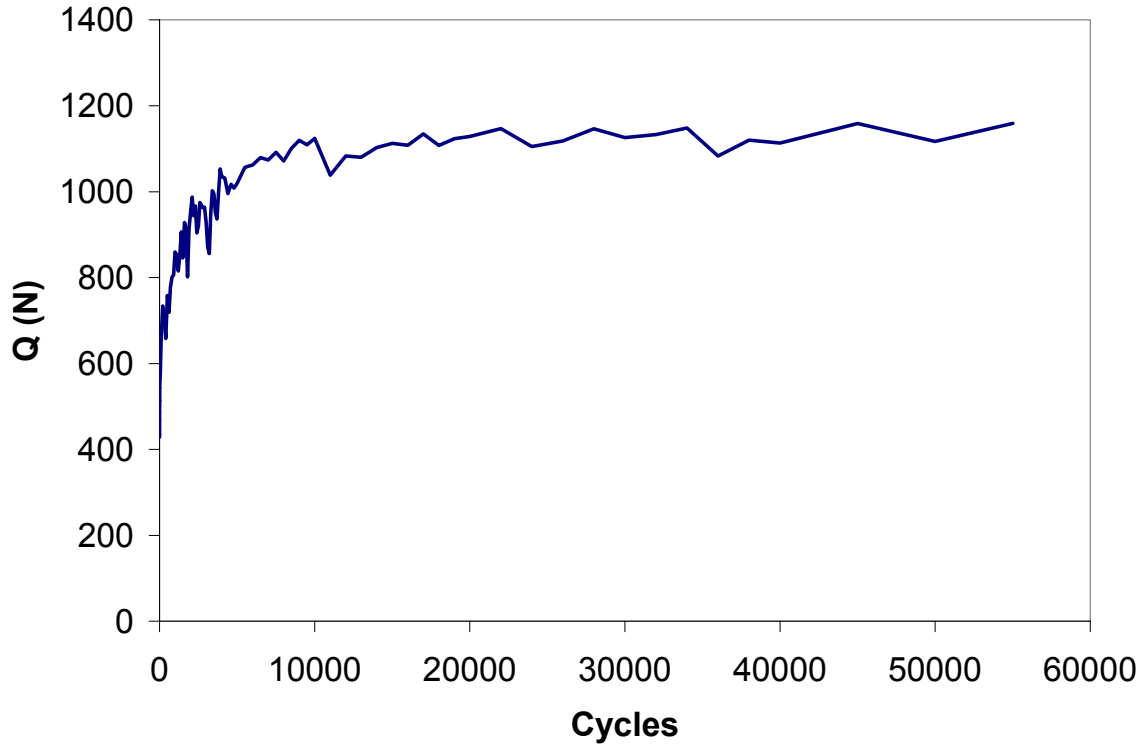

A1.4 Q vs Cycle Curve for Experimental Test Using Pad R=0.01524 m, span=1.02E-4 m

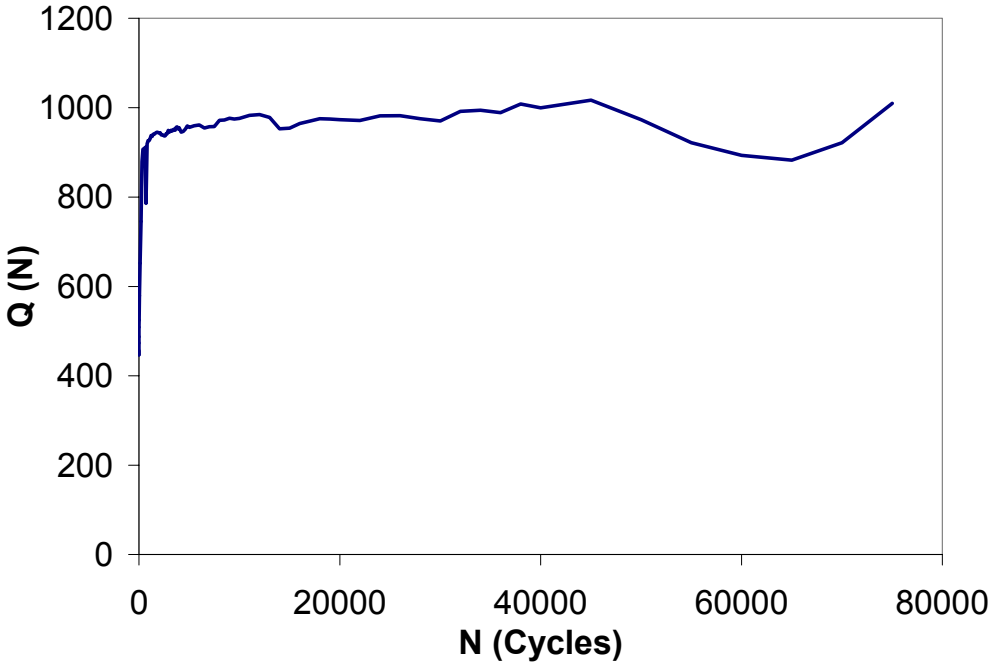

A1.5 Q vs Cycle Curve for Experimental Test Using Pad R=0.01524 m, span=1.27E-5 m

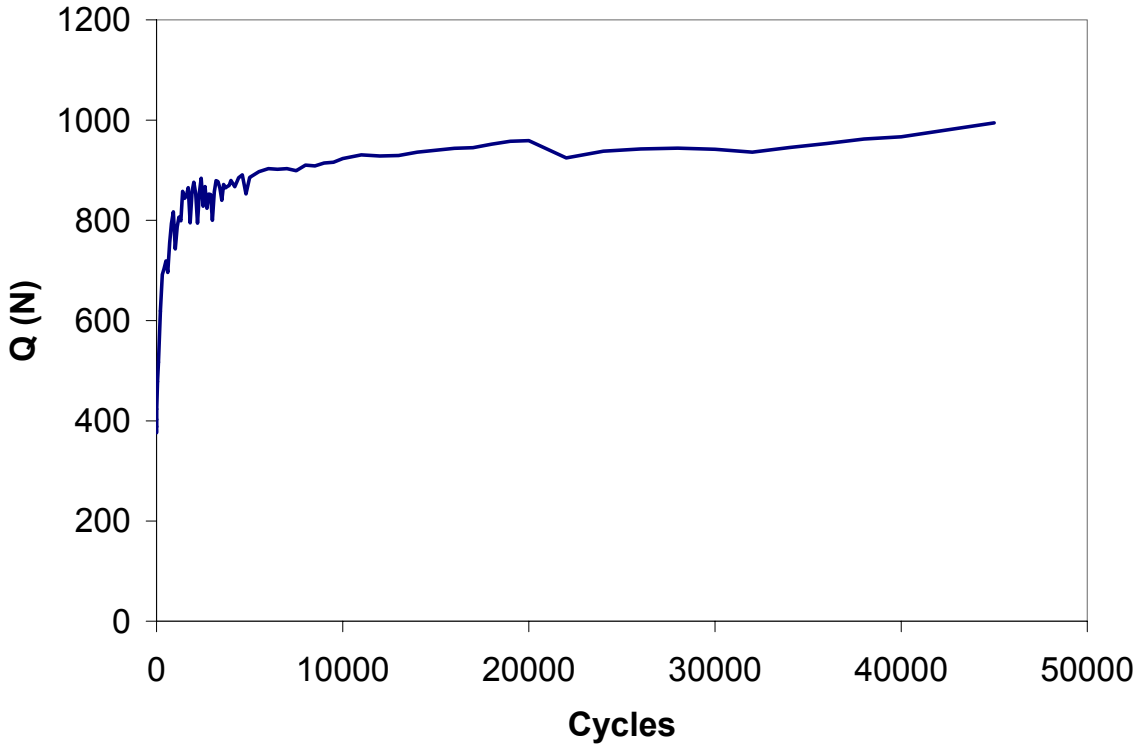

A1.6 Q vs Cycle Curve for Experimental Test Using Pad R=0.0127 m

A2 Unanalyzed Experimental Results

As experimental tests were run in the laboratory, 5 important types of output were digitally received and recorded on the computer from sensors on the system: two load readouts, a strain readout, time and corresponding cycle number. The two load readouts were from load cells attached to the upper and lower actuators. The first load readout was labeled as the "axial force" and was in series with the fixed hydraulic arm, while the second load cell readout, titled "Axial 5 kip Load Cell," was in line with the lower actuator. A sample of their output can be seen in Figure A2.1. The half-inch gage extensometer produced a voltage output, as shown in Figure A2.2.

A2.1 Load Cells: The load cell readouts were used to calculate the shear traction force, Q. It can be noted that the force versus time graph, Figure A4.1., below is in English units. This is how the computer originally recorded this parameter. The Axial 5 Kip Load Cell read the applied bulk load, σ_N. The Axial Force load cell read the force experienced by the fixed end of the specimen. Shear tractions (the frictional forces), between the fretting pads and the sample, oppose some of the applied bulk stress. The fixed end of the specimen opposes all remaining concentration of the applied bulk stress. Therefore, the difference between the two load cells is the shear traction generated by both fretting pads, or 2Q.

$$Q = \frac{(L_1 - L_2)}{2} \tag{19}$$

Q could then be determined at any time during the test when the loads were recorded.

A2.2 Extensometer: The voltages output from the extensometer were converted to displacements. The half-inch extensometer was calibrated at various known

displacements to determine the relationship between voltage output and measured displacement. The curve of voltage versus displacement, as shown in Figure A2.3., shows a linear relationship. The determined calibration relationship was:

Displacement = 0.0074680*Voltage + 0.0001535 (?)

Therefore, the extensometer-measured displacements could be determined at any time during a test in which voltage output was received. This measured displacement was later used to determine slip amplitude.

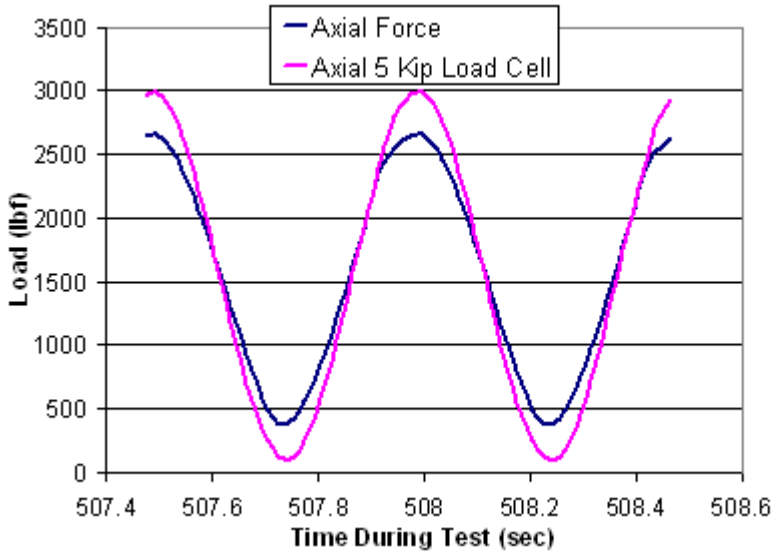

Figure A2.1 Sample Load Cell Output (R=.0127m Test Cycle 1000)

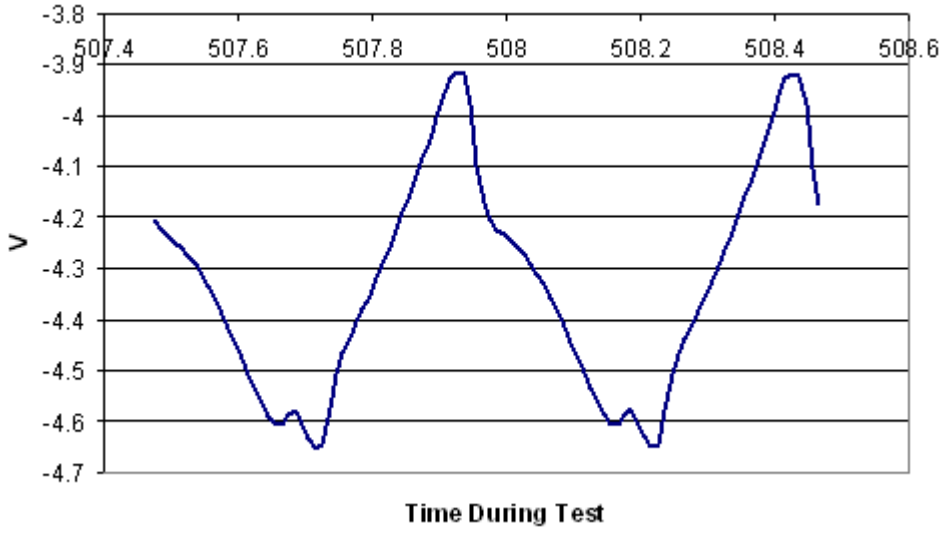

Figure A2.2 Sample Extensometer Output (R=.0127m Test Cycle 1000)

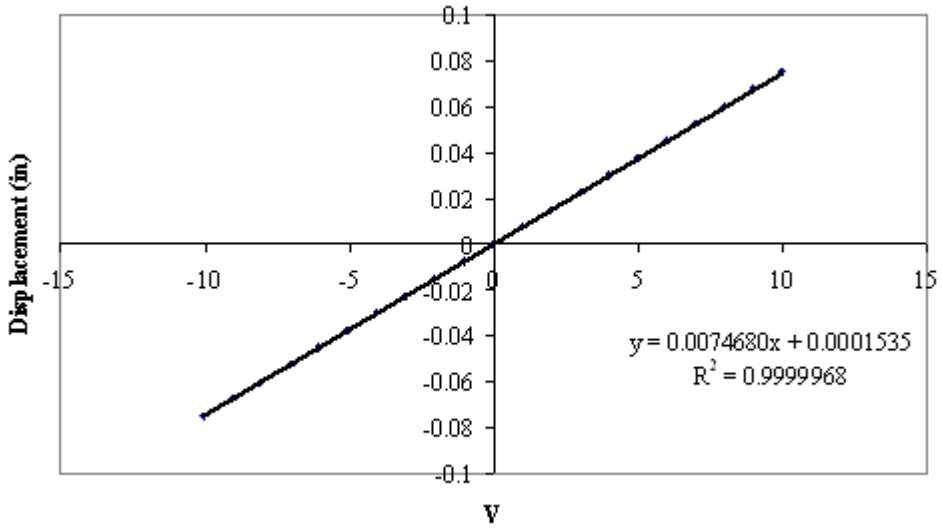

Figure A2.3 Half-Inch Extensometer Calibration Curve

A3 Best Use of Finite Element Analysis:

Iyer used FEA before his experiments to show what would happen. In this study FEA was used after the experiments to show what happened. Ideally both before and after would be preferred.

Iyer used an iterative process to determine what the experimental values of P should be to get desired values of a or p_0 for each pad radius. He initially used the analytical equations to find the value of P for a certain desired a or p_0 at a certain R. Then he ran the finite element code to see the more realistic value of what a or p_0 would be. Then he re-estimated P and ran the model again and again until he found a value for a or p_0 that was exactly what he wanted.

A similar approach was used to determine what global value of bulk stress, $\sigma_{N,max}$ and $\sigma_{N,min}$, in order to obtain the desired local bulk stresses, $\sigma_{L,max}$ and $\Delta\sigma_{L,max}$. Due to stress concentrations produced by the normal pressure only between the cylinder and specimen, the nominal bulk stress leads to unexpected values of the local stress distribution. The exact values of this local stress are a function of cylindrical radius, normal load, friction coefficient and of course the nominal bulk stresses.

A4 Analysis of FEA P-only Stresses:

Step 1 in the finite element analysis was to apply to pressure load of the cylinder onto the specimen and output all the stresses and displacements. The only applied force was the normal load applied to the cylindrical pad and transferred through the contact area to the substrate surface. The existence of tensile stress concentrations at the edge and outside of the contact zone before application of the bulk nominal stresses had been previously noticed [14]. By looking closely at the step 1 output, the effects of the cylindrical contact independent of applied bulk stresses, can be examined. In order to investigate these issues, stress distribution data for the different pad radii finite element tests with only normal load being applied was closely examined. These stresses, as well as the entire step 1 output for all of the different radii processed through finite element analysis, were thoroughly analyzed.

The first area looked at from the step 1 finite element analysis output was the stress distributions in the x-direction. The σ_{xx} stress distributions for the different radii can be seen in following figures. The tensile stress concentrations Iyer noted can be seen to indeed exist at the edges of the contact area. The peaks of these tensile stress concentrations lie exactly on the edges of the contact zones. For example the edge of the step 1 contact zone for the 0.0508 m radius fretting pads case was $x = \pm .75*10^{-3}$ m. The peak tensile stresses at this position was $222.115*10^{6}$ Pa, located at $-.75*10^{-3}$ m and $222.115*10^{6}$ Pa at $.75*10^{-3}$ m. Their peaks represent the maximum values of σ_{xx}, or maximum tensile stress values, along the substrate surface. The sharpness of these tensile stress peaks dulled for the smaller radii pads tested. The figures shows the trend

of how the maximum σ_{xx} changes with different pressure loads. Assuming that the tensile stress concentration is a function of normal load and not radius, then it should not matter that the pad radius is changing for the different normal loads. The ratio of P to maximum σ_{xx} did remain almost constant, at a slope of 383.52 Pa/N, for nine the different values of normal force tested. It can be seen from the figures that the ratio changed slightly for the lower magnitudes of normal force. All in all, the existence of tensile stress concentrations, located at the edge of the contact zone, when only pressure loads are applied, is well complimented by the findings in this study.

The σ_{xx} curves, in the pressure load only case, are symmetric in the y-direction about the center of the contact zone (where x=0). At the center of contact the curve is at its greatest magnitude of compressive stress. Looking in the $\pm$ direction from the center, the curve almost parabolicly slopes up to a tensile stress peak, which happens to be located just at the edge of the contact zone (the same peak that was just discussed). From this tensile peak, the σ_{xx} concentration begins to once again lower until σ_{xx} goes to zero in both the positive and negative x-directions. It was interesting to note that the location along the specimen where the tensile stresses again reached zero was approximately the same for all of the different cases tested. From the data it was observed that all the curves leveled off and crossed zero on the y-axis between x = $\pm 5.6*10^{-4}$ m to $5.75*10^{-4}$ m along the specimen surface, at which point they had a greatly damped oscillation about zero as the distance from the center of contact continued to increase.

Directly centered under the area of contact, concentrations of compressive σ_{xx} stresses were found. From the figures it can be seen that the peak compressive σ_{xx} stress was always located on the center of the contact. The figures at the end of the appendix

shows how this point of maximum compressive stress changed with the different test cases. The trend was linear except for tests using the smaller radii fretting pads and had lower pressure loads and correspondingly smaller contact semi-widths. The .0106m radius test actually had the greatest compressive stress concentration of all radii numerically analyzed.

Also interesting to note when looking closely at the σ_{xx} stresses in the step 1 analysis were the ridges along the stress distributions as they transitioned from the maximum compressive stress to the maximum tensile stress. They were only present in the tests that had larger radii fretting pads. These ridges seemed to decrease in magnitude as the radius of curvature (or pressure load or contact semi-width) decreased. They could be best observed on the 0.0508 m σ_{xx} distribution curve and they did not seem to be present on the 0.00762 m curve. They seemed to indicate that the transition from compressive to tensile stresses is not always smooth and the distribution was not a simple parabola.

The step 1 finite element stresses in the σ_{yy} direction seemed to be what one would expect and could predict. Each test produced a Hertzian ("bell curve") pressure distribution as can be seen in the figures. The center of contact had the greatest magnitude of σ_{yy} stress. This point represents the peak contact pressure and will be discussed in greater detail in the results chapter of this study. From the peak contact pressure, in the P-only case, the curve is symmetric in both the positive and negative x-direction. σ_{yy} decreases from the peak contact pressure until it approaches zero value at the edge of contact.

The σ_{yy} versus x distribution curve along the specimen surface was used to determine the finite element value for contact width. On the curve, the length of the specimen surface that experiences non-zero σ_{yy} values is representative of the contact region. This makes logical sense because when the fretting pad is pressed against the substrate the part that actually comes into contact with the substrate generates pressure. Where the pad no longer touches the specimen, there is no σ_{yy} stress. To be technical, the finite element σ_{yy} distribution curves did not go directly to zero at the edge of contact, but instead approached zero and there was a dramatic change in curve slope (the curves generated from the analytical program did go directly to zero). The contact widths were measured from the various test cases and compared to the theoretical values of the contact width. From comparison of the data, it can be seen that the theoretical values of contact width only varied from the finite element values by 1.56% at most (which was the case in the 0.0508 m radius test). Good agreement was shown between the numerical and analytical approaches for contact width.

There are two primary noticeable differences in σ_{yy} distributions between each of the different test cases. The first noticeable difference between each test is the width of these curves where the stress value is not zero. The different curve widths represent the different contact widths of each of the tests. The second noticeable difference between the curves is that the tip of each bell curve is at a different magnitude. This means that the peak contact pressures varied between each test. The analysis showed that as the contact semi-width decreased, the peak contact pressure ever so slightly decreased as well. According the analytical formulas the peak contact pressure should have held constant at 5.269E+8 Pa for the given global boundary conditions. Maintaining a constant

peak contact pressure while varying other parameters was one of the aims of this study, but the finite element analysis shows that the peak contact pressure was probably not held exactly constant. The variance of finite element calculated peak contact pressure from the analytical solution is greatest in the 0.00762 m radius pad test, with a difference of 2.219% for the normal load only case.

The third stress output by the finite element program for the step 1, pressure load only situation, was shear stress, τ_{xy}. It is commonly known that the normal stresses and shear stress at a point are linked. Incidentally a good illustration of this relationship is Mohr's Circle. The ridges that were noted in with the σ_{xx} curves are probably an effect of the shear stresses present. Shear stress distribution changed very little for the different cases tested. The ranges of the spiked areas correspond to the different contact widths. The cause of the spikes in shear stress has not yet been explored.

Iyer's finite element model and the models for this study revealed details about the tests that were not evident in the analytic model previously used by Nowell and Hill. A result of the numerical analysis was the presence of a tensile stress concentration on the substrate generated by just the normal load, P, even if the bulk nominal stresses were not being applied. This local stress, σ_L, produced solely by the normal load, P, was the same for the same magnitude of normal load independent of cylindrical radius. According to Dr. Mall, this is also true for the analytical solution and not significant. Furthermore, the ratio of the peak σ_{xx} to P was held constant throughout the different radii pad tests and respective different normal loads. The stress concentration was found to be located just outside the contact boundary. The σ_{yy} distributions could be used to

measure the numerical simulation's computed values of contact width and peak contact pressure. Examination of the shear stresses revealed spikes within the region of contact.

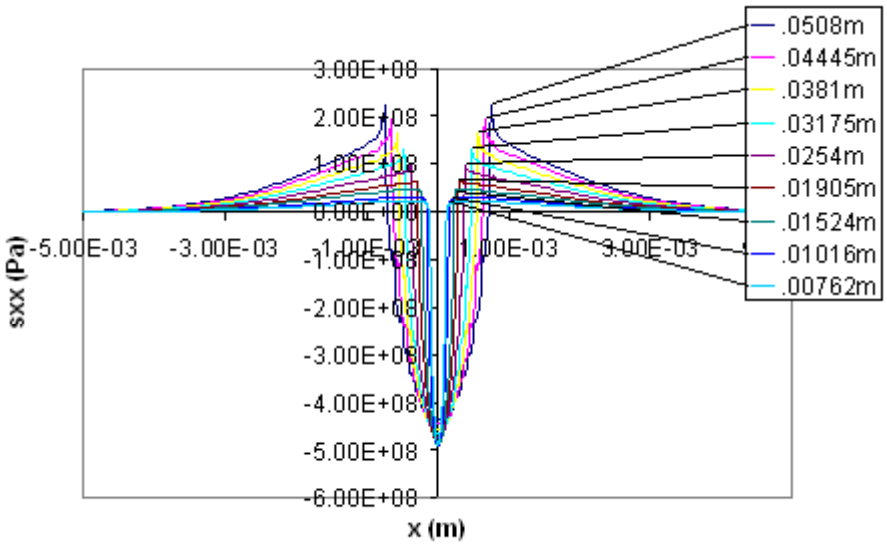

Figure A4.1 P-Only Sxx Distributions Along the Substrate Surface Centered About the Center of Contact.

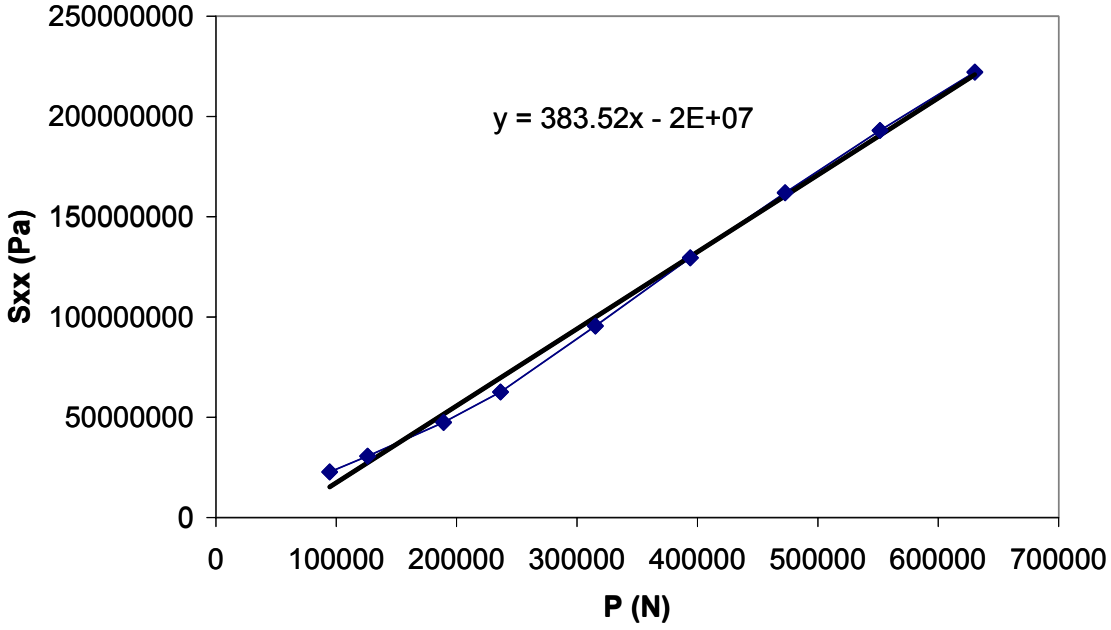

Figure A4.2 P-Only Maximum Tensile Stresses Versus Applied Pressure Load and Equation of Linear Regression. (Note: each different pressure load is also with a different radius fretting pad, yet the ratio of Sxx to P is essentially linear.)

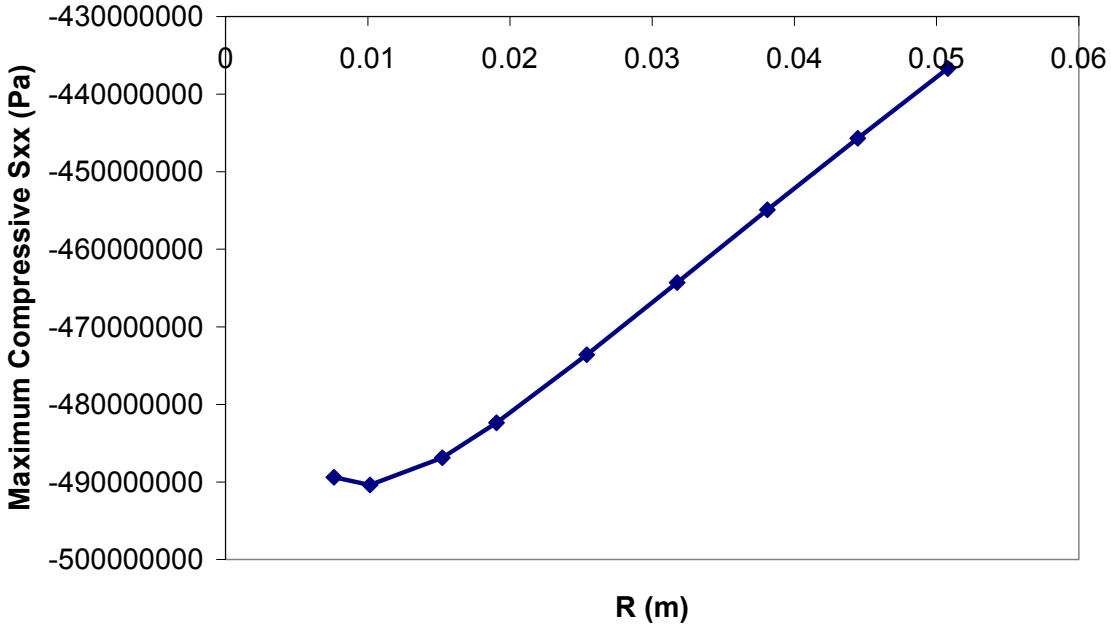

Figure A4.3 Maximum Compressive Sxx Versus Fretting Pad Radii.

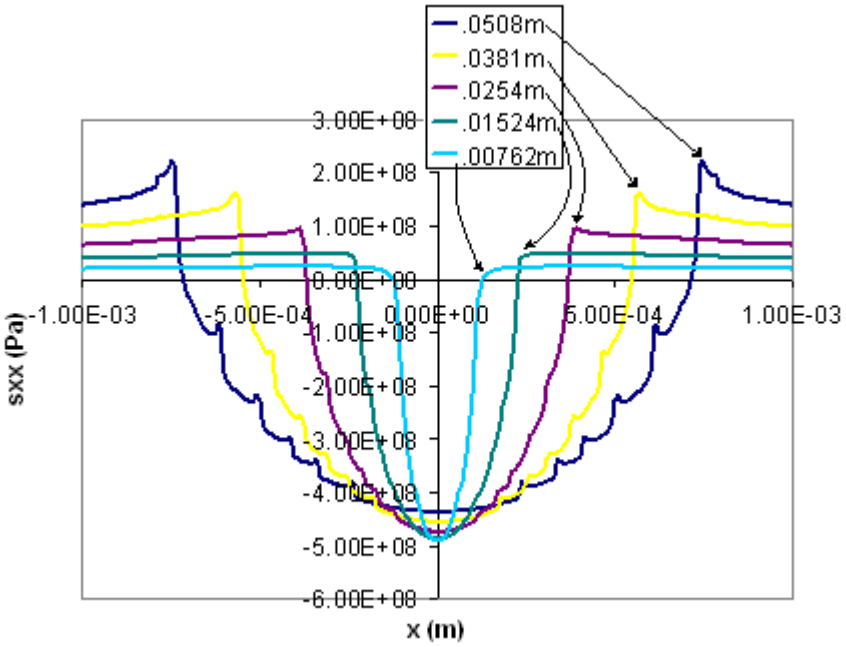

Figure A4.4 The trend from ridged to smooth transition on the curve form compressive maximum to tensile maximum in the P-only analysis of 5 different radii fretting pads.

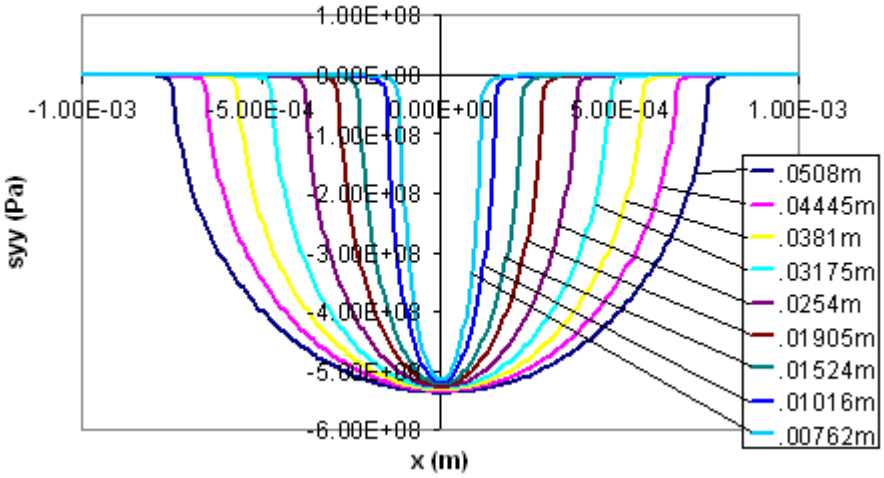

Figure A4.5 Syy Versus X Position Along the Specimen Surface for 9 Different Radii Fretting Pads With Only Pressure Load Applied.

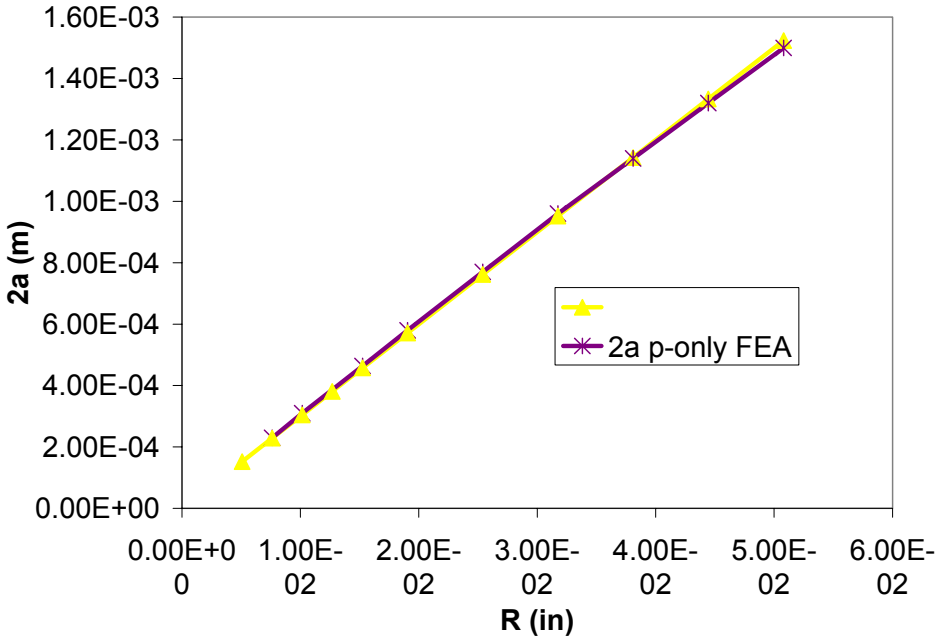

Figure A4.6 Contact Widths from Finite Element Output for Pressure Force Only Case and the Theoretical Contact Widths from the Analytical Solutions Versus Pad Radius

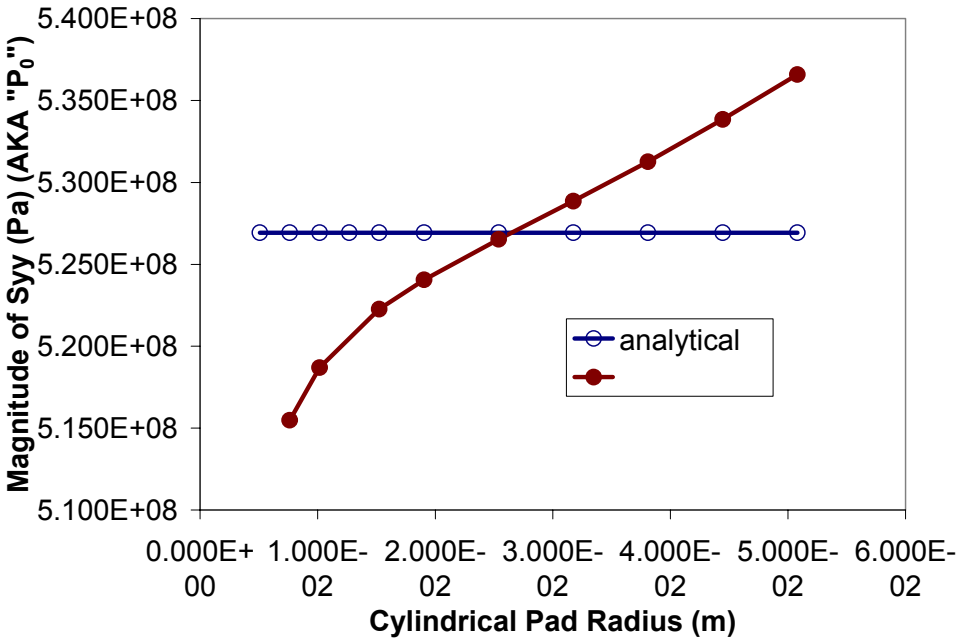

Figure A4.7 Magnitude of the Minimum Value of the Syy (Peak Contact Pressure) Versus Pad Radius.

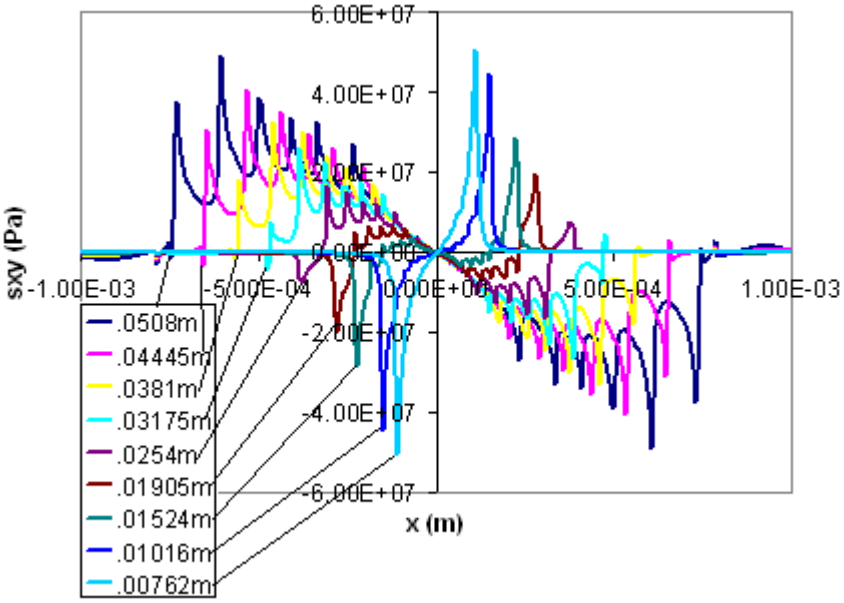

Figure A4.8 Sxy Versus X-position Along the Contact Surface for 9 Different Radii Fretting Pads With Only Pressure Load Being Applied.

A5 Analysis of FEA Combined Loading Stresses:

The second stage of the finite element analysis is to apply the bulk nominal stresses to non-fixed end of the substrate while continuing to apply the normal pressure load. For each radius test, a step 2 finite element analysis is performed twice, for both a minimum and maximum loading case. The maximum or minimum bulk stress and its respective Q value, determined from the actual test, are input along with the normal load and geometric constraints. Stress distributions for the minimum and maximum loading cases are output. It is assumed that loading cases in between the maximum and minimum loadings will not produce stress distributions or displacements that are outside of those found for the two extreme loading states. These stress distributions were the ones compared to the analytical FORTRAN program solutions in the validation section. The figures show an example typical of the loading distribution of sxx, syy, and sxy under Qmax and sN,max for both the analytical and numerical solution methods. The figures show an example of the minimum loading case stress distributions along the substrate surface.

Of the three stresses looked at, sxx, syy, and sxy, the stress distribution in the syy direction changed the least with the application of bulk stresses (which in turn caused Q loads) to the free end of the specimen. As was demonstrated in the normal load only section, from the syy distribution along the x-axis of the substrate specimen graph both the peak contact pressure and contact width (half of which is the contact semi-width, a) can be determined. The syy distributions of the combined loading stage of the finite element analysis are also valuable for measuring the eccentricity caused when bulk stresses are applied.

The figures at the end of this appendix section show the syy distribution for the three cases of loading for the 0.0254 m radius pads test case. The magnitude of peak contact pressure, the maximum compressive syy stress, changed very little between normal load only, maximum, and minimum combined loading cases. The peak contact pressures were –5.27001E+8 Pa for the maximum loading conditions, –5.26960E+8 Pa for the minimum loading case, and –5.26525E+8 pa for the normal load only case. The difference between these values is negligible. The differences in the contact width were also slightly different between loading conditions, but also negligible and not worth close examination.

It significant is that the peak contact pressures as well as the syy curves shifted to different points along the substrate surface for each of the different cases. The distance of this shifting from the P-only, or analytical case is called eccentricity, e. Whereas the applied bulk stress cases in the finite element model both have eccentricity. The FORTRAN program Syy curve almost perfectly overlaps the P-only FEA curve. The only real difference between the two curves is at the edge of contact. The FORTRAN program's Syy curve goes immediately to zero outside of the contact region. But, the FEA's Syy curve does not go directly to zero outside of the contact region. Instead it leaves the parabola shape at the edge of contact and slowly ascends back to zero. The cause of this eccentricity is illustrated in the figures.

The general trend of how eccentricity changed for the different test cases can be seen in the figures. For the large fretting pad radii, the eccentricity was greater than for smaller radii pads. This makes sense. Firstly, if eccentricity is caused by the pads rolling such that the contact region changes, as was shown in the figures, then pads of smaller

radii would not be able to roll as far and hence have small eccentricity. Furthermore, if it is the Q force that causes the pads to rotate, through the translation of pressure on the fretting fixture causing it to flex, then a greater magnitude of Q force would cause a greater pad rotation. In the smaller radii test cases, the magnitude of Q was also proportionally reduced. As this eccentricity becomes more and more prevalent, the locations of stress peaks (not only on the syy distribution) diverge between the analytical and numerical models' different stress distributions.

Once the bulk stresses were applied to the simulated fretting specimen, the sxx stress distribution was no longer symmetric about the original center of contact. Instead the sxx distributions were asymmetric and their general shape was flipped between maximum and minimum loading cases. The figures show an example of the three types of sxx distributions looked at for each test case. The normal load, P, only case was discussed in the P-Only Stress Distributions section. Because both the maximum and minimum bulk stresses are greater than zero, the sxx distribution would never transition through the P-Only loading case in an actual test. Instead the stress distribution oscillates between the maximum and minimum combined loading condition.

Traveling from right to left along x-axis of the maximum combined loading sxx curves, certain trends can be noted. The far right side of the curve is flat. The maximum combined loading sxx curve is level at 550 MPa. This section of the curve, which was cut from the figures because it was relatively uninteresting, represents the length of substrate specimen that experiences the full stress of the bulk loading but is far enough from the normal load not to feel its influence. As the curve moves further to the left, the effects of the normal load begin to play a role. In the 0.0254m radius example, from the

Syy curve of maximum loading, the edges of contact were measured to be at x=-4.1E-4 m and x=3.597E-4 m. The maximum value of the sxx distribution for maximum combined loading was found to be 1.358E9 Pa just inside the edge of the contact area at x=3.473E-4 m. By looking at the displacements curve, through a process which will be discussed later, the the stick zone was measured to be from –2.65E-4 m to 1E-5 m for the maximum loading case. The distance from the edge of contact to the stick zone is the slip zone. In the slip zone, viewing from right to left, the stress quickly hit the peak and then decend becoming less and less tensile until they hit the compressive "plateau." The plateau in the center of the contact region of the curve corresponds with the stick zone. On the left side of the stick zone is the second slip zone whose stresses continue to drop and become more compressive until they hit a compressive peak. In the case of the .0254m radius this compressive peak is –4.526E+8 Pa and is located at x=-3.659m from the center of the coordinate system. This is just inside the contact region on the negative x side. From here the stress levels off at the value that is the bulk stress minus the stress cause by the Q force.

Traveling from right to left along x-axis of the minimum combined loading sxx curves, similar trends noted in the maximum loading case can be noted. The minimum combined loading sxx curve is level at 18 MPa on the far right of the curve. This section of the curve represents the length of substrate specimen that experiences the full stress of the bulk loading but is far enough from the normal load not to feel its influence. As the curve moves further to the left, the effects of the normal load begin to play a role. The minimum loading conditions contact region was found to be from –3.60E-4 m to 4.09E-4 m. Instead of hitting a maximum tensile peak on the positive x side of the coordinate

system, the sxx curve for the minimum load case drops compressive first. The maximum compressive load along the substrate surface was –7.943E+8 Pa located at x=3.659E-4 m. The curve then becomes less compressive until it hits the plateau, which corresponds with the stick region. The stick zone was measured to be from- 1.35E-4 m to 2.4E-4 m for the minimum loading case. It is the negative-x slip zone that has the peak tensile stress in the minimum combined loading case. This peak tensile stress occurs just inside the contact region at x=-3.535E-4 m and has a value of 8.949E+8 m. From here the stress levels off to the value of the difference of the bulk stress and Q stress.

The figures show the Sxx curves for all the different radii test cases at their maximum loading conditions. Several trends can be noted. The width of the effected area of the curve decreases as fretting pad radius decreases. This is because the width of the contact area decreased with fretting pad radius for the tests in this study. Also, as the fretting pad radius increases, the length of the plateau area in the center of the contact region increases as well. This is because for the loading conditions in this study, contact stick zone size increases with fretting pad radius. Aside from the width changes, the curves all look basically similar. The magnitudes of their peak tensile Sxx stress values seem pretty close. But there does seem to be a slight trend that as the radius decreases, the peak Sxx stress also decreases.

One possible explanation for this third noted trend is that the decrease in peak Sxx stress has nothing to do with combined loading fretting conditions at all. Instead it might be reflecting the trend noted earlier, that the tensile stress concentrations located just on the edge of the contact zone in the normal load only case, as was noted by Iyer, decrease with decreasing radius. Using the concept of superposition it can be logically assumed

total Sxx as seen in the combined loading stress distribution is simply the Sxx caused by the normal load only case plus some Sxx cause by the bulk stresses and Q stresses plus some possible confluence effect. If the influence of this confluence effect is not significant in the total Sxx distribution, then the total Sxx minus the Sxx of the P-only case (shifted for to negate eccentricity effects) would be the Sxx of bulk stresses and Q stresses. Going back to the original explanation of the trend noted about the peak Sxx values for the different curves, if this difference was a result of the P-only stress concentrations, the values of the total Sxx peaks minus the P-only Sxx values at points equal distance from the contact edge would produce equal difference in all test cases. This exercise as attempted in the figures, but the evidence was not very conclusive. The corresponding P-only values to the peak maximum loading condition sxx values did not form a consistent trend.

As can be observed from the figures, the trends for the minimum loading case of the Sxx stress distributions are the same as maximum combined loading, except it is as if the stress distributions in the region of contact are flipped in the x-direction. This is because the Q, shear traction force, is in opposing directions for the maximum and minimum loading cases.

The third stress output from the finite element program Step 2 was shear stress, Sxy. The figures show typical stress distributions for the maximum and minimum combined loading cases as well as the normal load only loading case. The maximum loading shear stress distribution is negative over the contact area and the minimum is positive. Both combined loading curves are basically parabolic in shape except for a "dent" over the vertex. This same dented-parabola shape can be seen in all of the

different radii test cases. The dent length corresponds well with the plateau on the Sxx curves and is therefore and effect of the stick zone.

At the end of this section, there is a graph containing the Sxy curves of six different radii test cases for the maximum loading conditions. The most interesting trend on this graph is the location and shape of the dents. They seem to all have one side starting from close to the same position, which is the peak minimum value of shear. The slopes of the dents are initially all the same for their ascent to a local peak Sxy. When they reach that local peak, which is different for each test case, they then curve back to a local minimum and then return to their respective the greater parabolic curves. The other three radii, which were analyzed using the finite element analysis, did not have Sxy distribution curves that met this trend.

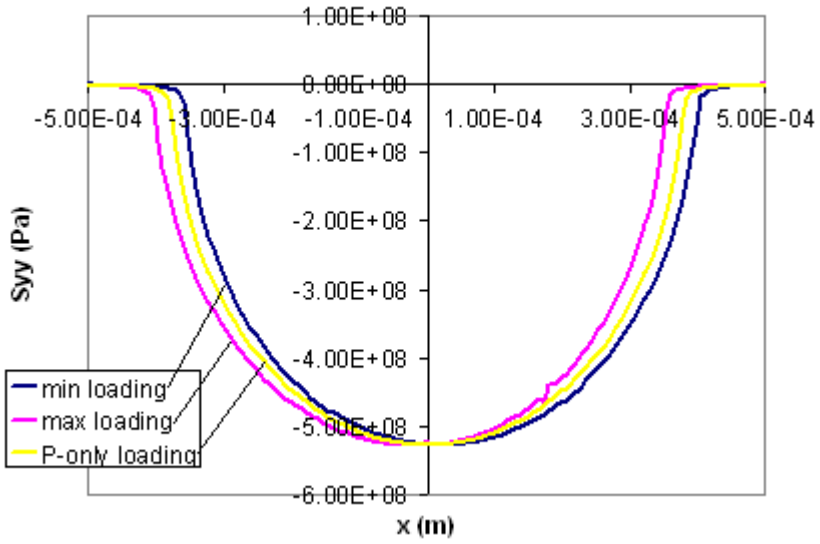

Figure A5.1 Syy Stress Distributions From the Finite Element Model for the Step 2 Maximum and Minimum Combined Loading Case Compared to the Step 1 Normal Load Only Case from the .0254m Pad Radius Test.

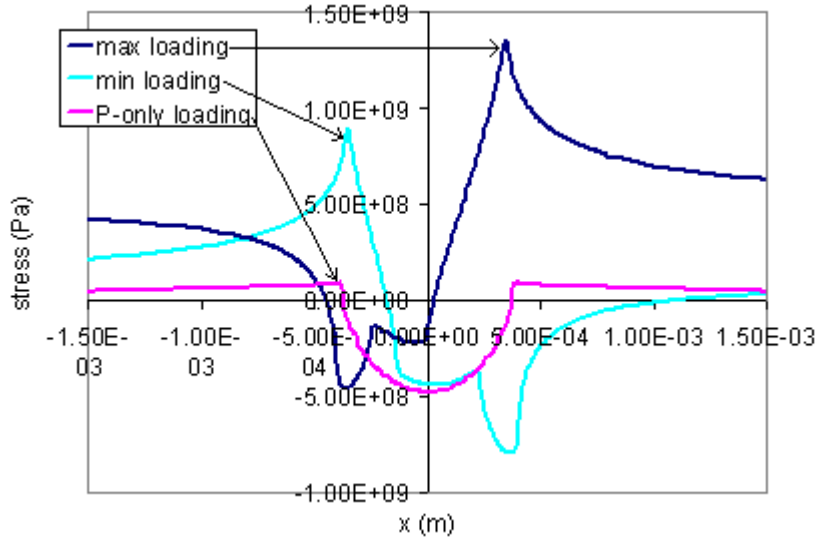

Figure A5.2 Sxx Stress Distributions From the Finite Element Model for the Step 2 Maximum and Minimum Combined Loading Case Compared to the Step 1 Normal Load Only Case from the .0254m Pad Radius Test.

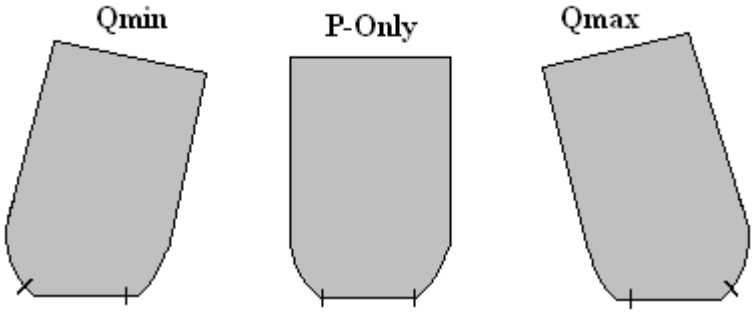

Figure A5.3 Shifting Contact Region

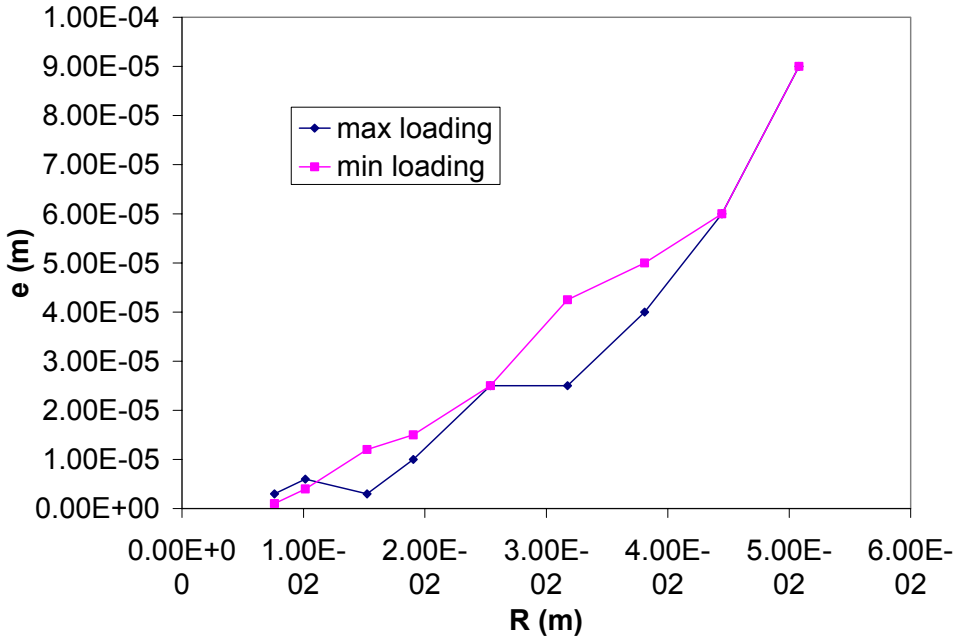

Figure A5.4 Eccentricity of the Maximum and Minimum Combined Load Cases from the Finite Element Output from Finite Element Analysis

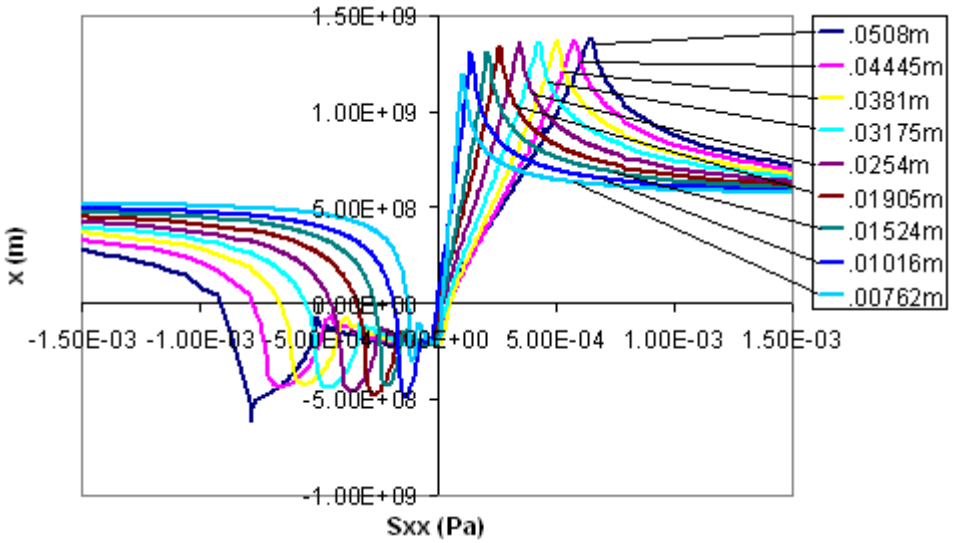

Figure A5.5 Sxx Distributions for Maximum Combined Loading Conditions.

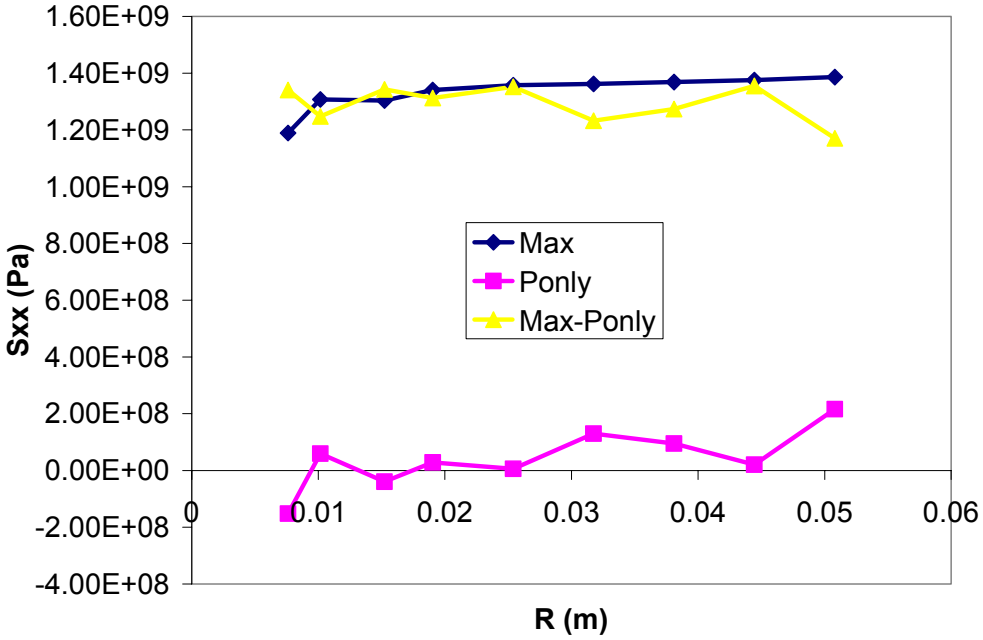

Figure A5.6 Maximum Tensile Sxx Stresses for Maximum Loading, P-Only Loading Sxx at Same Distance from Edge of Contact, and Difference

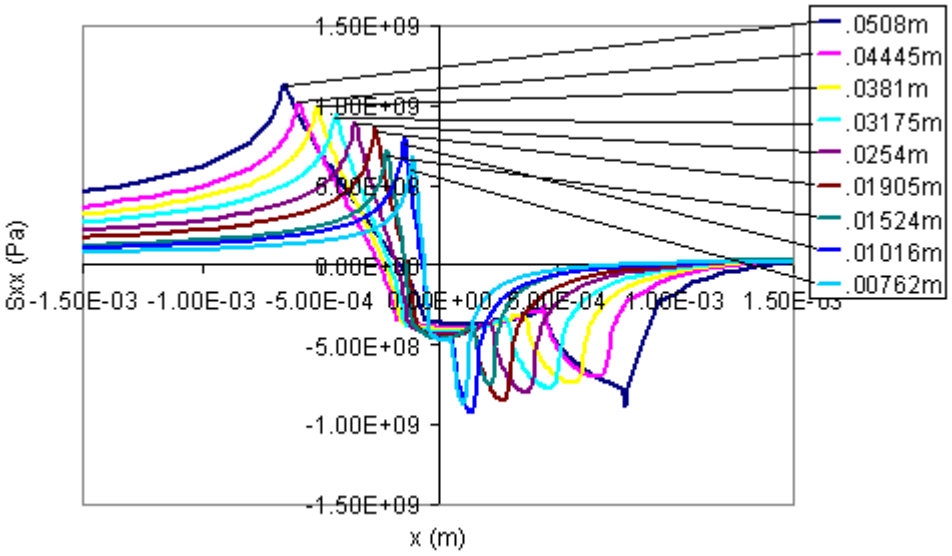

Figure A5.7 Sxx Distributions for the Minimum Combined Loading Conditions.

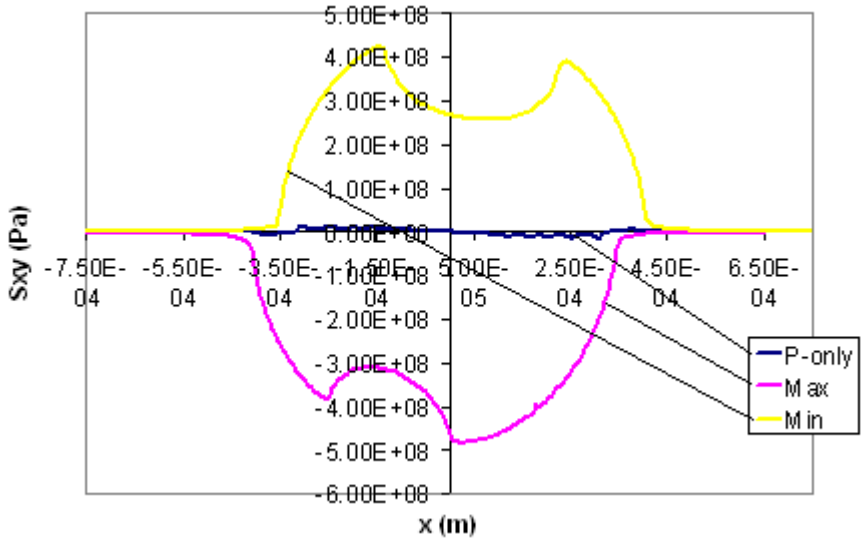

Figure A5.8 Example of Shear Stress Distributions Along Substrate Surface For Different Types of Loading Conditions (R=.0254m Test Case)

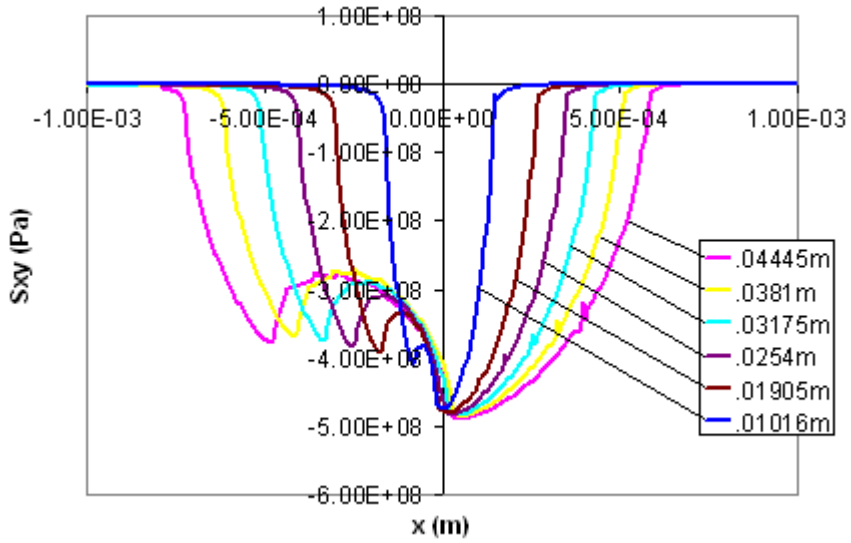

Figure A5.9 Sxy Distributions for the Maximum Combined Loading Conditions.

A6 Analysis of FEA P-only Displacements:

Another output of the finite element analysis was displacements for the Step 1, normal load only, and Step 2, combined loading cases. As stresses were applied to the mesh of elements, nodal points were displaced. Through comparison of the displaced nodes with their original nodal location, important trends and values from the different test cases can be studied. Nodal displacements of the specimen surface as well as nodal displacements along the pad surface were analyzed. The displacement output is given in terms of u1 and u2 values. U1 corresponds with displacement in the x-direction and u2 corresponds to the y-direction.

As normal load was applied, for the Step 1 finite element analysis, the contacting bodies displaced. The figures show how both the pad surface nodes and the substrate surface nodes, of the 0.01524 m pad radius test case, displaced relative to their respective zero loading positions across the total surface length analyzed by ABAQUS. Both curves are symmetric about the middle. The y-displacements are Gaussian in shape. As was expected the substrate deflected the greatest distance at the center of contact. These displacements go to zero along the surface further from the center of contact. The figures illustrates the substrate deflection in all the different test cases. Normal load was applied in proportion to pad radius such that the peak contact pressure was constant for all tests. Interestingly, while the peak displacements are not the same magnitude, the length of the substrate experiencing non-zero u2 displacements was approximately constant throughout the different test cases. The pad displacements mirror the specimen displacement as was shown in the figures

The figures display typical displacements in the u1 direction for the pad and substrate as a result of only normal loading. Both curves are "flip-symmetric" about the center of contact. The displacements level off as the move distant from the contact area. Because it was a boundary condition that the negative x end of the specimen in fixed, the displacement in the x-direction close to that boundary is essentially zero. The displacements change from zero in the proximity of contact and become positive in increasing, then decreasing, and then increasing relative displacements. Because this is a graph of total displacement experienced by points along the curve slopes in this curve indicate direction of relative displacement. The reason these curves are not symmetric is because the positive and negative ends of the specimen are experiencing different boundary conditions. The figures at the end of this section show how the x-direction displacements change for the different test cases. The magnitude of displacements increases with increasing pressure load and the central negative sloped region changes with changing contact width, but the same general trend is kept throughout all cases.

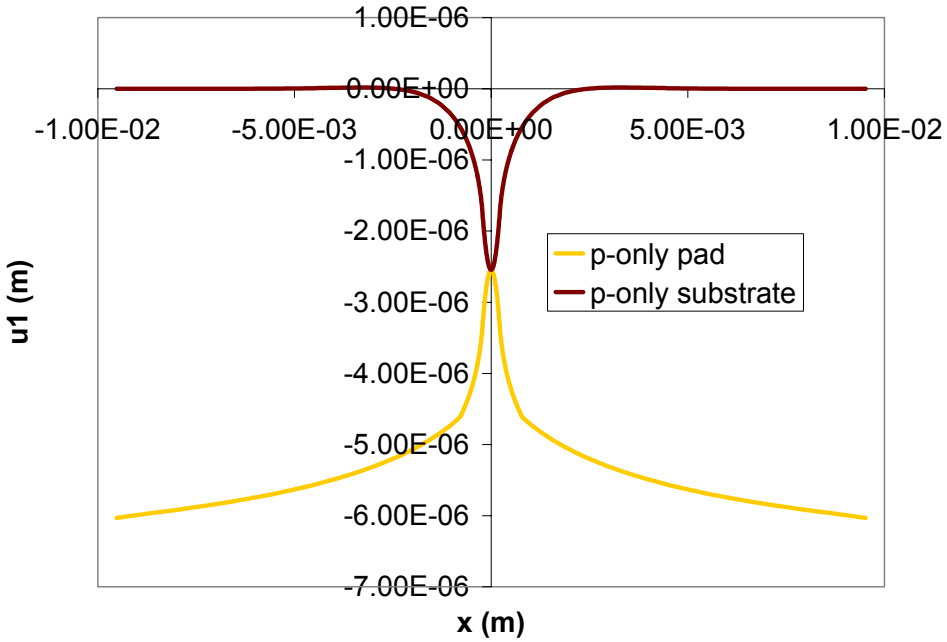

Figure A6.1. u2 (Along Y-Axis) Displacement of the Pad Surface and Substrate Surface as a Result of Normal Load Only for the .01534m Radius Fretting Pads Test Case

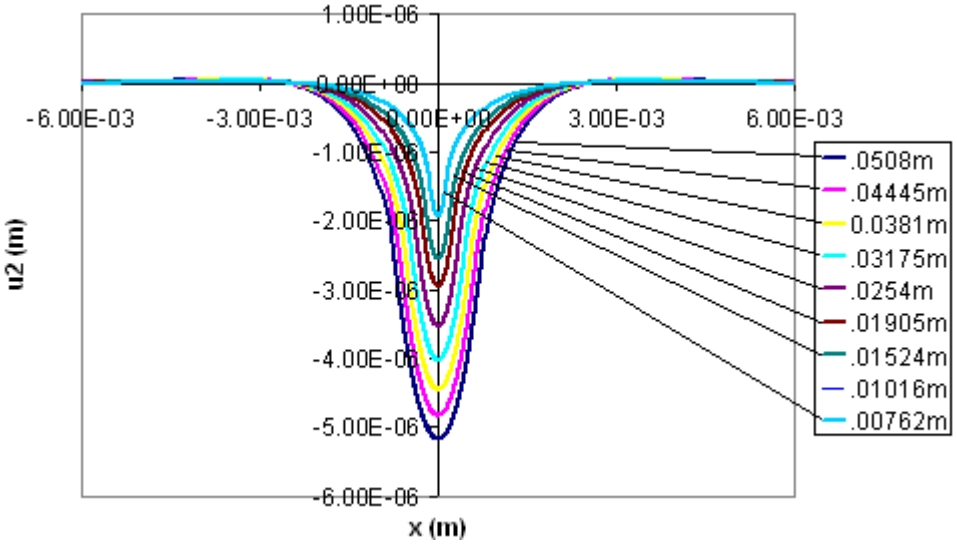

Figure A6.2. u2 Displacement of the Substrate Surface for the Various Test Cases as a Result of Normal Load Only

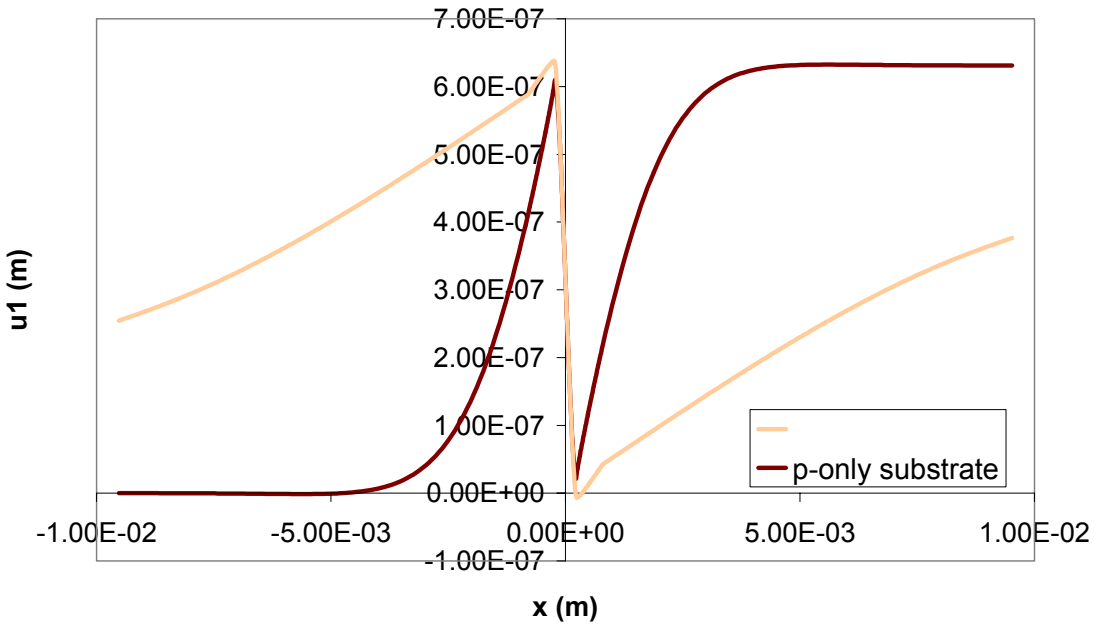

Figure A6.3. u1 (Along X-Axis) Displacement of the Pad Surface and Substrate Surface as a Result of Normal Load Only for the .01534m Radius Fretting Pads Test Case

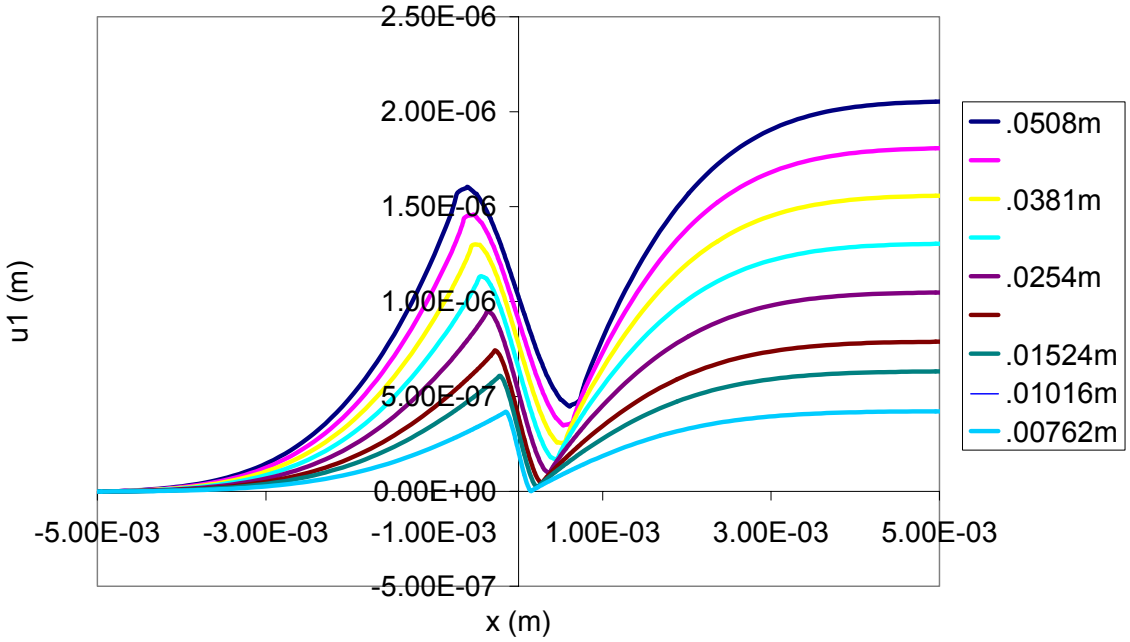

Figure A6.4. u1 Displacement of the Substrate Surface for the Various Test Cases as a Result of Normal Load Only

A7 Analysis of FEA Combined Loading Displacements:

The nodal displacements of the pad surfaces and substrate surfaces were analyzed under the step 2, minimum and maximum combined loading conditions. Several trends helping to explain what is really happening in fretting fatigue can be noted. A figure shows how the combined loading conditions effected the displacements in the .01524m test case.

There are two primary differences in between the combined loading cases and the normal load only case in the u2 distributions. The first noticeable change is that the Gaussian distributions in of pad and substrate displacements are slightly skewed. This dissymmetry reverses itself between the maximum and minimum loading cases, just as the Q force switches direction between the maximum and minimum loading conditions. Secondly, the displacements no longer return to the zero displacements line. Instead they level off at negative displacements, the magnitudes of which are proportional the Sxx stress experienced by the respective section of the sample. This negative displacement is mostly caused by the Poisson ratio squeezing effect generated from tensile stresses. Further evidence for the Poisson ratio explanation for this phenomena can be seen in a figure, which illustrates the substrate y-direction displacements for the maximum loading conditions of all test cases. On the positive x side of the curves all u2 distributions level off at the same magnitude of displacement. However on the negative x-side, the distributions level off at different magnitudes of y-displacement. This is because Q is different for each test case, which means that the combined stress level, bulk stress minus stress from shear traction, which is experienced by the negative x side of the distributions

is different as well. These different stress levels translate to different displacements due to the Poisson effect.

The u1 displacement distributions of the pad and substrate for maximum and minimum loading conditions can be seen in a figure. Unlike the u2 displacement distributions, the u1 distributions clearly show the influence of the contact region. This trend of the u1 displacements in the contact region will be examined closely in the section discussing slip amplitude. Another trend in the u1 distributions, which can be viewed in a figure at the end of this section, is that while the one end of the substrate remained fixed at zero displacement, the other end of the substrate extended to different lengths of x-direction displacement. This was again probably the influence of the different Q values. Whereas there are differences in the slopes on the left side of the contact region, where Q influences the combined stress, the u1 displacement distributions are all parallel on the positive x side of the contact region, where the stress is just a function of bulk stress, which was constant for every test in this study

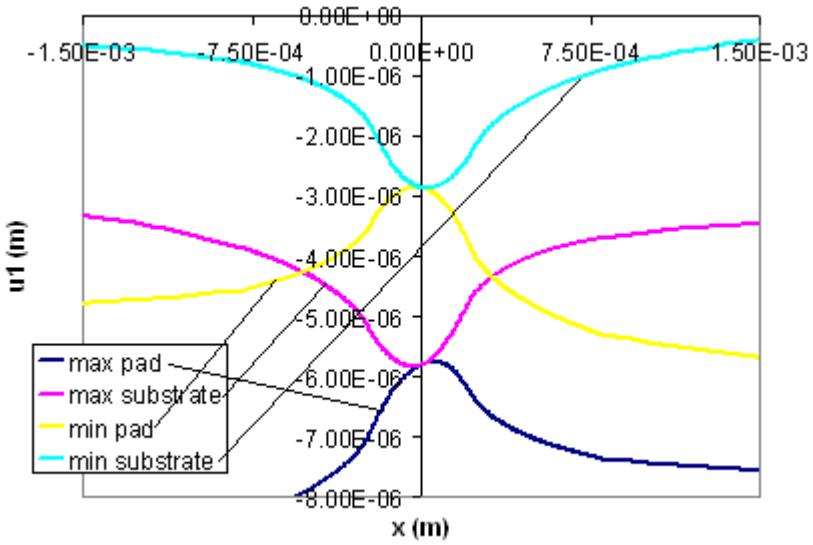

Figure A7.1. u2 (Along Y-Axis) Displacement of the Pad Surface and Substrate Surface as a Result of Normal Load, Minimum and Maximum Combined Loading for the .01534m Radius Fretting Pads Test Case

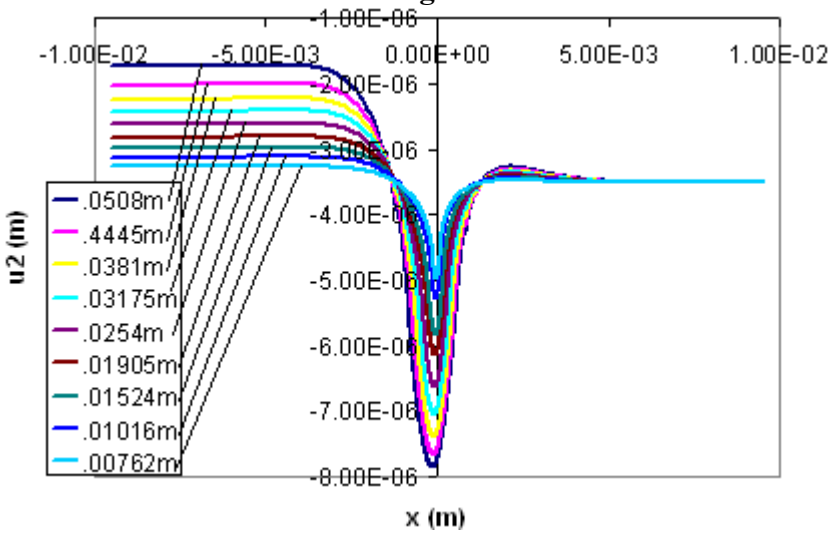

Figure A7.2. u2 Displacement of the Substrate Surface as a Result of Maximum Combined Loading for All Test Cases

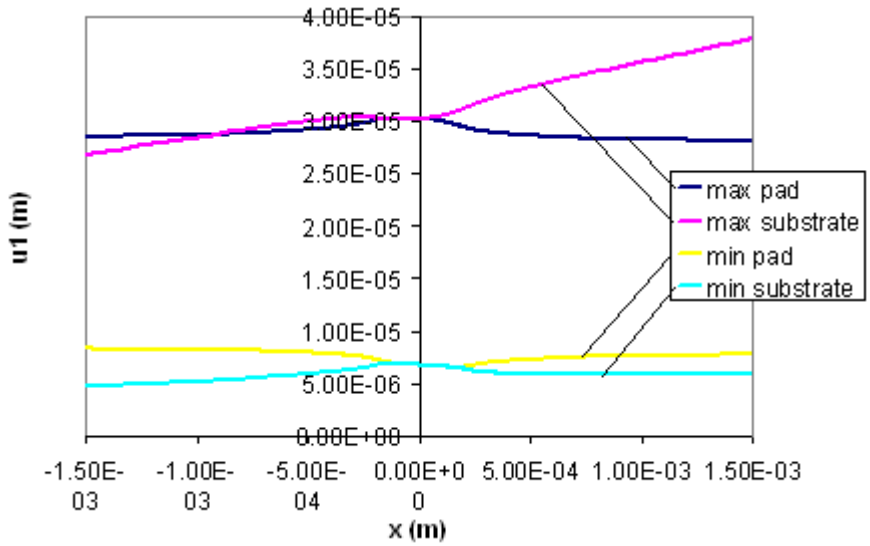

Figure A7.3. u1 (Along X-Axis) Displacement of the Pad Surface and Substrate Surface as a Result of Normal Load, Minimum and Maximum Combined Loading for the .01534m Radius Fretting Pads Test Case

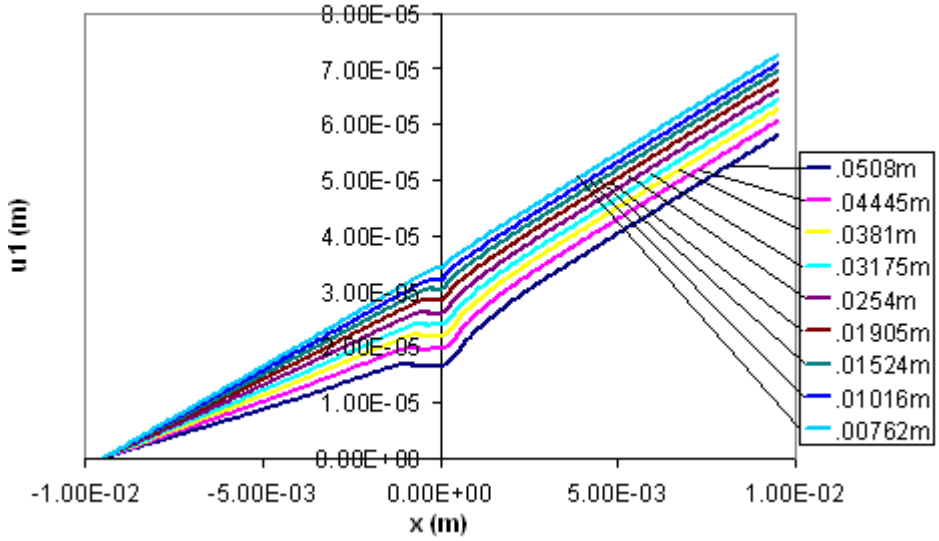

Figure A7.4. u2 Displacement of the Substrate Surface as a Result of Maximum Combined Loading for All Test Cases

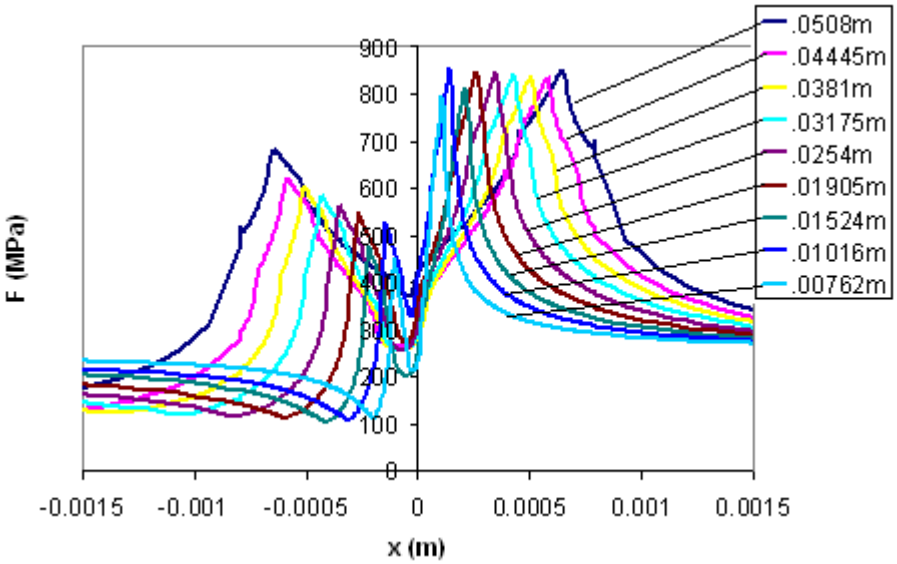

Figure A7.5. Findley Parameter Distribution of the Different Pad Radii Tests

A8. Critical Plane Based Fatigue Predictive Parameter Plots:

The following are plots of the maximum values of these parameters and Q/P:

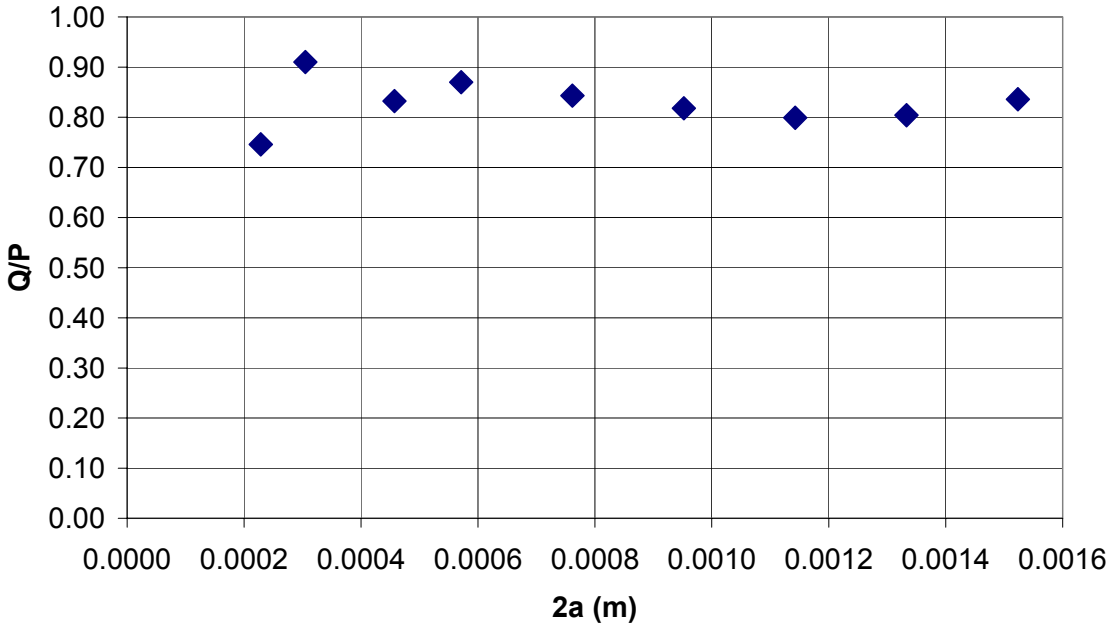

Figure A8.1 Q/P Ratio of Inputs to the Finite Element Analyses VS Contact Width

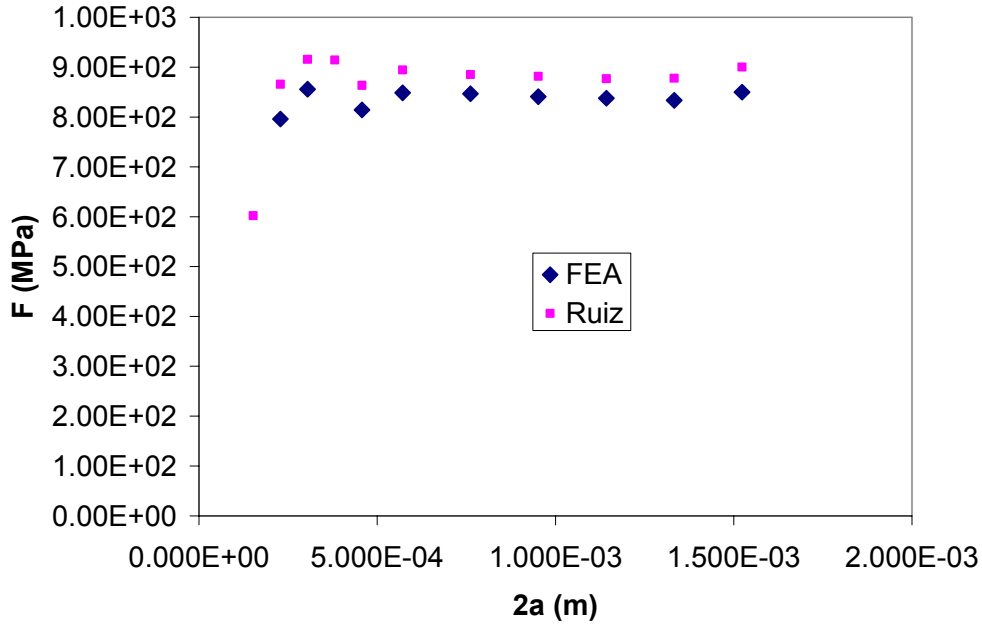

Figure A8.2 Maximum Findley Parameter Value from FEA and Analytical Program Output Versus Contact Width

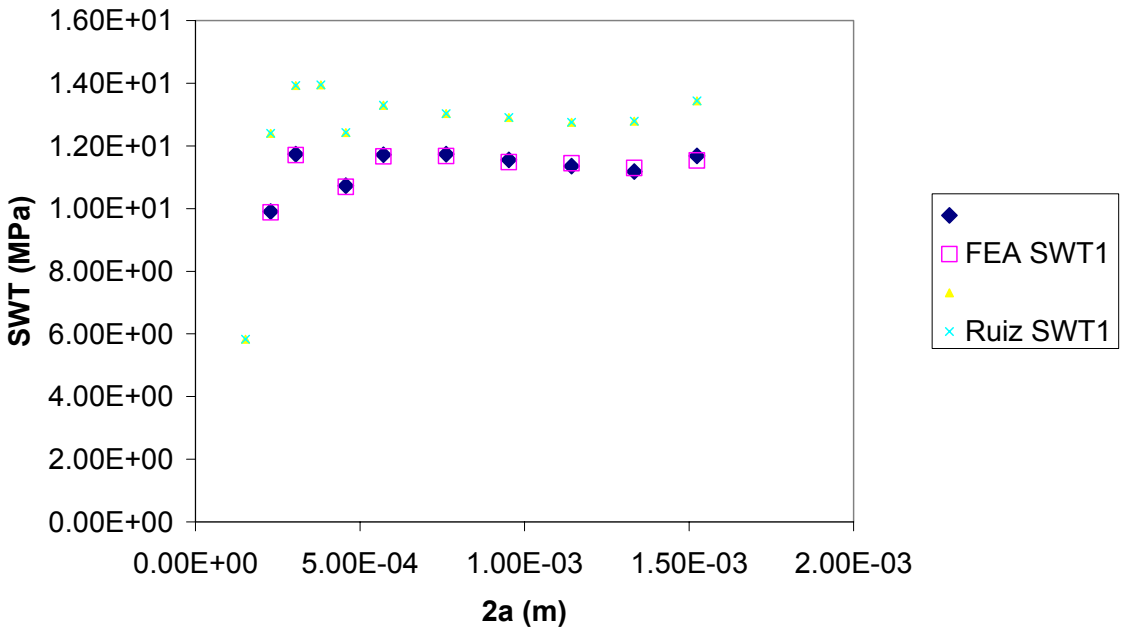

Figure A8.3 Maximum Smith-Watson-Topper 1 & 2 Values from FEA and Analytical Program Output Versus Contact Width

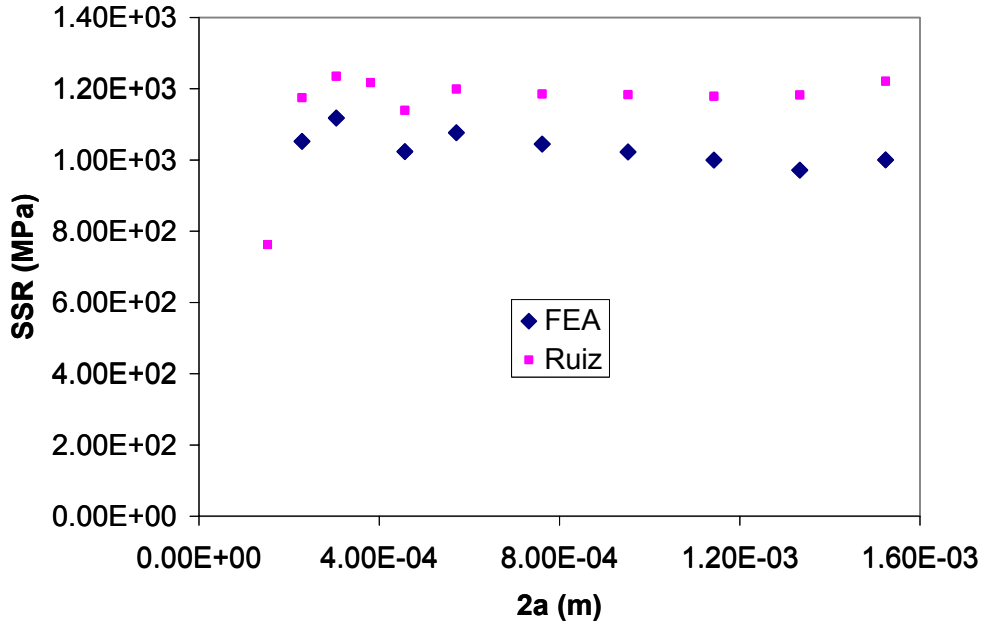

Figure A8.4 Maximum Shear Stress Range Values from FEA and Analytical Program Output Versus Contact Width

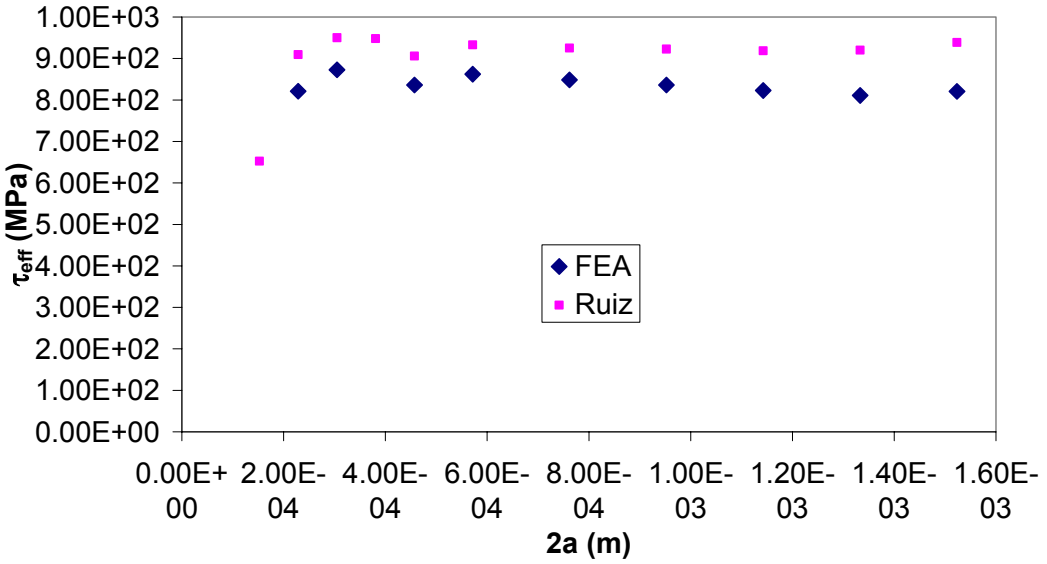

Figure A8.5 Maximum Effective Shear Stress Range Value from FEA and Analytical Program Output Versus Contact Width

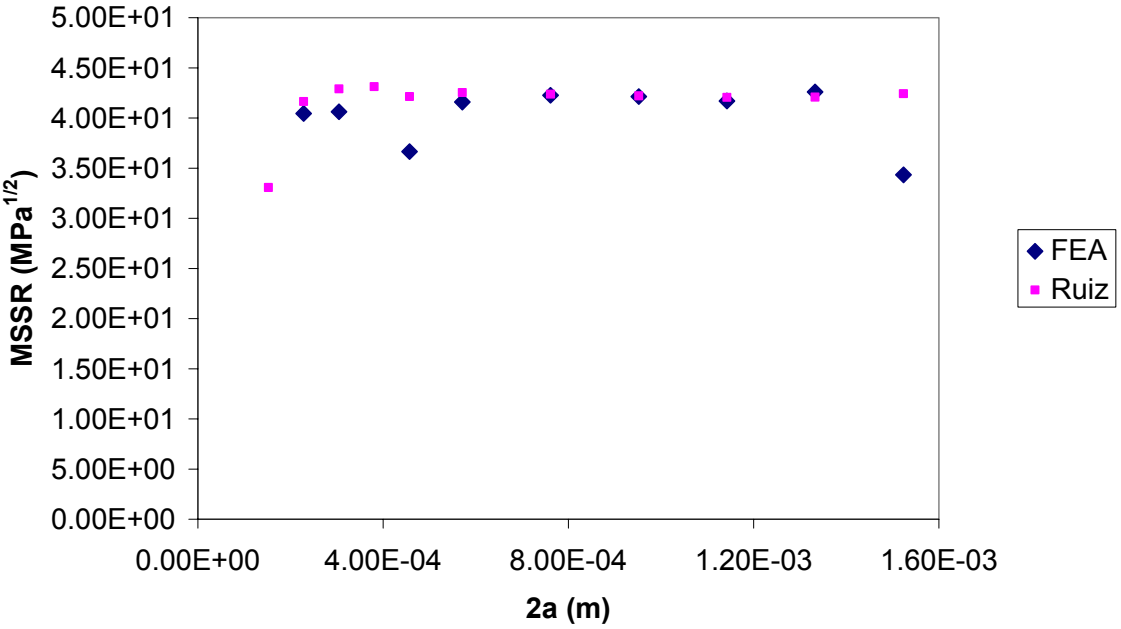

Figure A8.6 Maximum Modified Shear Stress Range from FEA and Analytical Program Output Versus Contact Width

A9: Comparing the Stick, Slip, and Total Contact Zone Sizes

The ratios of the stick zones size to total contact were determined, as shown in figure A9.1. The change in size of the stick zone to changes in total contact width was almost a linear relationship. However, the ration of the 1st slip zone, b1 as shown in Figure 2.3, to the total contact width stays constant. This trend leads one to the idea that the stick zone would eventually not exist in proportion to the slip zone as the contact width decreased towards zero. The absence of a stick zone would mean that gross sliding was occurring.

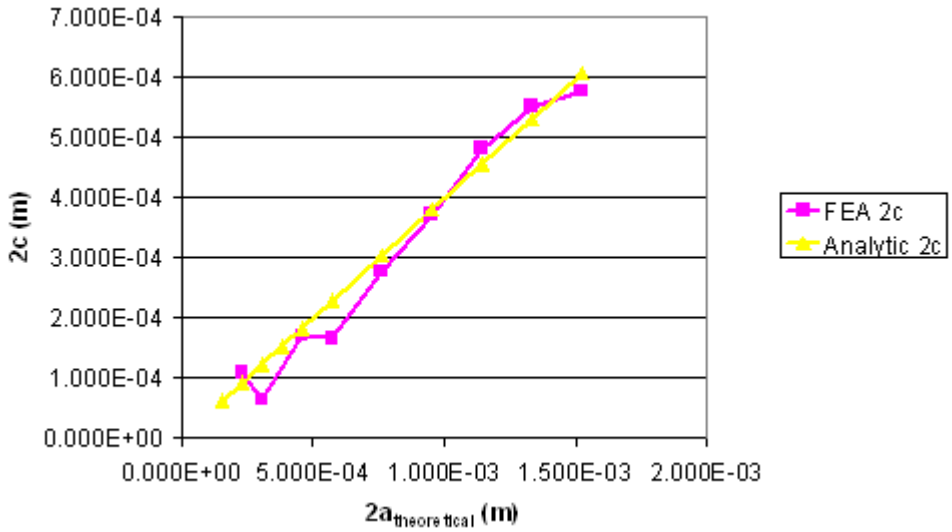

Figure A9.1. Stick Zone Width Versus Total Contact Width

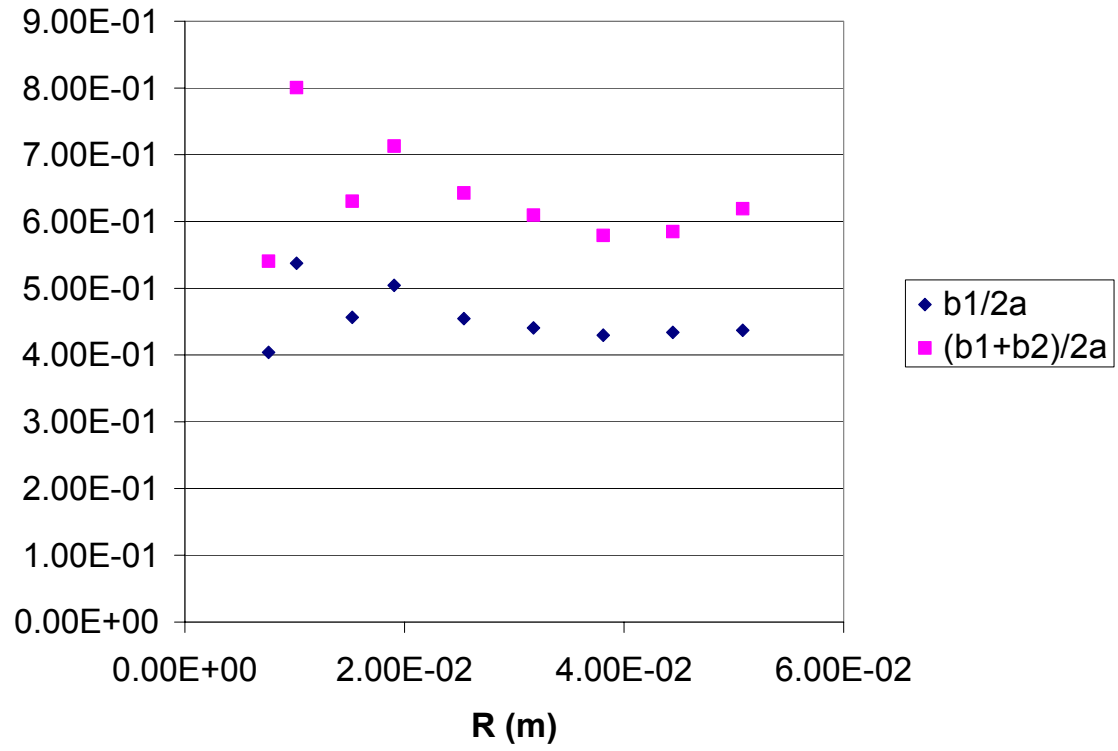

Figure A9.2. Ratio of Slip Zone Widths to Total Contact Width Versus Pad Radius

Bibliography

1. Bramhall, R. "Studies in fretting fatigue" D. Phil. Thesis, Oxford University, 1973.

2. Chan KS, Lee Y. FORTRAN program developed at South West Research Institute. Personal Communication of Lykins, 1998.

3. Cortez, Rebecca, Shankar Mall, Jeffrey R. Calcaterra. "Investigation of variable amplitude loading on fretting fatigue behavior of Ti-6Al-V." International Journal of Fatigue 21 (1999) 709-717.

4. Dowling, Normal E. Mechanical Behavior of Materials: Engineering Methods for Deformation, Fracture, and Fatigue. From pg 400

5. Endo K, Goto H, Nakamura T. Bull JSME 1969:12:1300.

6. Fellows, L., D. Nowell, D. Hills, "Contact Stresses in a Moderately Thin Strip (with Particular Reference to Fretting Experiments)," 1995, Wear, Vol 185, 235-238.)

7. Fenner, K.J., K.H.R. Wright and J.Y. Mann. "Fretting corrosion and its influence on fatigue failure, Proc. Int. Conf. On Fatigue of Metals." Institution of Mechanical Engineers, London, 1956.).

8. Goss G.L., Hoeppner D.W. Wear 1973;27:153-9.

9. H. Hertz, "Uber die Berugrung fester elastischer Korper," J. Reine Angew. Math., 92 (1882) 156 – 171.)

10. Hibbeler, R.C. Mechanics of Materials. pgs 452-4

11. Iyer, K, Mall S. "Effects of cyclic frequency and contact pressure of fretting fatigue under two-level block loading." Fatigue fract Engng Mater Struct 2000;23(4):335-46.

12. Iyer, K, Xue M, Kasinadhuni R, Bastias PC, Rubin CA, Wer JJ, Hahn GT. In: Chang CI, Sun CT, editors. Structural integrity in aging aircraft. New York: ASME. 1995.

13. Iyer K, S. Mall. "Analyses of contact pressure and stress amplitude effects on fretting fatigue life." ASME J Engng Mater Technol 2001. in press.

14. Iyer, K. "Peak contact pressure, cyclic stress amplitudes, contact semi-width and

slip amplitude: relative effects on fretting fatigue life." International Journal of Fatigue. 23 (2001) 193-206.

15. Jin, O. and S. Mall. "Effects of Independent Pad Displacement on Fretting Fatigue Behavior of Ti-6Al-4V."

16. Jin, O. and S. Mall. "Influence of Contact Configuration on Fretting Fatigue Behavior of Ti-6Al-4V Under Independent Pad Displacement Condition."

17. Johnson, K.L. Contact mechanics. Cambridge: Cambridge University Press, 1985.

18. Kuno, M., R. B. Waterhouse, D. Nowell and D. A. Hills, "Initiation and growth fretting fatigue cracks in the partial slip regime," Fatigue Fract. Eng Mater 12(5)(1989)387-398)

19. Lykins, Christopher Douglas. "An Investiation of Fretting Fatigue Crack Initiation Behavior of the Titanium Alloy Ti-6Al-4V." Dissertation December 1999.

20. Lykins, Christopher D., Shankar Mall, Vinod Jain. "An evaluation of parameters for predicting fretting fatigue crack initiation." International Journal of Fatigue. 22 (2000) 703-716.

21. Lykins, C.D., S. Mall, and V.K. Jain, "A shear stress based parameter for fretting fatigue crack initiation", Fatigue and Fracture of Engineering Materials and Structures.

22. Lykins, C.D., S. Mall, V.K. Jain. "Combined experimental-numerical investigation of fretting fatigue crack initation." International Journal of Fatigue 23 (2001) 703-711.

23. Namjoshi, Shantanu A., Shankar Mall, Vinod K. Jain, Ohchang Jin. "Fretting Fatigue Crack Initiation Mechanism in Ti-6Al-4V"

24. Namjoshi, S.A. "Parameters Program."

25. Nishioka K. Hirakawa K. Bull JSME 1972;15:135-44.

26. Nowell D., Hills, D.A. Mechanics of fretting fatigue. The Netherlands: Kluwer Academic Publishers, 1994.

27. Nowell, D., Hills, D.A. "A Discussion of: 'Peak Contact Pressure, Cyclic Stress Amplitudes, Contact Semi-width and Slip Amplitude: Relative Effects on Fatigue Life' by K. Iyer." 2 April 2001. International Journal of Fatigue 23 (2001) 747-748.

28. Nowell and Hill. “Crack Initiation Criteria in Fretting Fatigue.” Wear, 136 (1990) 329-343.

29. Pape, J.A., R.W. Neu. “Influence of Contact Configuration in Fretting Fatigue Testing.” Wear 225-229 (1999) 1205-1214.

30. Ruiz, C., P.H.B. Boddington and K.C. Chen. “An investigation of fatigue and wear in a dovetail joint.” Exp. Mech., 24(3)(1984)208-217.

31. Szolwinski MP, Farris TN. Wear. 1996:198:93-107

32. Walker, K. “The effect of stress ratio during crack proagation and fatigue fro 2024-T3 and 7075-T6 Aluminum”, Effects of Environment and Complex Load History on Fatigue Life. American Society for Testing and Materials, West Conshohocken, PA. STP 462, pp. 1-14, 1970.

33. Waterhouse, R.B. Fretting corrosion. New York: Pergamon Press, 1972.

34. Wittkowsky, U., P.R. Birch, J. Dominguez, and S. Suresh. “An apparatus for quantitative fretting fatigue testing.” Fatigue Fract Engng Mater Struct 22, 307-320. Blackwell Science Ltd., 1999.

Vita

Lieutenant Russell S. Magaziner was born in 1978 in Arlington, TX and grew up in Randolph, NJ from the age of three until college. He graduated from Randolph High School, Randolph, NJ in June 1996. In May 2000 he graduated from the United States Air Force Academy with a Bachelor of Science in Mechanical Engineering with minors in Mathematics and German Language. He was commissioned upon graduation of the Academy in May 2000. In August 2000 he was assigned to AFIT as a direct accession to earn a Masters of Science in Aeronautical Engineering with emphases in Materials and Structures. Upon graduation, LT Magaziner will be assigned to the National Air Intelligence Agency, WPAFB, OH to work as a tactical analyst.

REPORT DOCUMENTATION PAGE

Form Approved
OMB No. 074-0188

1. REPORT DATE *(DD-MM-YYYY)*	2. REPORT TYPE	3. DATES COVERED *(From – To)*
26-03-2002	**Master's Thesis**	Aug 2001 – Mar 2002

4. TITLE AND SUBTITLE

EXAMINATION OF CONTACT WIDTH ON FRETTING FATIGUE

5a. CONTRACT NUMBER

5b. GRANT NUMBER

5c. PROGRAM ELEMENT NUMBER

6. AUTHOR(S)

Magaziner, Russell S., 2LT, USAF

5d. PROJECT NUMBER

5e. TASK NUMBER

5f. WORK UNIT NUMBER

7. PERFORMING ORGANIZATION NAMES(S) AND ADDRESS(S)

Air Force Institute of Technology
Graduate School of Engineering and Management (AFIT/EN)
2950 P Street, Building 640
WPAFB OH 45433-7765

8. PERFORMING ORGANIZATION REPORT NUMBER

AFIT/GAE/ENY/02-8

9. SPONSORING/MONITORING AGENCY NAME(S) AND ADDRESS(ES)

AFRL/MLLMN
Attn: Dr. Jeffrey Calcaterra
2230 Tenth Street, Suite 1 DSN : 785-1360
WPAFB, OH 45433-7817 e-mail:Jeffrey.Calcaterra@wpafb.af.mil

10. SPONSOR/MONITOR'S ACRONYM(S)

11. SPONSOR/MONITOR'S REPORT NUMBER(S)

12. DISTRIBUTION/AVAILABILITY STATEMENT

APPROVED FOR PUBLIC RELEASE; DISTRIBUTION UNLIMITED.

13. SUPPLEMENTARY NOTES

14. ABSTRACT

The primary goal of this study was to find the effects on the fretting fatigue life when systematically holding the fretting fatigue variables, peak contact pressure, maximum/minimum nominal bulk stress, and the ratio of shear traction to pressure force constant while varying the contact semi-width through changes in pad radius and normal load. Experimental tests were performed on a test setup capable of independent pad displacement. Analytical and finite element simulations of the different experimental tests were performed. The local mechanistic parameters were inspected. Five different critical plane based fatigue predictive parameters lacked effectiveness in predicting changes in life with changes in contact width. The Ruiz parameter, and a modified version of the Ruiz parameter performed better than the five critical plane based parameters. Correlations between slip amplitude and fretting fatigue life were found. Tests experiencing infinite fatigue life, in contrast to the typical shortened fretting fatigue life, were experiencing the *gross slip* condition, which led to fretting wear instead of fretting fatigue.

15. SUBJECT TERMS

Fretting Fatigue, Fretting Wear, Critical Contact Width

16. SECURITY CLASSIFICATION OF:			17. LIMITATION OF ABSTRACT	18. NUMBER OF PAGES	19a. NAME OF RESPONSIBLE PERSON
a. REPORT	b. ABSTRACT	c. THIS PAGE			Prof. Dr. Shankar Mall, AFIT (ENY)
U	U	U	UU	186	19b. TELEPHONE NUMBER *(Include area code)* (937) 255-3636, ext 4587; e-mail: Shankar.Mall@afit.edu

Standard Form 298 (Rev. 8-98)
Prescribed by ANSI Std. Z39-18